1-1-2015

Therapeutic Targeting Of Bmp2 In Nf1-Deficient Malignant Peripheral Nerve Sheath Tumors (mpnsts)

Sidra Ahsan
Wayne State University,

THERAPEUTIC TARGETING OF BMP2 IN NF1-DEFICIENT MALIGNANT PERIPHERAL NERVE SHEATH TUMORS

by

SIDRA AHSAN

DISSERTATION

Submitted to the Graduate School

of Wayne State University,

Detroit, Michigan

in partial fulfillment of the requirements

for the degree of

DOCTOR OF PHILOSOPHY

2015

MAJOR: CANCER BIOLOGY

Approved By:

_____

Advisor Date

_____

_____

_____

_____

DEDICATION

This work is dedicated to my parents

For Ammi: Thank you for always being there for me. I would not have been able to complete this without your tremendous support and encouragement. Your strength and resilience has always inspired me to never give up.

For Abbu: Even though you are not here amongst us, your zest for life, kindness, patience, and gentle character inspires me to do better each day.

ACKNOWLEDGEMENTS

I would like to acknowledge my mentor Dr. Michael A. Tainsky for his invaluable guidance and support towards my training as a scientist. Thank you for providing me with countless opportunities to learn scientific techniques, participate in grant writing, encouraging internships and professional development opportunities. Most of all, thank you for allowing me to evolve into an independent thinker and teaching me how to ask complex scientific questions and answer them in a logical manner.

I would like to express tremendous gratitude to my committee members, who have contributed immensely to this project. This work would not have been possible without your insights and guidance. I would like to acknowledge Dr. Yubin Ge for helping me understand and design the cell viability studies. Thank you for always having your door open for questions and discussions. I would like to thank Dr. Raymond Mattingly and Dr. John Reiners Jr. for their input and advice on the pharmacology studies. Thank you for your dedication to this project and my training as a graduate student.

I would like to acknowledge and thank the WSU SOM Cancer Biology graduate program for their continuous financial support and funding of my graduate degree. I would like to acknowledge Dr. Matherly and Dr. Brush for their guidance through the PhD process and always taking time out of their busy schedules to address my concerns.

TABLE OF CONTENTS

LIST OF TABLES

LIST OF FIGURES

LIST OF ABBREVIATIONS

AKT: AK mouse strain T-thymoma

ALK: Activin-receptor-Like-Kinase

AU: Adenylate-Uridylate

BI: Bliss Independence

BMP: Bone morphogenetic protein

CI: Combination Indice

CSRD: cysteine and serine rich domain

Dox: Doxycycline

ECM: Extracellular cellular matrix

EGFR: Epidermal growth factor receptor

ERK: Extracellular signal-related kinase

FDA: Food and drug administration

GAP: GTPase activating protein

GBM: Glioblastoma multiforme

GC: Guanine Cytosine

GEF: Guanine nucleotide exchange factor

GFP: Green fluorescent protein

GRD: GAP-related domain

HP: high passage

ID: Inhibitor of Differentiation

JNK2: Janus Kinase 2

K_{decay}: decay rate constant

LP: low passage

MAPK: Mitogen-activated protein kinase

miR: microRNA

MEK: Mitogen-activated protein/Extracellular signal-related kinase Kinase

MPNST: Malignant peripheral nerve sheath tumor

mTOR: mammalian Target Of Rapamycin

MTT: 3-[4,5-dimethyl-thiazol-2-yl]-2,5-diphenyltetrazolium-bromide

NF1: neurofibromin I

NF1: Neurofibromatosis Type I

NSCLC: non-small cell lung carcinoma

PARP: poly(ADP-ribose) polymerase

PH: PH-like domain

PI3K: Phosphoinositide 3-Kinase

PTEN: Phosphatase and Tensin homolog

qRT-PCR: quantitative Real time-polymerase chain reaction

RAF: Rapidly Accelerated Fibrosarcoma

RFP: Red fluorescent protein

SDS-PAGE: SDS-polyacrylamide gel electrophoresis

Sec: Sec-14 domain

SMAD: Small Mothers Against Decapentaplegic

ssDNA: single stranded DNA

STAT3: Signal Transducer and Activator of Transcription-3

SYN: Syndecan binding region

TF: Transcription factor

TGF-β: Transforming Growth Factor-beta

TNF-α: Tumor Necrosis Factor-alpha

TSG: Tumor suppressor gene

TSS: Transcription start site

TUB: Tubulin binding domain

$t_{1/2}$: half-life

UTR: Untranslated region

Wnt: Wingless/int

CHAPTER I: Introduction

Malignant peripheral nerve sheath tumor (MPNST) is a rare form of cancer that originates from Schwann cells associated with the peripheral nerves. MPNST accounts for 5-10% of all soft tissue sarcomas (Strauss et al. 2001), which may occur sporadically or in association with Neurofibromatosis Type I (NF1). Up to half of MPNST cases are diagnosed in people with NF1 (King et al. 2000), and NF1 patients have an 8-13% chance of developing MPNSTs (Anghileri et al. 2006). NF1 is an autosomal dominant hereditary disorder due to loss of function in one parental copy of the neurofibromin (*Nf1*) gene, which predisposes individuals to a variety of disorders including MPNSTs as well as musculoskeletal abnormalities, developmental and cognitive disorders, and other cancer subtypes. *Nf1* is a tumor suppressor gene, which encodes for a RAS-GTPase activating protein (GAP) related domain (GRD) that negatively regulates Ras signaling by accelerating the hydrolysis of the active GTP-bound RAS (Xu et al. 1990). Neurofibromin deficiency results in constitutively active Ras signaling, which plays a central role in development and maintenance of NF1-related tumors.

MPNSTs are bulky, complex, debilitating tumors with grave prognosis. Mortality associated with MPNSTs is primarily due to its aggressive invasiveness and motility. Surgery is the primary treatment option for MPNSTs; however its success is limited by tumor infiltration, resulting in a high relapse rate. Due to the size and location of MPNSTs, surgery is often performed with wide margins, leaving behind cancer cells needing additional chemotherapy. Based on the crucial role of NF1 RAS-GRD in development of MPNSTs, therapies have been targeted towards the RAS-driven oncogenic pathways; however these therapeutic strategies have met with limited success.

The NF1-mediated regulation of Ras pathway is controlled by RAS-GRD (330 amino acids), which comprises a small portion of the NF1 protein that contains 2818 amino acids. The function of other NF1 domains is not very clear, and represents an understudied aspect of NF1-related pathologies. Interestingly, various single nonsense and missense mutations in the *Nf1* gene outside the GRD sequence can lead to NF1 disease manifestation in patients (Messiaen & Wimmer 2008). Another study reported that induced expression of *Nf1* RAS-GRD does not rescue the lethality associated with *Nf1*$^{(-/-)}$ mouse models (Ismat et al. 2006), suggesting that NF1 regulates vital mechanisms of development and tumorigenesis, independently of RAS-GRD. This project addresses the need to understand the functionality of NF1 in cancer cellular processes, independent of RAS-GRD, which can be employed as a therapeutic strategy in NF1-related MPNSTs.

Our lab conducted a systematic gene expression profiling study using MPNST cell lines with variable NF1 statuses to identify signaling cascades associated with NF1 malignancy, but independent of RAS-MEK1/2 signaling, to identify novel druggable targets for MPNSTs. In doing so, we have identified the bone morphogenetic protein 2, BMP2-SMAD1/5/8 signaling pathway, independent of the RAS-MEK1/2 regulation, as a therapeutic target in MPNSTs (Sun et al. 2013). The functional significance of targeting BMP2-SMAD1/5/8 signaling is demonstrated by the reversal of invasiveness and cellular motility in MPNST cell lines by inhibition of BMP2 (Sun et al. 2013). Gene expression data mined by our lab from NF1 patient tissue samples independently established that increased expression of BMP2 is associated with the degree of malignancy in Schwann cell-related tumors in NF1 patients (Miller et al. 2009).

In this study, I present the case for targeting of BMP2-SMAD1/5/8 signaling based on its role in motility and invasiveness in combination with current therapeutic strategies in MPNSTs. To design a rational targeted therapeutic approach, identification of the regulatory mechanisms leading to over-expression of BMP2 upon NF1 deficiency is warranted. To provide a comprehensive understanding of targeting BMP2-SMAD1/5/8 signaling in MPNSTs, we assessed the feasibility of targeting BMP2 at the protein level, and identified genetic targets mediating the increase in BMP2 signaling upon NF1 deficiency. The aim of this project is to utilize gene expression profiling studies to identify a novel druggable target, understand the regulatory mechanisms, and therapeutic utility of multiple targeted pathways in NF1-related MPNSTs.

1.1 Hereditary Cancers

Cancer is a disease of underlying genomic alterations. Mutations within the genetic material in tumor cells drive the initiation, progression, and evolution of cancers. Loss of function mutations result in deficient or complete loss of activity in proteins such as tumor suppressors, whereas gain of function mutations in oncogenes enhance protein activity. Accumulation of mutations in genes that maintain genomic stability is a hallmark of cancer. These genomic aberrations are mostly sporadic in nature, however some mutations can be inherited from parents to offspring.

Approximately 5-10% of cancers are caused by hereditary mutations (Garber & Offit 2005). The mechanism of genetic predisposition to cancer was described in the early 1970s, based on studies of hereditary retinoblastoma families, which led to the generation of the Knudson “two-hit” model of tumorigenesis (Knudson 1971). The Knudson model proposes that patients with hereditary susceptibility to cancers inherit

only one functional copy of the gene. Due to genomic instability or loss of heterozygosity, the affected patients lose the last functional copy of the gene resulting in absence of protein function (Knudson 1971), and ultimately leading to tumorigenesis. It is important to note that the Knudson model is specific to tumor suppressor genes (TSGs). Loss-of-function mutations are characteristic of TSGs, which require mutations in both alleles of a gene prior to manifestation of an effect. In contrast, gain-of function mutations occur in oncogenes where mutations in a single parental allele of a gene can result in novel or enhanced protein functionality.

Mutations within TSGs comprise the greatest proportion of inherited susceptibility to cancer (Hodgson 2008). These mutations often occur in pathways that regulate essential cellular processes including chromosomal stability (e.g. *p53*), DNA damage repair (e.g. *BRCA1, MLH1*) and cell cycle (e.g. *Rb, p53*) (Vineis et al. 2010). In the case of germline *p53* (Li-Fraumeni syndrome) and *Rb1* (Retinoblastoma) mutation carriers, malignancy is the defining characteristic of the hereditary syndrome. In other cases, such as *APC* (Familial Adenomatous Polyposis) and *Nf1* (Neurofibromatosis Type I) mutation carriers, afflicted individuals are not just at an increased risk for malignancy, but also present with non-cancerous features and congenital anomalies.

1.2 Neurofibromatosis Type I (NF1)

Neurofibromatosis Type I, formerly known as von Recklinghausen disease, is one of the most common heritable genetic conditions of the nervous system with a birth incidence of 1 in 2500-3000 individuals (Friedman 1999). The NF1 disease is caused by mutations in the neurofibromin I (*Nf1*) gene. *Nf1* is a TSG due to its well-characterized RAS-GRD, which negatively regulates RAS activity by accelerating the hydrolysis of the

activated GTP-bound RAS (Xu et al. 1990). Therefore loss of NF1 activity leads to activation of the wild-type Ras proto-oncogenes. NF1 is an autosomal dominant condition with nearly complete penetrance of the associated phenotypes (Friedman 1999). However, these traits are extremely variable in expression. Heterozygosity of the *Nf1* gene leads to a wide variety of clinical pathologies including café-au-lait macules, axillary freckling, Lisch nodules, cognitive disorders, bone deformities such as osseous lesions, and neurofibromas. (Brems et al. 2009). Presence of two or more of these aforementioned benign clinical features encompasses the diagnostic criteria for the NF1 disease (Hirbe & Gutmann 2014). NF1 patients are also susceptible to various forms of cancers, development of which requires a complete loss of *Nf1* gene function (Roma 2001). NF1 patients are at risk for developing glioma of the optic pathway (15-20%), MPNSTs (8-13%), gastrointestinal stromal tumors (4-25%), rhabdomyosarcomas (1.4-6%), leukemia, breast cancers, and other brain tumors (Hirbe & Gutmann 2014). Cancer subtypes among NF1 patients exhibit severe pathology with poor prognosis. NF1 patients have a five-fold increased chance of breast cancer occurring at a younger age (Sharif et al. 2007; Wang et al. 2012), and the mortality rate for breast cancer in NF1 patients is higher compared to the general population (Evans et al. 2011). NF1 patients also have a five-fold increased chance of developing glioblastomas with poor prognosis (Hatori et al. 2006; Gutmann et al. 2002).

Café au lait spots and multiple neurofibromas are distinguishing features of NF1 patients, as over 90% of NF1 patients display either one or both of these symptoms (Compston 1994a; Huson 1989a). Neurofibromas mostly occur during adulthood in NF1 patients, however early onset of optic gliomas, plexiform neurofibromas, cognitive

defects, and other neurologic syndromes have been reported in many cases (Watson 1967). Neurofibromas are complex benign peripheral nerve sheath tumors composed of Schwann cells, fibroblasts, perineural cells, and mast cells (Rutkowski et al. 2000). Cutaneous neurofibromas grow along the nerves or underneath the skin and are largely asymptomatic (Gerber et al. 2009). Approximately 56-57% of all NF1 patients develop plexiform neurofibromas which are extensive, larger neurofibromas that can occur anywhere within the body (Kluwe et al. 1999; Mautner et al. 2008). Plexiform neurofibromas are thought to be congenital lesions that manifest themselves during childhood in NF1 patients (Nguyen et al. 2011). Most importantly, plexiform neurofibromas are painful lesions that can transform into the most aggressive cancer subtype seen in NF1 patients called malignant peripheral nerve sheath tumors.

1.3 Malignant Peripheral Nerve Sheath Tumors (MPNSTs)

MPNST is a spindle cell soft-tissue sarcoma, which generally occurs on peripheral nerves in the trunk, extremities and head and neck regions (Nikumbh et al. 2013). MPNST is a rare form of cancer with a prevalence of 0.001% in the general population (Ducatman 1986a). The lifetime risk for NF1 patients to develop MPNSTs is estimated at 8-13% (Anghileri et al. 2006), with a recent study documenting the risk at precisely 11.7% in the NF1 population (Evans et al. 2012). In a Kaplan-Meier analysis, the five-year survival rate from diagnosis for MPNST patients with hereditary NF1 disease was 21%, compared to 42% for sporadic cases of MPNSTs (Evans et al. 2002). The majority of hereditary MPNST cases occur in the adult population between 20-40 years of age (Ducatman 1986b; Widemann 2009), however, MPNST is one of the more frequent soft-

tissue sarcomas seen in the pediatric population with a higher incidence among the 10-20 years age group (Bates et al. 2014).

Approximately 50% of MPNST cases occur in patients with NF1 disease (King et al. 2000), and 41% of the remaining sporadic MPNST cases present with sporadic mutations in the *Nf1* gene (Bottillo et al. 2009). Interestingly, a retrospective study of the northwest regional genetic registry in England reported a significant correlation between *p53* mutation carriers (Li Fraumeni Syndrome patients) and an increased risk of MPNST development (Anghileri et al. 2006). This is surprising because mutations of *p53* are not commonly found in NF1-related MPNSTs. In one study, only 11% of MPNST cases presented with mutations in *p53*; however, presence of these mutations was significantly associated with high tumor grades (Holtkamp et al. 2007).

1.4 Role of NF1 in MPNSTs

Mutations of the *Nf1* gene play a critical role in MPNST development given that the majority (~70.5%) of MPNST cases harbor either germline or sporadic mutations in the *Nf1* gene (Bottillo et al. 2009). Various types of mutations including nonsense mutations, missense mutations, intronic mutations, deletions and insertions occur in the *Nf1* gene, however no clear correlation between the specific type of mutations and their effects (genotype-phenotype relationships) have been identified (Shen et al. 1996). 80% of *Nf1* mutations in hereditary NF1 patients are frameshift or nonsense mutations, which result in a non-functional truncated protein (Jett & Friedman 2010). Microdeletions of the *Nf1* gene, specifically 1.5Mb deletions, confer increased risk of MPNST development in NF1 patients (De Raedt et al. 2003). Additionally, carriers of *Nf1* microdeletions present with severe cognitive dysfunction, early onset neurofibromas, and poor prognosis for MPNSTs

(Shen et al. 1996; De Raedt et al. 2003). The *Nf1* locus is the most highly mutable locus in the genome with a rate of mutation 100-fold greater than the average mutation rate (Shen et al. 1996). This is further supported by the fact that approximately half of NF1 individuals present with de novo mutations in the *Nf1* gene not found in their parents (Hirbe & Gutmann 2014).

1.5 Role of microenvironment in NF1-related malignancies

In-vivo disease modeling of *Nf1*-related tumors in genetically engineered mice has emphasized the role of *Nf1*-heterozygous tumor microenvironment and other molecular pathways (Munchhof et al. 2006). Complete deletion of the *Nf1* gene in mice results in embryonic lethality, whereas $Nf1^{(+/-)}$ mice do not develop neurofibromas or optic gliomas classically associated with NF1 disease (Jacks et al. 1994). Heterozygosity of the microenvironment of $Nf1^{(-/-)}$ Schwann cells or other cells of cancer origin has been identified as a requirement for development of optic gliomas as well as plexiform neurofibromas in mice (Bajenaru et al. 2002; Zhu et al. 2002). The *in vivo* neurofibroma model required tissue-specific deletion of *Nf1* in Schwann cells using the Cre/Lox transgene system, leaving intact the heterozygous state of the surrounding neurons, fibroblasts and mast cells (Zhu et al. 2002). $Nf1^{(+/-)}$ microglia and mast cells are identified as key players in development and maintenance of *Nf1*-related tumors (Daginakatte & Gutmann 2007; Riccardi 1993). A serum biomarker study showed increased expression of inflammatory cytokines such as IFN-γ, TNF-α, IL-6 and EGFR in patients with plexiform neurofibromas or MPNSTs (Park et al. 2013), emphasizing the role of the $Nf1^{(+/-)}$ heterozygous microenvironment particularly mast cells and monocytes in tumorigenesis. Interestingly, the neurofibroma mice models do not develop MPNSTs. The development

of an *in vivo* disease model of MPNST required haploinsufficiency of both *Nf1* and *p53*, in *cis* orientation on chromosome 11 (Cichowski et al. 1999).

1.6 Neurofibromin *(Nf1)* gene and function

The *Nf1* gene is located on chromosome 17q11.2 encoding an ~280kD cytoplasmic protein (Gutmann et al. 1995). The *Nf1* gene is composed of 60 exons covering over 350 kb of genomic DNA (Li et al. 1995), which results in a protein of 2818 amino acids (Bernards et al. 1992; Takahashi et al. 1994). Four alternative transcripts of *Nf1* have been identified called GRD I, GRD II, 3'ALT, and 5'ALT (Gutmann et al. 1995). The NF1 protein is highly conserved with more than 98% homology between human and mouse amino acid sequences (Bernards et al. 1993). NF1 protein is found in the cytoplasm where it co-localizes with cytoplasmic microtubules (Gregory et al. 1993). Although NF1 is ubiquitously expressed in a variety of tissues and cell types, functional studies indicate that NF1 is highly expressed in neurons, glial cells, Schwann cells, and oligodendrocytes (Daston & Ratner 1992).

The NF1 protein contains several domains in addition to the RAS-GRD, which is the most extensively studied domain of NF1. Protein-ligand interactions have been reported in the PH-like domain (PH), Sec-14 domain (Sec), tubulin binding domain (TUB), cysteine and serine rich domain (CSRD), and Syndecan binding region (SYN) of NF1 [Fig. 1.1] (S. Welti, 2008). NF1 forms a complex with CASK and syndecan via its SYN domain *in vivo* (Hsueh et al. 2001). Yeast two-hybrid system studies have shown that NF1 binds caveolin 1, a protein that regulates p21ras, PKC and growth response factors (Boyanapalli et al. 2006). NF1 also regulates adenyl-cyclase activity in the ATP-PKA-cAMP pathway in astrocytes (Tong et al. 2002; Dasgupta et al. 2003).

The most well-studied functional domain of NF1 is the RAS-GRD encoded by exon 21 to 27a, which shares sequence homology with the p120GAP (Daston & Ratner 1992). Increased RAS activity has been reported in NF1 patient-derived MPNST cells (Mattingly et al. 2006) as well as mouse models. Results from an NF1 patient screen demonstrated that a missense mutation, R1276P, in *Nf1* RAS-GRD leads to an 8000-fold loss of the GAP activity of NF1-GRD which can induce most NF1-related pathologies including malignant Schwannomas (Klose et al. 1998). Furthermore, overexpression of *Nf1* RAS-GRD restores cellular growth, proliferation and signaling in $Nf1^{(-/-)}$ cells (Hiatt et al. 2001). These reports highlight the importance of NF1 as a tumor suppressor, which inhibits cellular transformation by attenuation of Ras signaling and subsequent downstream effector pathways.

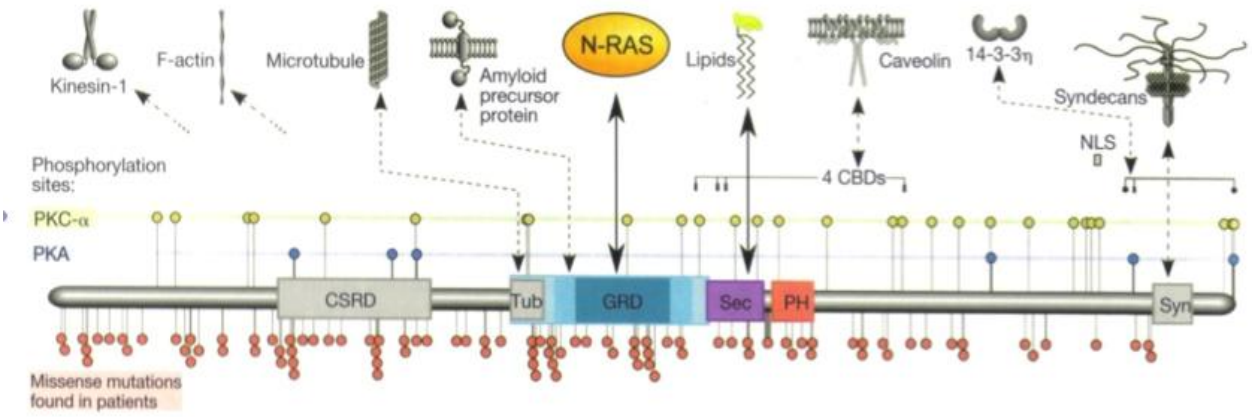

Figure 1.1: Domains of Neurofibromin I (NF1). Diagram of the prominent domains of NF1. The GRD highlighted in blue is the RAS GAP-related domain of NF1, which shares sequence homology to the p120-GAP protein. The GRD domain is flanked by a tubulin binding region (Tub) in grey, Sec-14 domain (Sec) in purple, and a Ph-like domain (PH) in red. NF1 protein also contains a cysteine/serine rich domain (CSRD) in grey, which contains a number of cAMP-dependent PKA binding sites. Blue circles indicate phosphorylation sites for PKA and yellow circles for PKC-α. Positions of missense mutations are marked by red circles. Figure adapted from *Neurofibromatoses* (S. Welti, 2008).

1.7 Signaling pathways regulated by NF1

1.7.1 Ras pathway

A proposed model of the underlying biological mechanism of *Nf1*-related MPNSTs suggests that de-differentiation of Schwann cells is driven by the Ras pathway, via activation of the MEK1/2-ERK1/2 axis (Harrisingh et al. 2004). NF1 inactivates Ras, thereby promoting the differentiation of Schwann cells. This hypothesis is further supported by the *Nf1* mouse model where Parada and colleagues demonstrated that the congenital lesions of plexiform neurofibromas occur during a short stage in Schwann cell development when immature and precursor cells, which are de-differentiated, are most abundant (Le et al. 2011). It logically follows that in the absence of NF1, Ras pathway is constitutively active, maintaining Schwann cells in a pre-mature stem like state. This stem cell-like state of cancer cells is distinctively associated with poorly differentiated, aggressive tumor sub-types (Monteiro & Fodde 2015). NF1 also plays an important role during self-renewal of neuroglial progenitor cells and differentiation of astrocytes in the peripheral nervous system (Hegedus et al. 2007). Spyra et al. have shown that an established MPNST cell line, S462, expresses stem cell markers and characteristics of stem-like cells such as self-renewal, clonality and an increased rate of tumor formation *in vivo* (Spyra et al. 2011).

Given the critical role of *Nf1*-RAS GRD in development of NF1-related phenotypes, including MPNSTs, members of the Ras pathway have been significant targets in treatment of MPNSTs. There are 4 forms of the RAS protein: H-RAS, N-RAS, K-RAS A and B, with N-RAS constitutively activated in *Nf1*-null MPNST cell lines (Mattingly et al. 2006). Members of the Ras protein family are mutated in over 30% of cancers, where

they are involved in cellular transformation, proliferation, survival, growth and metastases (Midgley & Kerr 2002). The Ras pathway is activated upon binding of growth factor ligands (e.g. PDGF, EGF, etc.), which stimulate signaling cascades leading to recruitment of guanine nucleotide exchange factors (GEFs). Prenylation, a post-translational modification, of the RAS protein facilitates its attachment to inner cell membrane where GEFs allow exchange of Ras-GDP (inactive state) with pools of intracellular GTP, thereby activating the Ras pathway (Basso et al. 2006; Gilman 1987). The Ras pathway is inactivated when Ras-GTP is hydrolyzed to Ras-GDP by an intrinsic Ras-GTPase. The hydrolytic activity of the intrinsic Ras-GTPase is weak, therefore inactivation of the Ras pathway requires binding of extrinsic GAPs, such as the one encoded by *Nf1*, to accelerate hydrolysis and inactivate Ras (Leondaritis et al. 2009). In absence of NF1, constitutively active GTP-bound Ras activates several downstream signaling pathways.

1.7.2 RAF-MEK-ERK and PI3K-AKT-MTOR axis

Ras exerts its diverse array of effects through activation of two prominent downstream effector pathways: rapidly accelerated fibrosarcoma (RAF)-Mitogen activated protein/extracellular signal-regulated kinase (ERK) kinase (MEK)-ERK (RAF-MEK1/2-ERK1/2) pathway and Phosphoinositide 3 kinase-mouse strain AK thymoma-mechanistic target of rapamycin (PI3K-AKT-mTOR) pathway [Fig. 1.2]. Both these signaling pathways regulated by RAS are hyperactivated in various forms of cancers, specifically those with aberrant RAS signaling. Active MEK1/2-ERK1/2 signaling promotes cellular proliferation and survival via regulation of cell cycle genes such as cyclin D1, pRB, and CDK4 (Samatar & Poulikakos 2014). The significance of the RAF-MEK1/2-ERK1/2 is well documented in proliferation and survival of NF1-associated

MPNST cell lines (Mattingly et al. 2006). The activation of MEK1/2 occurs in 91% of MPNST patient tissue samples, as compared to 21% of benign neurofibromas (Zou et al. 2009).

The induction of RAS also activates the PI3K/AKT/mTOR axis. Phosphatase and tensin homolog (PTEN), the master negative regulator of PI3K/AKT/mTOR axis, is frequently methylated in MPNST cell lines leading to increased AKT signaling in these cells (Bradtmoller et al. 2012). *Nf1* via its RAS-GRD negatively regulates the PI3K-AKT-mTOR axis (Johannessen et al. 2005). The pathogenic role of PI3K/AKT/mTOR pathway in MPNSTs is demonstrated by decreased cellular proliferation and angiogenesis in NF1-associated MPNSTs upon inhibition of mTOR by rapamycin (Bhola et al. 2010). MEK1/2-ERK1/2 and PI3K-AKT-mTOR signaling can be modulated independently of RAS by extracellular ligands that bind the epidermal growth factor receptors (EGFR). Accordingly, a recent study found that overexpression of EGFR via Janus kinase 2/signal transducer and activator of transcription 3 (JNK2/STAT3) activation transformed neurofibromas into MPNSTs in genetically engineered mice models (Wu et al. 2014). These molecular pathways have been the main focus of targeted therapies in NF1-related plexiform neurofibromas and MPNSTs; however, these therapies have exhibited limited clinical success.

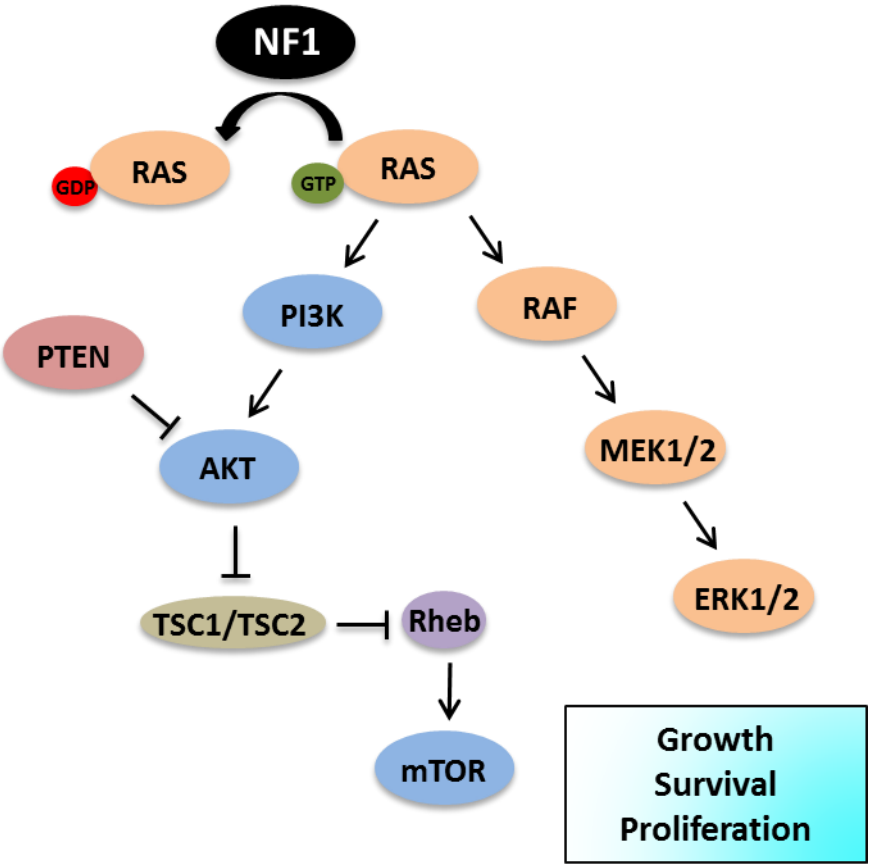

Figure 1.2: Prominent NF1-related RAS-associated signaling pathways. Simplified schematic of the NF1-related RAS-associated signaling axis. NF1 via its GRD attenuates Ras signaling. Upon *Nf1* deficiency, RAS bound by GTP is constitutively activated leading to activation of downstream signaling cascades, notably RAF-MEK1/2-ERK1/2, and PI3K-AKT-mTOR pathways. These pathways can be independently regulated by tumor suppressors such as PTEN, which is often methylated in MPNSTs. Activation of the RAF-MEK1/2-ERK1/2 and PI3K-AKT-mTOR signaling induces increased growth, proliferation and survival of MPNSTs.

1.7.3 RAS-independent pathways in NF1-related malignancies

Several studies have documented the role for NF1 as a tumor suppressor, independent of its RAS-GRD. The importance of NF1 domains other than the RAS GRD, is demonstrated by the failure to rescue embryonic lethality of *Nf1*$^{(-/-)}$ mice by induced expression of the GRD. Even though over-expression of *Nf1*- RAS GRD rescued mid-gestation lethality in *Nf1*$^{(-/-)}$ mice, it did not restore aberrant neural crest tissue development resulting in death (Ismat et al. 2006). NF1 has been shown to have effects independent of its regulation of RAS in *Nf1*$^{(-/-)}$ Drosophilia melanogaster where Ras signaling is intact and aberrant cyclic AMP dependent protein kinase A signaling is responsible for reduced larvae and adult body size (Guo et al. 1997).

In fibrosarcoma cell lines, NF1 regulates the Rho-ROCK-LIMK2 pathway independent of RAS effector pathways, to induce cytoskeletal reorganization (Ozawa et al. 2005). A deficiency in the RAS-related protein R-RAS2/TC21 in *Nf1*$^{(-/-)}$ Schwann cells results in up-regulation of TGF-β, leading to an increase in brain tumors and sarcomas while decreasing neurofibromas (Patmore et al. 2012). Moreover, gene expression profiling of MPNST patient samples revealed a positive correlation between the activation of the canonical Wingless/int (Wnt) signaling and malignancy of MPNSTs; in addition, subsequent downregulation of Wnt signaling reduced cell viability and tumorigenic potential in MPNST cell lines (Watson et al. 2013). Finally, by using the sleeping beauty transposon based somatic mutagenesis system in mice models, a recent study identified several new proto-oncogenes and tumor suppressors: FOXR2, PTEN, STAG1, TAOK1, BMPR2, etc. that cooperate with the classical Ras-associated pathways in formation of MPNSTs (Rahrmann et al. 2013).

1.8 Clinical management of MPNSTs

Surgery is the major curative option for MPNSTs, however it is performed with wide margins due to the size and location of these tumors (Friedman 2002). Even with surgery, radiation therapy, and adjuvant chemotherapy, survival for NF1 patients with MPNSTs is relatively poor. The poor prognosis of patients with hereditary NF1-related MPNSTs appears to be correlated with the presence of *Nf1* microdeletions which are associated with increased severity of any NF1-related phenotype (De Raedt et al. 2003). Another analysis suggests that poor survival of MPNST patients with NF1 is due to the size of tumors that are bulkier in NF1 patients compared to those with a sporadic MPNST (Anghileri et al. 2006). Concomitantly, large tumor size at presentation (typically >5 cm) has been the most consistent adverse prognostic factor for MPNST patients (Zou et al. 2009; LaFemina et al. 2013). A meta-analysis of the effect of NF1 status on survival of patients with MPNSTs shows a higher odds ratio of survival within the non-NF1 group compared to the NF1 group, however within the last decade survival between the two groups seems to have converged (Kolberg et al. 2013).

Chemotherapy for NF1 patients is primarily used in cases of unresectable plexiform neurofibromas or metastatic disease such as MPNSTs (Kolberg et al. 2013). Doxorubicin and ifosfamide have traditionally been used as the chemotherapy regimen for MPNSTs (Zehou et al. 2013). However, a ten-year institutional review of treatment of MPNSTs with doxorubicin and ifosfamide showed no correlation between chemotherapy and patient survival, questioning the use of such chemotherapies in MPNST patients (Zehou et al. 2013). In some cases, anthracycline is administered for palliative care in MPNST patients (Kroep et al. 2011).

Due to the failure of conventional chemotherapy, there has been a push towards targeted therapy of specific molecular pathways involved in the biogenesis of NF1-related MPNSTs. Based on the indispensable role of mast cells in MPNST maintenance, pre-clinical studies targeting the tumor microenvironment of MPNSTs have translated into human clinical trials using Gleevec, targeting c-kit function [NCT02177825]. The most well-studied function of NF1 is attenuation of the constitutively active Ras pathway in MPNSTs. Hence, inhibitors of the Ras pathway and rapamycin analogues have been used to treat gliomas, MPNSTs and plexiform neurofibromas, but with limited success. Tipifarnib, a farnesyl transferase inhibitor (FTI) that blocks the prenylation step in activation of the RAS protein, failed Phase II clinical trials [NCT00021541] in young NF1 patients with plexiform neurofibromas. It was determined that geranylgeranyl transferase compensates for the inhibition of prenylation of N-RAS and K-RAS by FTIs (Lerner et al. 1997; Whyte et al. 1997), suggesting that the prenylation, membrane association, and transforming activity of N-RAS and K-RAS was unaffected by the inhibition of farnesyl transferase. BRAF inhibitors, such as sorafenib exhibited increased toxicity in NF1 patients in clinical trials (Kim et al. 2013), whereas mTOR inhibitor sirolimus did not affect tumor burden, but prolonged time to disease progression by four months in plexiform neurofibroma patients (Weiss et al. 2015).

Due to the failure of targeting RAS in patients with plexiform neurofibromas, new strategies with re-designed agents targeting the downstream effectors of RAS pathway are being employed. Selumetinib, an ATP-independent inhibitor of the MEK1/2 pathway, was recently approved by the U.S. Food and Drug Administration (FDA) for the treatment

of uveal melanomas. Over 80% of uveal melanomas harbor mutations in *GNAQ* or *GNA11*, which behave similarly to *BRAF* mutations and result in constitutive activation of the Mitogen-activated protein kinase (MAPK) pathway (Van Raamsdonk et al. 2010; Van Raamsdonk et al. 2009). Also, selumetinib is currently in over twenty clinical trials for various types of cancers, specifically those dependent on increased MAPK signaling. It has proven patient tolerance in clinical trials, although, its effects as a single drug seem to be limited (Adjei et al. 2008). Most importantly, therapeutic efficacy of selumetinib is currently being investigated in PHASE II clinical trial for young adults with plexiform neurofibromas [NCT02407405]. Due to the inherent complexity of NF1-related MPNSTs, a single targeted agent therapy may not be efficacious, and therefore a combinatorial approach that targets multiple disease related pathways is the obvious option for comprehensive treatment and management of NF1-related MPNSTs. Targeting of Ras-associated pathways such as MEK1/2-ERK1/2 and PI3K-AKT-mTOR is necessary in plexiform neurofibromas and MPNSTs as these pathways play an important role in tumor development and maintenance. Nonetheless, identification and targeting of Ras-independent pathways is crucial for management of MPNSTs due to limited therapeutic benefits associated with targeting Ras-dependent signaling.

1.9 The case for targeting BMP2-SMAD1/5/8 signaling in NF1-related MPNSTs

Our lab conducted a systematic gene expression profiling study using MPNST cell lines with variable NF1 status to identify signaling cascades associated with NF1 malignancy, independent of the RAS-MEK1/2-ERK1/2 signaling, to identify new druggable targets for MPNSTs. Using pathway specific intervention, BMP2 was identified as a neurofibromin-dependent gene, independent of NRAS and MEK1/2 regulation (Sun

et al. 2013). Functional significance of BMP2 in MPNSTs was supported by decreased cellular migration and invasion upon inhibition of the BMP2 pathway in MPNST cell lines (Sun et al. 2013). The role of BMP2 in progression to MPNSTs is evident by changes in its expression levels at various stages of neurofibroma development in clinical specimens. *Bmp2* expression levels are significantly higher in MPNST patient samples, as compared to the benign forms of neurofibromas [Fig. 1.3].

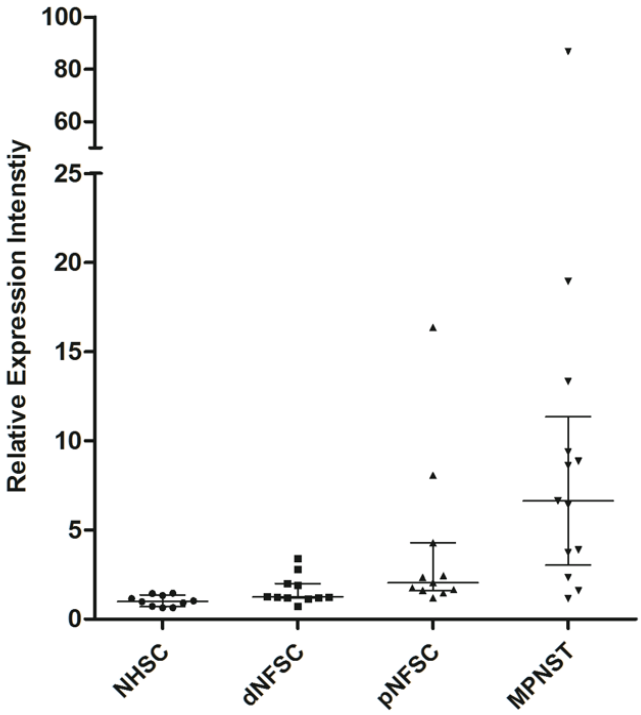

Figure 1.3: *Bmp2* expression levels in various stages of NF1-related Schwannomas. Data mined from a gene expression profiling study of Schwann cells derived from neurofibroma patient samples (Miller et al. 2009). Low levels of *Bmp2* are detected in normal human Schwann cells (NHSC) as well as cutaneous neurofibromas: dermal (dNFSC). *Bmp2* levels in plexiform neurofibromas (pNFSC) are similar to those in samples of dNFSCs, with a few outliers. MPNST patient samples show a remarkable increase in relative *Bmp2* expression levels. Analysis of *Bmp2* expression in neurofibroma patient samples suggests a stage-specific increase in *Bmp2* levels, which is associated with increased malignancy in NF1 patients (Sun et al. 2013).

1.10 Bone Morphogenetic Protein 2 (BMP2)

Based on amino acid sequence homology, BMP2 belongs to the transforming growth factor beta (TGF-β) family, which comprises the largest family of developmental peptides (Wozney et al. 1988). The *Bmp2* gene maps to chromosome 20p12, resulting in a 396 amino acid glycosylated polypeptide (Rao et al. 1992). BMP2 is highly conserved as mature regions of human, mouse and rat BMP2 are nearly identical (Chen et al. 2004a). BMP2 shares 98% amino acid sequence homology with BMP4, another member of the TGF-β subfamily (Wozney et al. 1988). Homozygous *Bmp2* mutant mice are non-viable, due to defects in development of exocoelomic cavity of the cardiac system (Zhang & Bradley 1996).

BMPs signal via hetero-oligomeric complexes of serine/threonine kinase receptors, type I and type II receptors. Specifically, BMP2 signals through three type I receptors: BMPR-IA or ALK-3, BMPR-IB or ALK-6, and ActR-IA or ALK-2 (Koenig et al. 1994). Upon ligand binding, type I and type II receptors form a hetero-tetrameric receptor complex (Moustakas et al. 2002) that initiates a signaling cascade involving Small Mothers Against Decapentaplegic (SMAD) family of proteins [Fig. 1.4]. SMAD 1, 5 and 8 are phosphorylated by the BMP receptor complex, which then associate with SMAD4 (Chen et al. 2004b). The SMAD1/5/8-SMAD4 complex translocates to the nucleus and initiates gene transcription in a tissue and developmental stage specific fashion (Moustakas et al. 2002; Akhurst & Hata 2012).

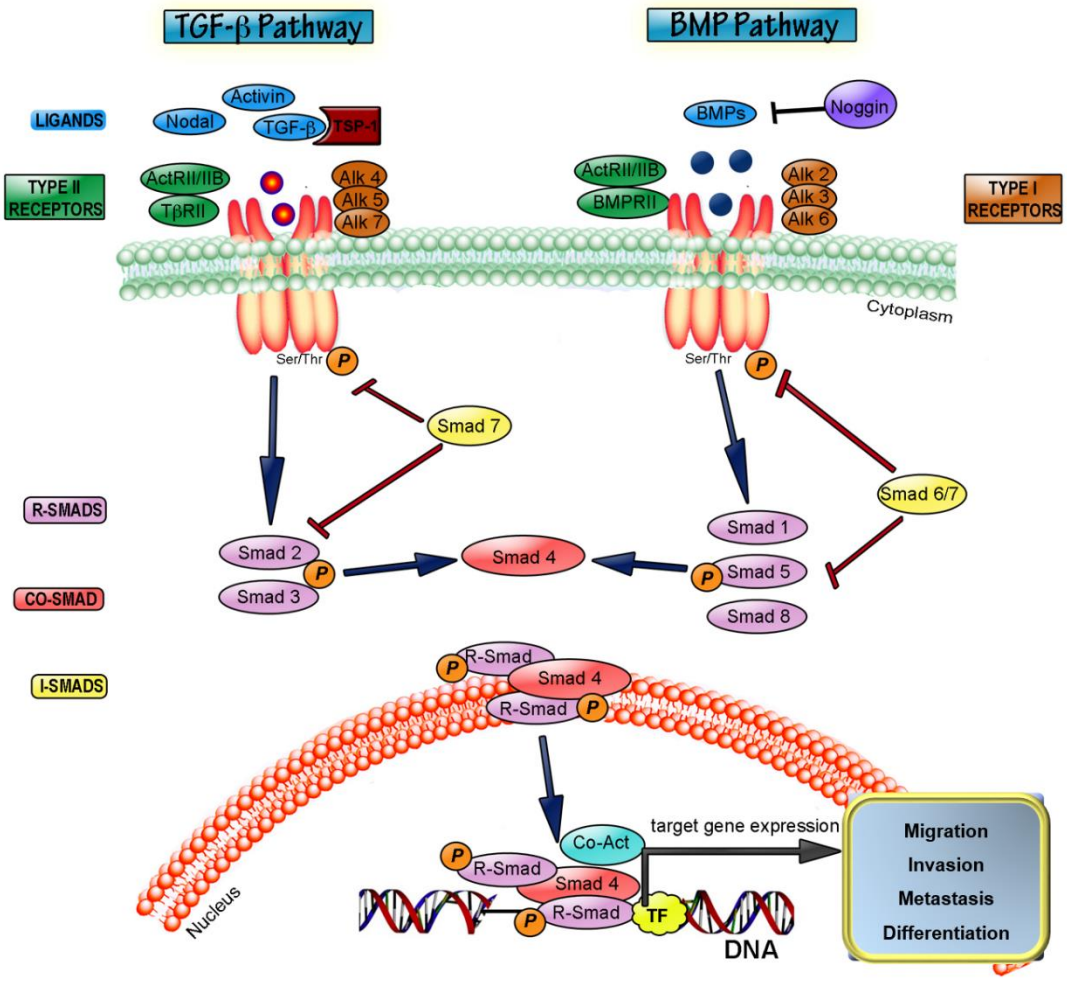

Figure 1.4: Signaling cascade of BMP and TGF-β pathway. TGF-β ligands such as Activin, Nodal and TSP-1 signal through Type II receptors, whereas the BMP sub-family signals via the Type I receptor. As BMPs bind Type I serine/threonine kinase receptors, Type I receptors form a hetero-oligomeric complex with Type II receptors resulting in phosphorylation of SMAD1/5/8. Phosphorylated SMAD1/5/8 associates with SMAD4, which results in its translocation to the nucleus. Various transcription factors regulate the nuclear SMAD1/5/8 complex to direct gene expression changes in cell differentiation, migration, invasion, and metastasis in a tissue and context-dependent manner. Noggin protein directly binds BMPs to inhibit their binding to the Type I receptor, whereas SMAD6/7 negatively regulate phosphorylation, thereby activation of SMAD1/5/8. This diagram is adapted from (Villapol et al. 2013)

1.11 Biological functions of BMP2

BMPs are involved in regulation of growth, differentiation, motility, and apoptosis in mesenchymal, epithelial, hematoepoetic, and neural cells during embryogenesis, organogenesis, and tissue homeostasis (Chen et al. 2004a; Wu & Hill 2009). The BMP sub-family has been extensively studied for its role in bone development and cartilage formation. BMP2 induces chondrocyte and osteoblast pre-cursor formation by interacting with the Sonic Hedgehog pathway during limb development (Niswander & Martin 1993). Subcutaneous injections of recombinant BMP2 have been shown to induce periosteal bone formation in mice (Chen et al. 2004a). Due to its extensive role in bone development, recombinant human BMP2 (rhBMP2) is administered to patients with various forms of fractures, spinal fusions and other bone and cartilage related abnormalities (Nauth et al. 2009). The use of rhBMP2 has been controversial based on comparison of its therapeutic benefits versus side effects in clinical trials (Lubelski et al. 2015). Interestingly, one of the side effects associated with administering rhBMP2 is tumor formation. A two year follow-up study of lumbar spinal arthrodesis patients who received rhBMP2 with bone grafts showed a higher incidence (4.6%) of cancer occurrence, as compared to the control group (0.8%), which only received bone grafts (Carragee et al. 2013).

BMPs play multiple essential roles in development of the central and peripheral nervous system. BMP/SMAD signaling is repressed during neural induction and development of the nervous system (Liu & Niswander 2005). BMP2 negatively regulates maturation of oligodendrocytes, myelinating cells of the central nervous system, by shifting neural precursors towards an astrocytic lineage (See et al. 2004). BMP2

cooperates with the Wnt signaling pathway to maintain pluripotency and suppress differentiation of the neural crest stem cells (Kleber et al. 2005). Although BMPs promote early glial development to immature Schwann cells from the neural crest (Dore et al. 2005), they prevent glial maturation by activation of AP-1 and Sp1 transcription factors (TF), which regulate promoter activity of glial fibrillary acidic protein in the peripheral nervous system (Dore et al. 2009).

1.12 Regulation of BMP2

1.12.1 Molecular inhibitors of BMP2/SMAD Signaling

Various members of the SMAD family negatively regulate BMP2 by binding its receptors and inhibiting their function. SMAD6 binds type I receptors and prevents the binding and phosphorylation of SMAD1/5/8 with SMAD4 (Imamura et al. 1997). SMAD6 is part of a negative feedback regulatory mechanism which is regulated by BMPs, given that SMAD1 and SMAD5 binding sites have been identified in the promoter of SMAD6 (Ishida et al. 2000). Another prominent inhibitor of BMP2 signaling is Noggin, which blocks the molecular epitope interfaces of both type I and type II BMP receptors (Krause et al. 2011). Transgenic mouse models of *Noggin* develop osteoporosis with a significant reduction in bone density, volume and formation (Devlin et al. 2003).

1.12.2 Transcriptional regulation of *Bmp2*

Mechanistic studies have demonstrated that *Bmp2* is primarily regulated at the transcriptional level. The promoter region of *Bmp2* has two major transcription start sites (TSS), with greater activity reported in the proximal promoter TSS as compared to the distal promoter in osteoblasts (Ghosh-Choudhury et al. 2001; Helvering et al. 2000).

Bmp2 is regulated by *cis*-regulatory elements with most enhancers located between 2.7 kb of the *Bmp2* TSS; however, distant enhancer elements located as far as 153.7 kb of the *Bmp2* promoter have been shown to drive *Bmp2* transcription in osteoblasts. (Pregizer & Mortlock 2009; Chandler et al. 2007).

Multiple pathways converge to activate BMP2 signaling. Wnt/β-catenin pathway controls *Bmp2* transcription through the Tcf/Lef response elements in the *Bmp2* promoter (Zhang et al. 2013). Retinoic acid is a known inducer of BMP2 signaling which activates BMP2 signaling via binding to retinoic acid response elements within the *Bmp2* promoter in osteoblasts and embryonic carcinoma cells (Rogers et al. 1992; Abrams et al. 2004). Inflammatory cytokines such as NF-κB, TNF-α and IL-β regulate *Bmp2* transcription in chondrocytes and chondrosarcoma cell lines (Fukui et al. 2003; Feng et al. 2003). p53 and delta-NP63α in association with SMAD1/5/8 occupy promoters of BMP target genes, such as inhibitor of differentiation (ID-1), to repress epithelial-mesenchymal transformation in mammary epithelial cells (Balboni et al. 2015). *Bmp2* has also been shown to be regulated at the post-transcriptional level by mRNA stabilization. Tumor necrosis factor-alpha (TNF-α) stabilizes *Bmp2* mRNA in rat chondrocytes via activation of the p38 MAPK pathway (Fukui et al. 2006). These studies suggest that *Bmp2* is primarily regulated at the transcriptional level via TF-binding to promoter regions, and/or through post-transcriptional mechanisms that modulate *Bmp2* transcript stability.

1.13 Significance of BMP2 in tumorigenesis

Role of BMP2 in cancer development and maintenance is dependent on the affected cell type and microenvironment. BMP2 is over-expressed in carcinomas of the prostate, lung, colon, breast, and ovary (Dai et al. 2008; Katsuno et al. 2008; Bieniasz et

al. 2015; Yu et al. 2008). BMP2 and BMP4 increase cellular motility and invasion in prostate cancer cell lines *in vitro* and *in vivo* (Dai et al. 2008). However, the role of BMP2 in prostate and pancreatic cancer cells is dependent on the hormonal status of the cells, where BMP2 stimulates tumor growth in androgen-independent prostate and pancreatic cancer cell lines but represses tumor formation in androgen-dependent cell lines (Kleeff et al. 1999; Ide et al. 1997). Moreover, BMP2 negatively regulates tumor growth in myelomas (Hsu et al. 2005). The role of BMP2 signaling in breast cancer is also controversial. In MCF-7 breast cancer cells, over-expression of *Bmp2* induced a G1 arrest and promoted apoptosis by increasing levels of cleaved caspase 3 (Chen et al. 2012). In contrast, inhibition of BMP2 by LDN-193189 reduced ALDH+ stem-like cells and expression of mesenchymal markers inhibiting epithelial to mesenchymal transition thus invasion, in mammary epithelial cells (Balboni et al. 2013).

BMP2 is over expressed in approximately 98% of lung carcinomas with little to no expression in normal or benign lung tissue (Langenfeld et al. 2005). Serum levels of BMP2 are two-fold higher in non-small cell lung cancer (NSCLC) patients as compared to the controls, correlating with advanced clinical stage of disease (Fei et al. 2013). BMP2 promotes tumor proliferation in A549 NSCLC cells via activation of the canonical SMAD1/5/8 pathway (Langenfeld et al. 2006), in which inhibition of BMP2 leads to decreased cellular proliferation and migration (Chu et al. 2014). A recent study demonstrated that BMP2 in NSCLC cell lines is regulated by microRNAs (miRs). Induced expression of miR-34b, miR-34c, and miR-486 attenuated BMP2 signaling and migration and invasion in A549 cells (Fotinos et al. 2014). Similarly, over-expression of BMP2 in epithelial ovarian cancers is well-documented where attachment and motility of epithelial

ovarian cancer spheroids is regulated by increased expression of BMP2 via activation of the AKT pathway (Peart et al. 2012). Increased *Bmp2* mRNA levels in epithelial ovarian cancer patient tissue samples positively correlate with tumor grade and shorter survival (Le Page et al. 2009). There are conflicting reports on the role of BMP2 in glioblastoma multiforme (GBM). One study reported that BMP2 is an effective pro-differentiation treatment for GBM stem cells and sensitizes these cells to treatment with temozolamide (Persano et al. 2012). On the contrary, Guo et al. showed that BMP2 promotes GBM formation by increasing proliferation, migration, and self-renewal of GBM cancer stem cells which can be reversed by overexpression of miR-656 (Guo et al. 2014).

1.14 Proposed role of BMP2 in development of NF1-related neurofibromas and MPNSTs

By comparing conditional *Nf1* knockout transgenic mouse models of premature non-myelinating Schwann cells versus differentiated Schwann cells, Zheng et al. identified *Nf1* knockout premature Schwann cells as the cells of origin for plexiform neurofibromas (Zheng et al. 2008). This is in accordance with the neurofibroma development model proposed by Harrisingh et al., in which the absence of NF1 and constitutively active Ras pathway drives de-differentiation of Schwann cells to a pre-mature state (Harrisingh et al. 2004), often marked by non-myelinated axons. Models of plexiform neurofibroma and MPNSTs exhibit a premature stem cell-like Schwann cell phenotype (Zheng et al. 2008; Spyra et al. 2011), and BMP2 is involved in maintenance and differentiation of Schwann cell precursors during development. Exogenous addition of BMP2 to rat Schwann cells inhibits expression of mature myelin-associated genes, resulting in a phenotypic switch to a pre-myelinating, immature Schwann cell state (Dore

et al. 2005). Many studies have reported cross-talk between BMP/TGF-β family members and Wnt, Notch signaling pathways. These pathways maintain tumor stem cell niches (Giancotti 2015) during development and tumorigenesis (Wu & Hill 2009; Guo & Wang 2009), and active Wnt signaling promotes the tumorigenic potential of MPNSTs (Watson et al. 2013). These studies suggest a role for BMP2 in transforming neurofibromas to a pre-mature stem-like state, which is characteristic of aggressive malignant tumors such as MPNSTs.

One of the major questions in development of MPNSTs is the role of mutations at loci other than the NF1 locus, such as p53, Rb, or PTEN. Only a fraction of NF1 patients with plexiform neurofibromas develop MPNSTs, indicating that haploinsufficiency of NF1 is necessary, but not sufficient for tumor formation (Farid et al. 2014). Interestingly, the mouse models of neurofibroma do not develop MPNSTs (Zhu et al. 2002), as development of MPNST *in vivo* requires haploinsufficiency of both the *Nf1* and *p53* gene (Cichowski et al. 1999). Given that carcinogenesis is a multi-step process, we expect changes in multiple signaling pathways and cellular processes to govern the transformation, development and maintenance of MPNSTs. A retrospective immunohistochemical staining of benign Schwannoma patient samples reported increased staining of $p16^{INK4A}$, indicative of senescence, which was absent in MPNST patient samples (Simonetti et al. 2014). Furthermore, $Nf1^{(+/-)}$ melanocytes reprogrammed to induced pluripotent stem cells senesce upon complete loss of *Nf1 in vivo* accompanied by an up-regulation of $p16^{INK4A}$ (marker of senescence) and the senescence associated secretory phenotype (Larribere et al. 2015). Ras-induced senescence is a well-studied phenomenon where activation of oncogenic features driven by the Ras pathway are

impeded by cellular defense mechanisms leading to senescence (Dimauro & David 2010). Since NF1 deficiency leads to activation of the Ras oncogene, Ras-driven senescence or tumor dormancy may be the major barrier in transformation of benign neurofibromas to malignant MPNSTs. Thus, activation of tumorigenecity would require mutations or aberrations in similar cellular defense signaling pathways particularly those which regulate cell cycle such as p53, Rb, PTEN, etc. BMP2 is exclusively up-regulated in MPNSTs as compared to benign neurofibromas (Miller et al. 2009), suggesting that BMP2 may be one of the key players in transformation of a senescent or dormant state of benign neurofibromas to a malignant phenotype. It is also possible that activation of BMP2-SMAD1/5/8 may not trigger the tumorigenic switch but instead contribute to transformation and/or maintenance of MPNSTs.

1.15 Project Overview

Using gene expression profiling, our lab identified BMP2 as the principal mediator of TGF-β signaling in NF1-related MPNSTs, independent of NRAS and MEK1/2 regulation. Figure 1.5 shows the BMP/TGF-β pathway analysis of the gene expression profiling study, in which BMP2 is the only significant member of the TGF-β family up-regulated upon *Nf1* knockdown in MPNST cell lines. Other BMP family members did not exhibit significant changes in gene expression levels upon *Nf1* knockdown, whereas BMP4, the closest homolog of BMP2, was down-regulated.

The following chapters will address the role and significance of BMP2 in NF1-related MPNSTs. I will demonstrate the functional significance of targeting BMP2-SMAD1/5/8 signaling in conjunction with MEK1/2 inhibition in MPNSTs. I will examine the regulatory mechanisms that lead to activation of BMP2 upon knockdown of *Nf1* to

identify a specific genetic target for increased BMP2 signaling in MPNSTs. Overall, I will present the feasibility of a combinatorial therapeutic approach by combined inhibition of the BMP2 pathway with inhibitors of other relevant pathways, to provide a comprehensive treatment strategy for improving clinical outcome of NF1-related MPNSTs.

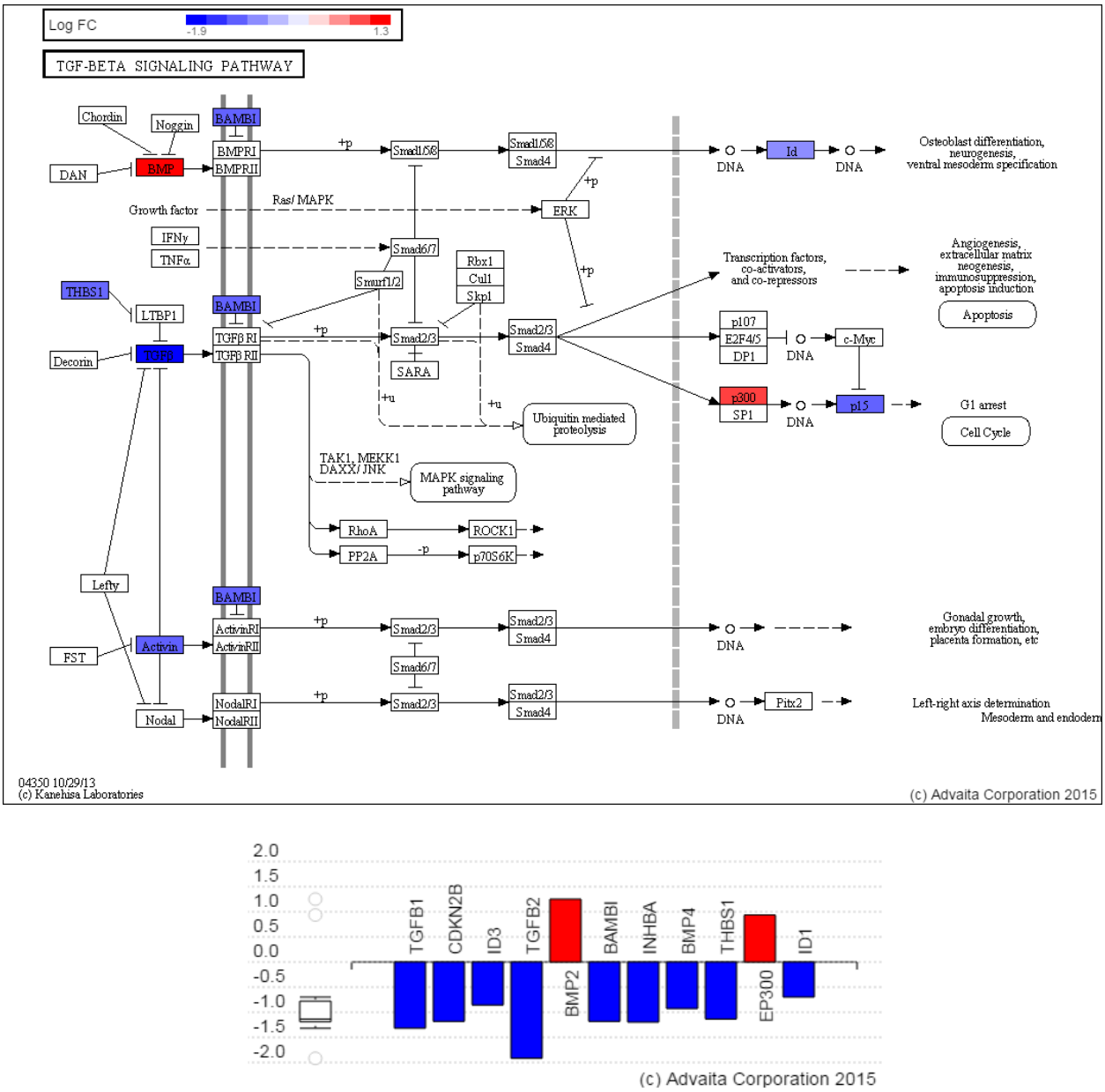

Figure 1.5: Pathway analysis of gene expression changes upon *Nf1* knockdown in MPNSTs. iPathway Guide software (Advaita Bioinformatics Co.) was used to analyze gene expression changes in the dataset (Sun et al. 2013) comparing STS26T-V($Nf1^{+/-}$) and STS26T-*Nf1* KD cells. Genes highlighted in color exhibit at least a two-fold change in expression levels with *p-value*<0.05. Red color denotes up-regulated genes and blue denotes down-regulation. According to pathway analysis of gene expression changes upon *Nf1* knockdown in MPNST cell lines, BMP2 is significantly up-regulated, BMP4 is down-regulated, whereas other BMPs do not change significantly. Other members of the TGF-β subfamily such as TGF-β, Activin, TMBS1 are down-regulated. No significant change is noted in Noggin, Chordin, or DAN (negative regulators of BMP2 signaling).

CHAPTER II: Regulation of BMP2 by NF1 in MPNSTS

2.1 Summary

NF1 suppresses MPNST formation by regulating RAS-MEK1/2-ERK1/2 and PI3K-AKT-MTOR signaling pathways, which are constitutively active upon NF1 deficiency and play a pivotal role in tumor initiation and maintenance. Using gene expression profiling of MPNST cell lines with variable NF1 status, our lab has identified that NF1 regulates an important signaling axis of BMP2-SMAD1/5/8 in MPNSTs. We have shown that BMP2 is up-regulated in *Nf1*$^{(-/-)}$ MPNST cell lines, and down-regulation of *Nf1* results in increased *Bmp2* mRNA expression and subsequent activation of the SMAD1/5/8 pathway (Sun et al. 2013). This chapter presents additional studies that validate the regulation of BMP2 by NF1 in novel MPNST cellular models. This chapter also serves as an introduction to the patient-derived *Nf1*-null MPNST cell lines and *Nf1* knockdown systems, which will be used to study the therapeutic targeting and mechanistic regulation of BMP2 in MPNSTs in the following chapters.

Data presented in this chapter establish that BMP2 is up-regulated upon NF1 deficiency at both transcript, protein, and secreted protein levels in MPNST cell lines. BMP2 expression levels were determined in low passage patient-derived *Nf1*$^{(-/-)}$ MPNST cells that are unaffected by artifacts of prolonged cell culturing, and better simulate the physiological condition of MPNSTs *in vivo* as compared to the high passage cells used previously. Furthermore, the regulation of BMP2 by NF1 is evaluated by using two independent knockdown systems: stable lentiviral-mediated *Nf1* knockdown and conditional *Nf1* knockdown.

2.2 Materials and Methods

2.2.1 Cell culture and cell lines

All MPNST cell lines used in this study were maintained in RPMI 1640 medium (Invitrogen, Waltham, MA, USA) supplemented with 5% fetal bovine serum (Hyclone Laboratories, South Logan, UT, USA). Low passage human MPNST ST88-14(*Nf1*$^{-/-}$), and low passage T265(*Nf1*$^{-/-}$) cells were a generous gift from Dr. Margaret Wallace (Department of Molecular Genetics and Microbiology, University of Florida, FL, USA). High passage human MPNST ST88-14(*Nf1*$^{-/-}$) cells (from T. Glover, University of Michigan, Ann Arbor, MI, USA), T265(*Nf1*$^{-/-}$) cells (from G. De Vries, Hines VA Hospital, Hines, IL, USA), and STS26T(*Nf1*$^{+/-}$) cells (from D. Scoles, Cedars-Sinai Medical Center, Los Angeles, CA, USA), were cultured for at least over 100 passages in our lab. STS26T*(Nf1*$^{+/-}$*)* cell line was used to establish a stable *Nf1* knockdown cell line, and the inducible *Nf1* knockdown cell lines. Cell lines were periodically checked and found negative for mycoplasma using MycoAlert Mycoplasma Detection Kit (Lonza, Basel, Switzerland). Cultures were propagated for no more than 3 months at a time.

2.2.2 Lentivirus shRNA mediated stable *Nf1* knockdown and inducible *Nf1* knockdown system

The pGIPZ lentiviral *Nf1* shRNA vector, Clone ID: V2LHS_76032 (Open BioSystems, GE Dharmacon, Lafayette, CO, USA), was used for targeted knockdown of *Nf1* in the STS26T*(Nf1*$^{+/}$*)* cell line. *Nf1* shRNA and scrambled control lentiviral particles were generated in HEK293T cells using a Trans-Lentiviral Packaging Kit (Thermo Fisher Scientific, Waltham, MA, USA). STS26T*(Nf1*$^{+/-}$*)* cells were infected with pGIPZ lentiviral particles and selected with puromycin (1.0 µg/mL) for 8 days post-infection. Selected

cells were confirmed by fluorescence microscopy for green fluorescence protein (GFP) expression, and a pooled population was maintained in selection media containing puromycin (0.5 µg/mL) for duration of experiments.

Conditional *Nf1* knockdown cell lines were established using the parent Schwann cell line STS26T*(Nf1*$^{+/-}$*).* STS26T was infected with two different clones of TRIPZ inducible lentiviral *Nf1* shRNA, Clone ID: V2THS_260806, and V3THS_380114 (GE Dharmacon, Lafayette, CO, USA). Conditional *Nf1* knockdown cells were selected with and maintained in puromycin (0.25 µg/mL). Individual colonies were picked to generate three stable tetracycline-regulated clonal cell lines. Selected clones were confirmed by fluorescence microscopy for expression of red fluorescence protein (RFP) present on the vector. Doxycycline (2 µg/mL) was added to cells to induce activation of the inducible lentiviral *Nf1* shRNA 24 hours prior to experiments.

2.2.3 Western blot analysis

Cells grown to 60-80% confluence were washed with cold PBS, scraped and lysed with RIPA buffer (150 mM NaCl; 1% Triton X-100; 0.5% deoxycholic acid, 0.1% SDS; 50 mM Tris-Cl; pH 8.0) supplemented with 1% protease inhibitor cocktail, 1% PMSF (from stock at 10 mg/mL in methanol), 1 mM Na_3VO_4, 1 mM $Na_4P_2O_7.10{\cdot}H_2O$, and 1 mM NaF. Eighty-five µg of whole cell lysate were loaded per well on 8% SDS polyacrylamide gel electrophoresis (SDS-PAGE) for subsequent detection of neurofibromin. Sixty five µg of whole cell lysate per well were run on 10% SDS-PAGE for subsequent detection of the phosphorylated and total forms of SMAD1/5/8 and ERK1/2. α-Tubulin was used as the loading control in all western blots. 0.45 µm nitrocellulose transfer membrane (Fisher Scientific, Waltham, MA, USA) was used for protein transfer.

Primary antibodies used in these experiments were rabbit polyclonal anti-neurofibromin 1:600 (#A300-140A, Bethyl laboratories, Montgomery, TX, USA), rabbit monoclonal anti-phospho-SMAD1/5/8 1:600 (#9516S, Cell Signaling, Danvers, MA, USA), mouse monoclonal anti-phospho-ERK1/2 1:1,000 (#9106S, Cell Signaling), rabbit polyclonal anti-SMAD1/5/8 1:400 (#9106S, Cell Signaling), rabbit monoclonal anti-ERK1/2 1:1,000 (#4695S, Cell Signaling), and mouse monoclonal anti-α-tubulin 1:5000 (#T5168, Sigma-Aldrich, St. Louis, MO, USA). Secondary antibodies 1:10,000, were conjugated to IRdye infrared dyes (Rockland Immunochemicals, Limerick, PA, USA). Signal was detected using the Odyssey infrared imaging system and software (Licor Biosciences, Lincoln, NE, USA) and the protein bands were quantified using ImageJ software.

2.2.4 ELISA test for secreted BMP2 protein

Cell culture supernatants were collected 24 hours post-incubation in RPMI-1640 supplemented with 0.5% FBS. Conditioned media was collected and concentrated using Amicon Ultra-4 Centrifugal filter units with 3 kDa cut-off (Merck Millipore, Billerica, MA, USA). Secreted BMP2 levels were analyzed using the BMP2 Quantikine ELISA kit (R&D Systems, Minneapolis, MN, USA). Duplicates of each sample were analyzed per experiment. A standard curve was generated using optical density (O.D.) of the BMP2 standards provided by the vendor. Secreted BMP2 levels for each sample were calculated against the standard curve and normalized to the standard medium as well as total protein concentration in conditioned media.

2.2.5 RNA extraction and quantitative real time PCR

RNA was extracted from 100 mm plates of 70-85% confluent cells using the RNeasy Mini Kit (#74106, Qiagen, Valencia, CA, USA). Three batches of total RNA (2.0 µg) for each cell line were reverse transcribed by SuperScript® II First-Strand Synthesis System (Invitrogen, Waltham, MA, USA). Q-RT-PCR was performed using Power SYBR Green MasterMix (Applied Biosystems, Carlsbad, CA, USA) and analyzed on the ABI 5700 Sequence Detection System (Applied Biosystems, Carlsbad, CA, USA). Primer sequences for each gene analyzed are listed in Table 2.1. The relative fold change was calculated using the CT method as follows: $2^{-\Delta\Delta CT}$, where, $\Delta\Delta CT = (CT_{Bmp2} - CT_{Gapdh})$ experiment - $(CT_{Bmp2} - CT_{Gapdh})$ control.

Table 1: Primer sequences used for gene expression studies by qRT-PCR

Gene	Forward	Reverse
Bmp2	GACACTGAGACGCTGTTCC	CCATGGTCGACCTTTAGG
Gapdh	ATCAAGAAGGTGGTGAAGCAG	TGTCGCTGTTGAAGTCAGAGG

2.2.6 Statistical Analyses

All experiments presented were replicated a minimum of three times. Paired t-test or ANOVA was used to determine the significant differences at 95% confidence interval.

2.3 Results

2.3.1 BMP2 is up-regulated in MPNSTs, independent of cell passaging effects

Our lab has previously demonstrated a significant increase in *Bmp2* mRNA levels in ST88-14($Nf1^{-/-}$) and T265($Nf1^{-/-}$) MPNST cell lines as compared to normal human Schwann cells ($Nf1^{+/+}$) (Sun et al. 2013). However, the $Nf1^{(-/-)}$ MPNST cell lines used in

the previous study had been cultured over many passages. Cells in culture are constantly subjected to environmental and manipulative stresses, which may introduce genotypic and phenotypic variations by selection of a dominant clone. These potential artifacts introduced by prolonged cell culturing are well-documented in literature. For example, PI3K-AKT signaling pathway inhibits activity of the androgen receptor in low passage prostate cancer cells, however this effect is reversed in the high passages of the same cell line (Lin et al. 2003). To circumvent the inherent bias of the cell culture system, low passage (LP) patient-derived MPNST cells, passages:8-16 for LP ST88-14($Nf1^{-/-}$), and passages:10-18 for LP T265 ($Nf1^{-/-}$) cell lines are used in this study to validate the role of BMP2 in MPNSTs. The results obtained from the LP ($Nf1^{-/-}$) MPNST cells are presented with those obtained from the high passages (HP) of the same ($Nf1^{-/-}$) MPNST cell lines.

To assess the steady-state expression levels of *Bmp2* mRNA in the LP *Nf1*-null MPNST cells, RT-PCR for *Bmp2* was performed using *Gapdh* as the housekeeping gene [Fig 2.1]. Fold changes for the tested cell lines were normalized to *Bmp2* expression levels in the *Nf1* heterozygous cell line: STS26T($Nf1^{+/-}$). Increased expression of *Bmp2* mRNA is detected in the LP MPNST cells similar to the HP cells [Fig. 2.1]. *Bmp2* mRNA levels are higher in the ST88-14($Nf1^{-/-}$) cells as compared to the T265($Nf1^{-/-}$) cell lines,

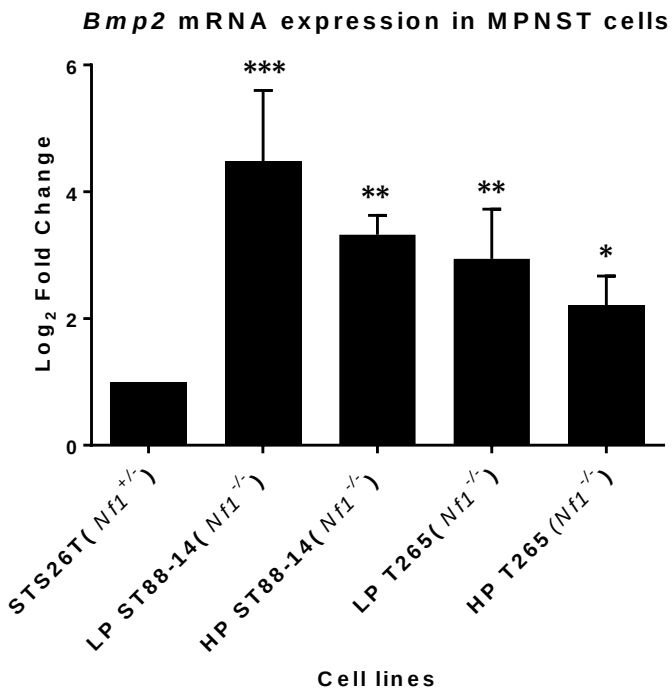

Figure 2.1: Quantitative RT-PCR of *Bmp2* mRNA in MPNST cells. In *Nf1*-null MPNST cells, the expression of *Bmp2* is significantly higher than in the STS26T($Nf1^{+/-}$) cells, which is used to calculate the relative fold change. RNA was extracted between passages 8-14 from LP ST88-14($Nf1^{-/-}$), passages 155-170 for HP ST88-14($Nf1^{-/-}$), passages 10-16 for LP T265($Nf1^{-/-}$) cells, and passages 208-230 for HP T265($Nf1^{-/-}$) cells. Data are presented as mean of three independent experiments ± SD (*P<0.05, **P<0.01, ***P<0.001, n=3 compared with the STS26T($Nf1^{+/-}$), One-way ANOVA followed by Tukey's test for multiple comparisons).

independent of passage numbers, however these differences are statistically insignificant.

Next, the abundance of BMP2 protein was assessed by using phosphorylation of SMAD1/5/8 as the readout in western blots in the low and high passage *Nf1*-null MPNST cells. Upon binding of its receptor, BMP2 activates a signaling cascade leading to the activation via phosphorylation of the SMAD1/5/8 complex. Figure 2.2 shows that phospho-SMAD1/5/8 is detected in all LP and HP ST88-14(*Nf1*$^{-/-}$) cells. Analysis of low and high passage T265(*Nf1*$^{-/-}$) cells shows an active BMP2-SMAD1/5/8 pathway as well, in which there is a slightly greater level of phospho-SMAD1/5/8 levels in the low passage T265(*Nf1*$^{-/-}$) cells as compared to its high passage counterpart. The presence of phospho-ERK1/2 in all of the tested cell lines is indicative of an active MEK1/2-ERK1/2 pathway, which is expected to be up-regulated in the absence of NF1 and subsequent RAS activation. The *Nf1*-null status of these cell lines is confirmed in the western blot, as no band for neurofibromin is detected in any of the cell lines [Fig 2.2].

The SMAD1/5/8 pathway can be activated by other members of the BMP sub-family such as BMP4, BMP7, BMP9, etc. As I used activation of SMAD1/5/8 as the surrogate for BMP2 in western blots, the secretion of BMP2 was assessed to ensure that the activation of SMAD1/5/8 is due to increases in BMP2 levels. This allows us to delineate the activation of SMAD1/5/8 pathway by BMP2 from other BMP family members. Furthermore, secretion of BMP2 is representative of its functional activity in both LP and HP *Nf1*-null MPNST cells. By using the sandwich ELISA methodology, conditioned media from each cell line was tested for levels of secreted BMP2 and normalized to the medium control without cells. Levels of secreted BMP2 in the

conditioned media of each cell line are significantly higher compared to the control medium [Fig 2.3]. LP and HP ST88-14(*Nf1*$^{-/-}$) cells secrete between ~150-200 pg/mL of BMP2. HP ST88-14(*Nf1*$^{-/-}$) cells secrete significantly higher levels of BMP2 (~200 pg/mL) as compared to the HP T265(*Nf1*$^{-/-}$) cells (~100 pg/mL). Otherwise, differences in the secretory concentration of BMP2 between low and high passage *Nf1*-null MPNST cell lines is statistically insignificant. In summary, profiling of BMP2 mRNA, protein, and secretion shows that BMP2 is expressed in *Nf1*-null MPNST cell lines, independent of passage numbers. The data presented in this section has validated our previous findings of BMP2 over expression in *Nf1*-null MPNSTs.

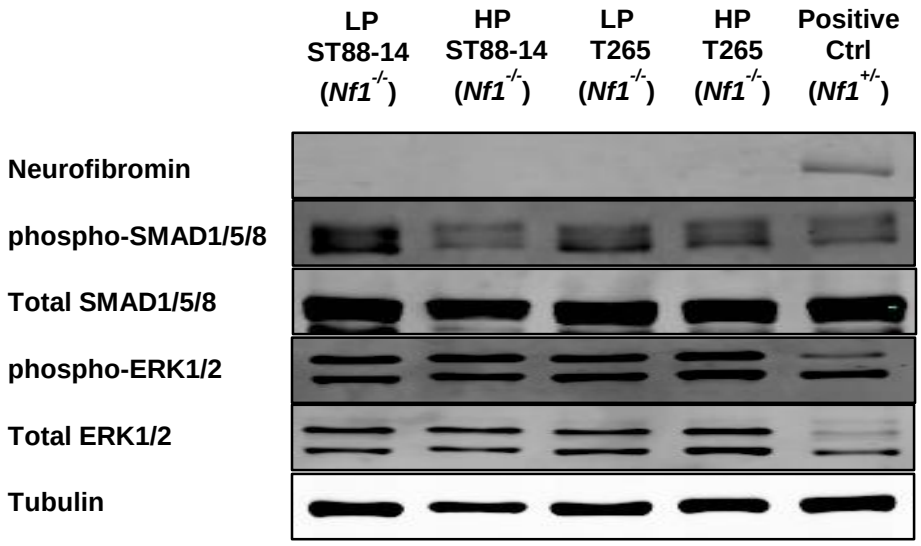

Figure 2.2: Activation of SMAD1/5/8 and MEK1/2-ERK1/2 pathways in MPNST cells. Representative western blot (n=3), of LP and HP (*Nf1*$^{-/-}$) MPNST cells lines confirms the NF1-null status of these cell lines as neurofibromin is not detected in any of the tested cells. Activation of the BMP2-SMAD1/5/8 pathway via detection of phospho-SMAD1/5/8 shows an activated BMP2-SMAD1/5/8 signaling axis. The discrepancy of phospho-SMAD1/5/8 levels between low and high passage ST88-14 (*Nf1*$^{-/-}$) cells can be explained by reduced loading in the HP ST88-14(*Nf1*$^{-/-}$) cells, as shown by the abundance of tubulin used as the loading control. Phosphorylation of both ERK1 and ERK2 is detected in all the cell lines, indicating an active RAS-MEK-ERK pathway.

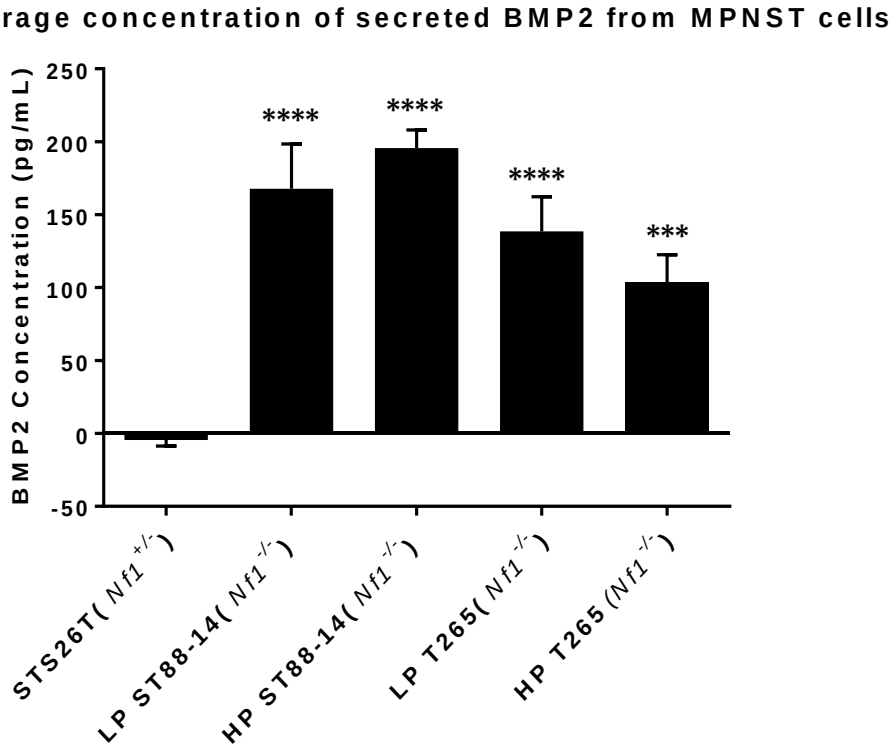

Figure 2.3: Secreted levels of BMP2 in NF1-null MPNST cells. Analysis of BMP2 secretion by ELISA using conditioned media from MPNST cell lines. BMP2 is secreted in both low and high passage *Nf1*-MPNST cells. Accounting for standard deviation, secreted levels of BMP2 vary minimally in both low and high passage ST88-14($Nf1^{-/-}$) cell lines, with 150-200pg/mL of secreted BMP2, respectively. BMP2 secretion in HP ST88-14($Nf1^{-/-}$) cells is significantly higher than in the HP T265($Nf1^{-/-}$) cells (P<0.01), however the difference between secretion of BMP2 in the LP ST88-14($Nf1^{-/-}$) and LP T265($Nf1^{-/-}$) is statistically insignificant . Cell culture supernatants from each cell line were collected 24 hours post-incubation in RPMI-1640 with 0.5% FBS, and plated in duplicates on to the BMP2 ELISA plate. Secreted BMP2 levels for each sample were calculated against the standard curve, and normalized for the medium, as well as total protein in conditioned media. Data are presented as mean of three independent experiments ± SD (***P<0.001, ****P<0.0001, n=3 compared with the STS26T($Nf1^{+/-}$), One-way ANOVA followed by Tukey's test for multiple comparisons).

2.3.2 BMP2 is regulated by NF1 in MPNST cells

We have established that BMP2 is overexpressed in *Nf1*-null MPNST cells, independent of prolonged cell culturing effects. This sub-section will demonstrate that the transcript and protein levels of BMP2 are dependent on the NF1 status in MPNST cells. Results from our gene expression profiling study of a transient *Nf1* knockdown in MPNST cells validated by RT-PCR has shown a two-fold increase in the levels of *Bmp2* mRNA upon knockdown of *Nf1*, which was followed by the activation of SMAD1/5/8 pathway (Sun et al. 2013). To validate the regulation of BMP2 by NF1, we generated two novel *Nf1* knockdown systems. The first approach was to generate a stable lentiviral *Nf1* knockdown cell line from a sporadic MPNST cell line STS26T($Nf1^{+/-}$). To eliminate any positional bias from the lentivirus site of chromatin integration, pooled populations of infected cells were used. The second approach was to generate an inducible *Nf1* knockdown cell model, in which down-regulation of *Nf1* can be temporally controlled in the same cell population. The inducible *Nf1* shRNA system provides the most specific cellular model to study the precise effect of *Nf1* on other signaling pathways by circumventing any bias introduced by off-target effects of the *Nf1* knockdown or control shRNA constructs. Moreover, by using multiple individual clones generated by the inducible *Nf1* knockdown shRNAs, the possibility of genotypic or phenotypic variations among clonal cell lines or introduced by the site of lentiviral integration is minimized.

2.3.2.1 Increased BMP2 expression upon down-regulation of neurofibromin

STS26T($Nf1^{+/-}$), a sporadic MPNST cell line, was infected with either an *Nf1* shRNA lentivirus to generate the STS26T-*Nf1* KD cells, or a scrambled control to generate the STS26T-V($Nf1^{+/-}$) cell line. The lentiviral infection was confirmed by

detection of the GFP-tag present on the plasmid vector by fluorescence microscopy. After selection for eight days, pooled populations from both stably-infected cell cultures were used. These cell cultures were propagated for maximum 6 weeks because at 8 weeks or thereafter, presence of the NF1 protein was detected in the *Nf1* knockdown cells. This can be possibly due to methylation of the long terminal repeats (LTR) of the lentiviral plasmid, or activation of a feedback mechanism by which *Nf1* is re-activated in these cell lines.

To validate the regulation of BMP2 by NF1, changes in the mRNA, protein, and secretory levels of BMP2 were assessed between the STS26T-V($Nf1^{+/-}$) and STS26T-*Nf1* KD cells. *Bmp2* mRNA levels upon *Nf1* KD were determined by calculating the fold changes in *Bmp2* levels relative to the STS26T-V($Nf1^{+/-}$) cell line [Fig. 2.4]. *Bmp2* mRNA levels increase approximately two-fold in the STS26T-*Nf1* KD cells as compared to the vector control, validating our previous findings based on the transient *Nf1* knockdown using miRNA oligonucleotides. RNA from HP ST88-14($Nf1^{-/-}$) cells was used as a positive control.

Results from the western blot and its quantification revealed ~75% knockdown efficiency of *Nf1* in the STS26T-*Nf1* KD cells [Fig. 2.5]. Although phospho-SMAD1/5/8 is detected in the STS26T-V($Nf1^{+/-}$) cells, indicative of an active SMAD pathway, there is increased phosphorylation of SMAD1/5/8 in the STS26T-*Nf1* KD cells [Fig. 2.5(A)]. Quantification of the western blot shows that upon knockdown of *Nf1*, levels of phosphorylated SMAD1/5/8 almost doubled in these cells [Fig. 2.5(B)]. As *Nf1* negatively regulates the Ras pathway, STS26T-*Nf1* KD cells show a significant increase in the levels of phospho-ERK1/2, indicative of activation of the MEK1/2-ERK1/2 axis of the Ras

pathway. Analysis of BMP2 secretion by ELISA demonstrates that levels of secreted BMP2 are dependent on the NF1 status [Fig. 2.6]. Approximately 90 pg/mL of BMP2 is secreted upon knockdown of *Nf1*, whereas insignificant differences in BMP2 secretion are noted between the vector control cells and the control media. Secreted levels of BMP2 in the STS26-*Nf1* KD cells are similar to those in the HP T265($Nf1^{-/-}$) cells at ~100 pg/mL [Fig 2.3]. Although phospho-SMAD1/5/8 is detected in the STS26T-V($Nf1^{+/-}$) cells in Fig. 2.5, the absence of BMP2 secretion in the same cell line [Fig. 2.6] highlights that NF1 exclusively regulates BMP2, independent of other BMP sub-family members, leading to phosphorylation of SMAD1/5/8 complex in MPNST cells. Data collected from the pooled *Nf1* knockdown cells suggests that mRNA, protein, and secreted protein levels of BMP2 are regulated by NF1, in which down-regulation of NF1 results in an increase in BMP2 expression levels and activity.

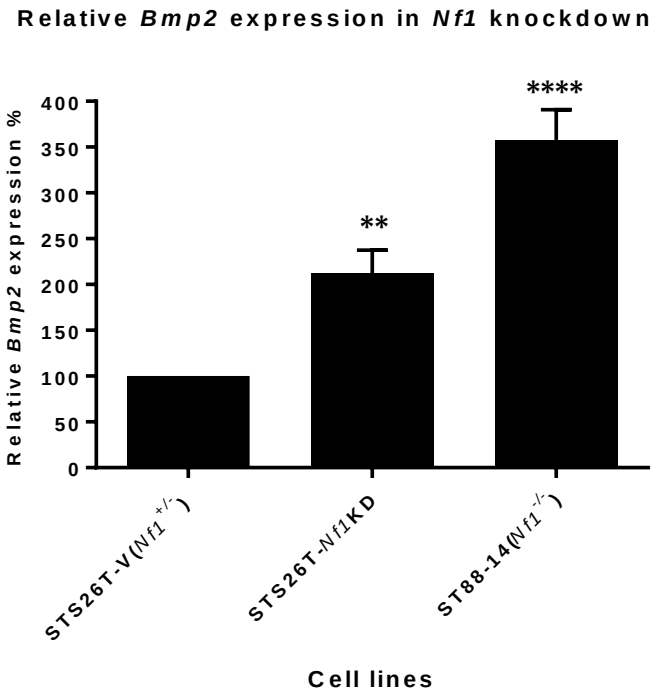

Figure 2.4: *Bmp2* mRNA changes upon *Nf1* knockdown. Upon knockdown of *Nf1* in the STS26T(*Nf1*$^{+/-}$) cells, expression of *Bmp2* increases two-fold as compared to the vector control cell line. Fold changes were normalized to steady-state mRNA levels in the STS26T-V(*Nf1*$^{+/-}$) cells. ST88-14(*Nf1*$^{-/-}$) cells were used as a positive control, where *Bmp2* expression was significantly higher than the expression in the sporadic MPNST cells (*P*<0.001). Data are presented as mean of three independent experiments ± SD (**P<0.01, ****P<0.0001, n=3 compared with the STS26T-V(*Nf1*$^{+/-}$), One-way ANOVA followed by Tukey's test for multiple comparisons).

A

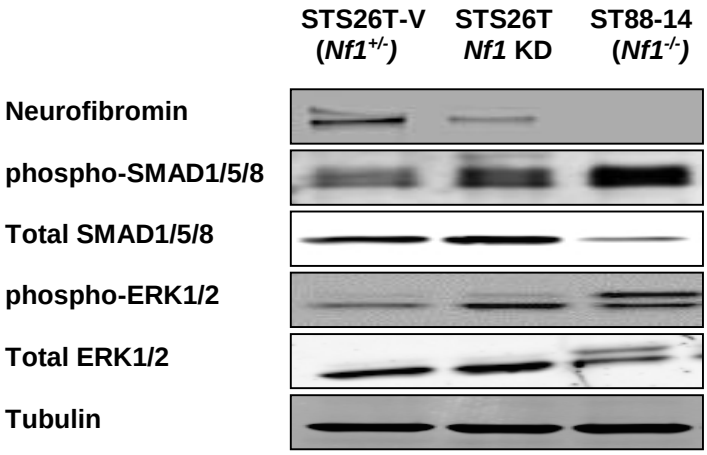

B

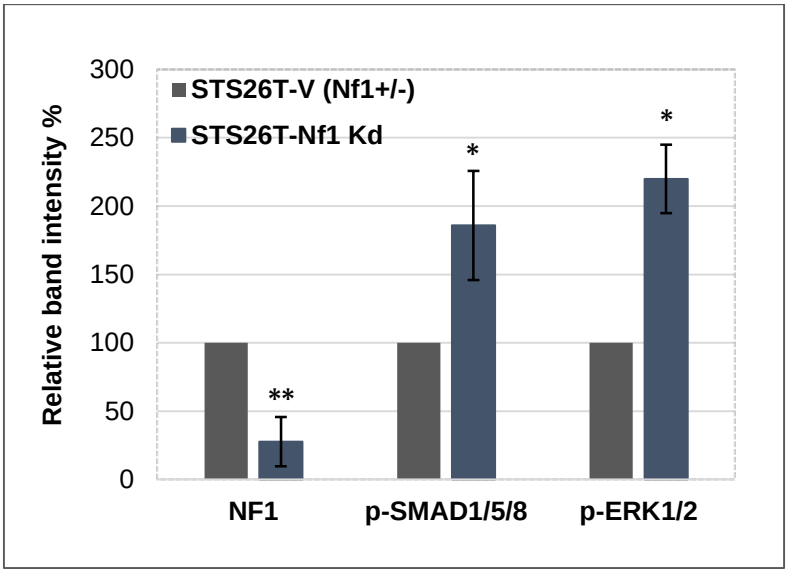

Figure 2.5: Activation of BMP2-SMAD1/5/8 pathway is dependent on NF1 levels. A: Representative western blot (n=3) shows that upon knockdown of *Nf1* in the STS26T(*Nf1*$^{+/}$) cells, levels of phosphorylated SMAD1/5/8, indicative of BMP2 status, and phospho-ERK1/2 increase. ST88-14 (*Nf1*$^{-/-}$) cells were used as a positive control. n=3. **B:** Quantification of the western blot shows that a knockdown efficiency of ~75% results in an almost 200% increase in levels of phosphorylated SMAD1/5/8. Phosphorylated ERK1/2 levels increase by ~220%. Paired t-test, n=3, **P*<.05, ***P*<.01. Data presented are mean quantification of 3 independent western blots ± SD.

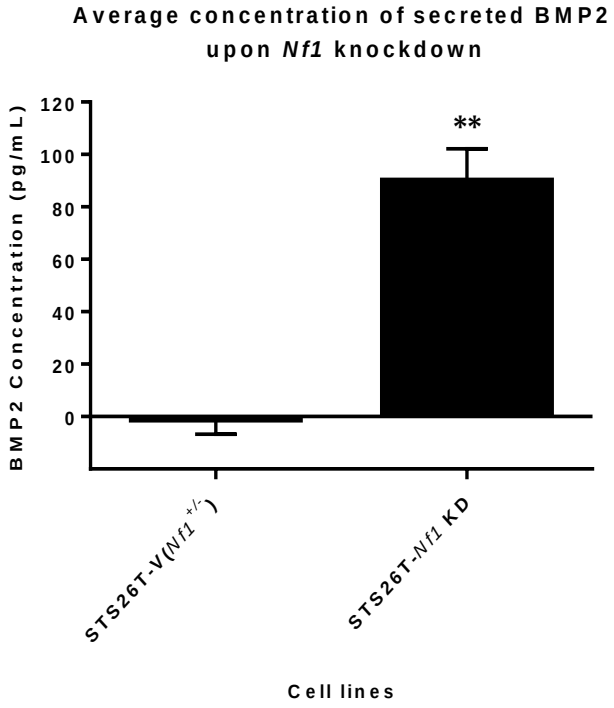

Figure 2.6: Secreted levels of BMP2 are regulated by NF1. Secreted levels of BMP2 are significantly higher from the STS26T-*Nf1* KD cells, as compared to the STS26T-V(*Nf1*$^{+/-}$) cells. Approximately 90 pg/mL of BMP2 is secreted from the STS26T-*Nf1* KD cells, whereas insignificant differences in BMP2 secretion are noted between STS26T-V(*Nf1*$^{+/-}$) cells and the media control. Cell culture supernatants from each cell line were collected 24 hours post-incubation in RPMI-1640 with 0.5% FBS, and plated in duplicates onto an ELISA plate coated with the BMP2 antibody. Secreted BMP2 levels for each sample were calculated against the standard curve, and normalized for the medium, as well as total protein concentration in conditioned media. Paired t-test, n=3, $^{**}P<0.01$. Data are presented as the mean of three independent experiments ± SD.

2.3.2.2 Changes in BMP2 levels are dependent on NF1 status in an inducible *Nf1* knockdown system

To verify that changes in BMP2 expression are exclusively dependent on the NF1 status of MPNST cells, an inducible *Nf1* knockdown system was chosen to study the regulation of BMP2 by NF1 in the same cell population. The inducible *Nf1* shRNA constructs used in these experiments are driven by a tetracycline-responsive promoter, in which *Nf1* shRNA is activated by addition of doxycycline (dox), a more stable derivative of tetracycline. We employed two tetracycline-regulated *Nf1* shRNA constructs as described in the methods section to generate three inducible *Nf1* KD cell lines. The plasmid backbone for both vectors is the same with variable *Nf1* shRNA sequences. Conditional knockdown (Cond. KD) #2 and #3 were generated from the same inducible *Nf1* shRNA, whereas Cond. KD #1 was generated from a different *Nf1* shRNA construct. Between eight to thirteen colonies were picked from cells infected with each *Nf1* shRNA construct after selection for twelve days. After which, these colonies were expanded and maintained in selection media. *Nf1* shRNA expression was induced by addition of doxycycline (2 µg/mL) for 24 hours prior to assays. The inducible *Nf1* shRNA vector contains a RFP-tag which along with the *Nf1* shRNA is driven by the tetracycline-responsive promoter. Hence, the presence of RFP expression is indicative of the activated *Nf1* shRNA. Based on RFP expression in dox-treated cells compared to the untreated, three colonies were expanded and used for further experiments [Fig. 2.7]. Increasing the concentration of doxycycline did not affect levels of RFP expression in these cells.

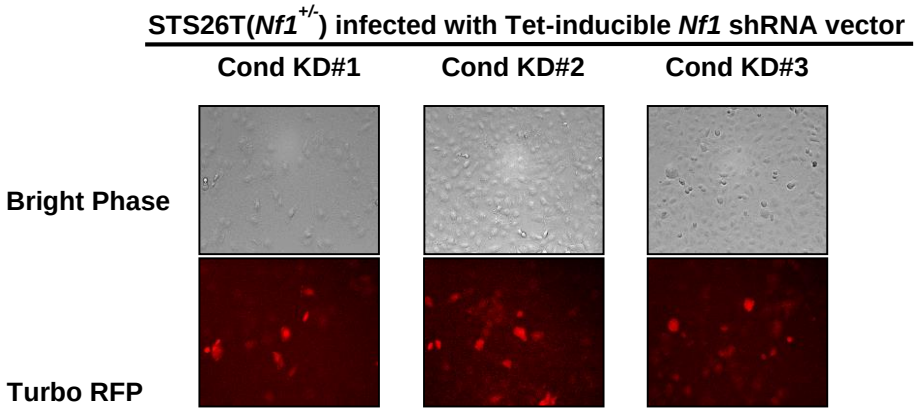

Figure 2.7: RFP expression in doxycycline-treated conditional *Nf1* KD cells. Using fluorescence microscopy, three clones generated from two inducible *Nf1*-shRNA constructs infected in the STS26T(*Nf1*$^{+/-}$) cells were selected based on RFP expression after 24 hours of treatment with doxycycline (2 µg/mL). Each clone is labeled as conditional knockdown (Cond KD) followed by the clone number. The conditional activation of the *Nf1* shRNA is dependent on treatment with doxycycline. The non-doxycycline treated cells of these clones did not show any RFP expression (data not shown). RFP was detected by the TRITC filter of the Olympus fluorescence microscope with an excitation/emission wavelength of 488/532 nm, respectively.

Changes in the mRNA levels of *Bmp2* were determined by RT-PCR of the untreated vs. the dox-treated conditional knockdown cells [Fig. 2.8]. As expected, levels of *Bmp2* mRNA increased upon induction of *Nf1* shRNA by doxycycline, as compared to the untreated controls. Levels of *Bmp2* mRNA increase between ~1.6-1.85 fold in each of the conditional KD cells, which is lower than the two-fold difference seen in the pooled STS26T-*Nf1* KD cells, as shown in Figure 2.1. Insignificant differences in *Bmp2* mRNA levels between the dox-treated STS26T($Nf1^{+/-}$) and untreated STS26T($Nf1^{+/-}$) cells suggests that the increased Bmp2 mRNA levels in the dox-induced conditional *Nf1* knockdown cells is not an off-target effect of doxycycline.

To evaluate changes in the protein abundance of activated SMAD1/5/8 complex and ERK1/2 upon knockdown of *Nf1* in the conditional KD cells, western blotting was used [Fig 2.9]. First, we established that 2 µg/mL of doxycycline (concentration used to induce the knockdown) does not affect phosphorylation of the SMAD1/5/8 complex [Fig 2.9(A)]. Fig 2.9(B) and (C) show that the induction of phospho-SMAD1/5/8 and phospho-ERK1/2 are dependent on the status of NF1, following the same pattern as the pooled stable *Nf1* KD cells. Upon treatment with doxycycline for 18-24 hours, the efficiency of *Nf1* knockdown remained fairly consistent in multiple western blots with Cond KD #2 and #3 displaying better knockdown efficiency as compared to Cond KD#1. Cond KD #2 and #3 are clones picked from infected cells derived from infection of the same *Nf1* shRNA construct, suggesting that the efficiency of KD in the inducible system is dependent on the specific shRNA construct.

In Figure 2.10, secretion of BMP2 was evaluated by ELISA from the conditional KD cells. As shown by insignificant changes in secreted BMP2 levels between dox-

treated STS26T(*Nf1*$^{+/-}$) cells and untreated control, 2 µg/mL of doxycycline does not affect secretion of BMP2. All conditional *Nf1* KD cells showed an increase in the secreted levels of BMP2 upon induction of the *Nf1* shRNA in a span of 24 hours. In the conditional KD cells, secreted BMP2 levels are dependent on the efficiency of KD as shown by the results of western blotting in the same cell lines. Cond. KD#1 cells secrete lower levels of BMP2 as compared to the Cond. KD#2 and #3, which exhibit better *Nf1* knockdown efficiency.

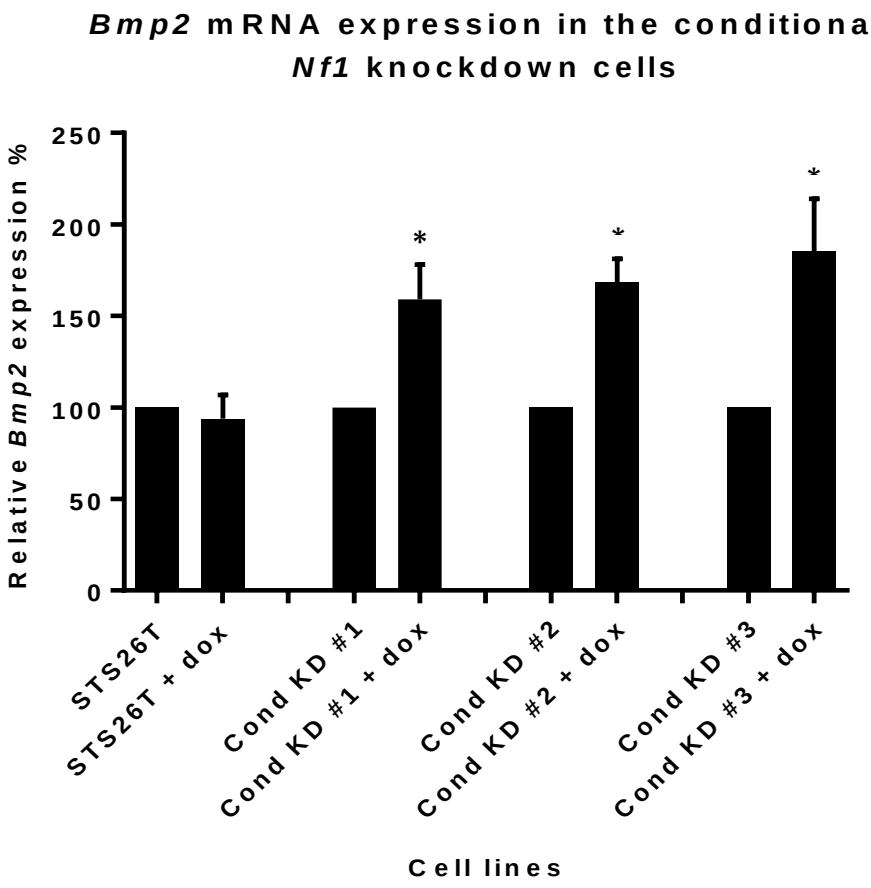

Figure 2.8: Quantitative RT-PCR of *Bmp2* mRNA in conditional *Nf1* knockdown cells. Upon treatment with doxycycline (2 µg/mL) for 24 hours, *Bmp2* mRNA levels increase between 160-185% in clones of the conditional *Nf1* knockdown cells. STS26T(*Nf1*$^{+/-}$) cells treated with dox (2 µg/mL) were used as a negative control to eliminate any dox-dependent changes in *Bmp2* mRNA levels. Percent fold change for each cell line were normalized to the untreated controls of each cell line which was set at 100%. Paired t-test, n=3, *P<0.05. Data are presented as the mean of three independent experiments ± SD.

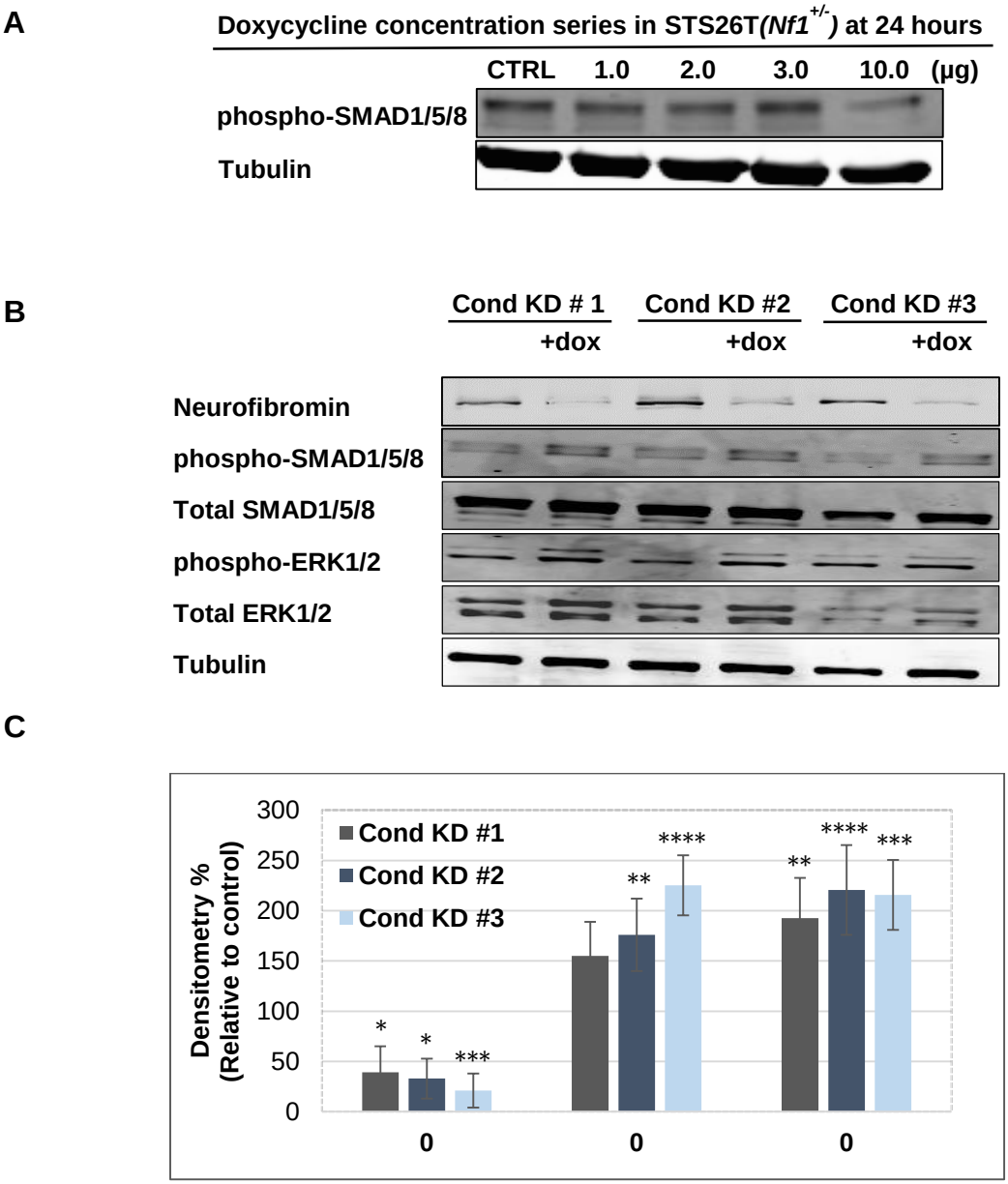

Figure 2.9: BMP2-SMAD1/5/8 pathway is activated upon induction of *Nf1* shRNA. **A:** Treatment of STS26T(*Nf1*$^{+/-}$) cells with various concentrations of doxycycline for 24 hours shows that 2 µg/mL doxycycline has no effect on the SMAD1/5/8 pathway. **B:** Representative western blot (n=3) of the inducible *Nf1* KD cells indicates that upon treatment with 2 µg/mL doxycycline for 24 hours, levels of NF1 are downregulated resulting in an increase in phospho-SMAD1/5/8 and phospho-ERK1/2 levels (n=3). **C:** Quantification of protein bands was normalized to untreated cells. Results suggest a proportional activation of p-SMAD1/5/8 and p-ERK1/2 based on the efficiency of KD of *Nf1*. Data presented are mean quantification of 3 independent western blots ± SD (**P*<0.05, ***P*<0.01, ****P*<0.001, *****P*<0.0001, n=3, compared to the untreated controls of each cell line, One-way ANOVA, followed by Tukey's test for multiple comparisons).

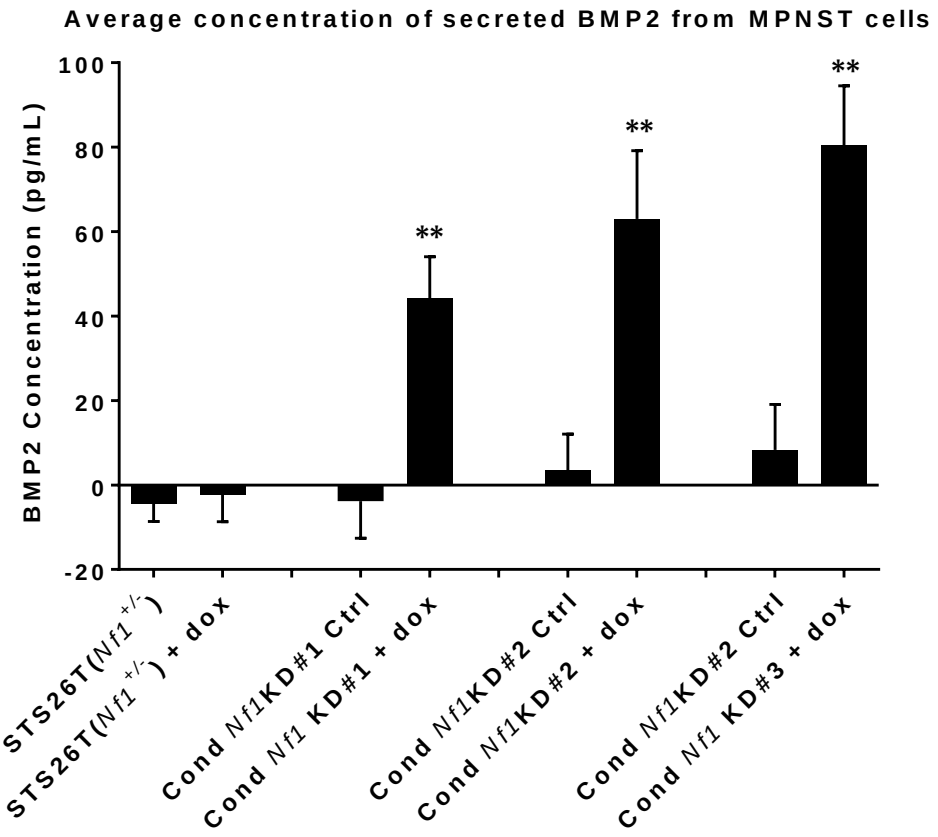

Figure 2.10: Secretion of BMP2 is regulated by NF1 in conditional *Nf1*-KD cells. Evaluation of secreted BMP2 levels level upon induction of *Nf1* shRNA. As shown by insignificant changes in BMP2 secretion of the parent STS26T(*Nf1*$^{+/-}$) cell line upon treatment with doxycycline (2 µg/mL), dox does not affect secreted levels of BMP2. Upon treatment with dox (2 µg/mL), secretion of BMP2 was induced in the conditional *Nf1* KD cells. Untreated control cells of conditional KD #1, #2, and #3 secrete little to none BMP2, levels of which significantly increase upon induction of the *Nf1* shRNA by treatment with doxycycline. Cell culture supernatants from each cell line were collected 24 hours post-incubation in RPMI-1640 with 0.5% FBS. Doxycycline (2 µg/mL) was added to the indicated cells at the start of the 24-hr incubation period. Collected conditioned media was plated in duplicate onto an ELISA plate coated with the BMP2 antibody. Secreted BMP2 levels for each sample were calculated against the standard curve, and normalized for the medium, as well as total protein concentration in conditioned media. Paired t-test, n=3, ***P*<0.01. Data are presented as mean of three independent experiments ± SD.

2.4 Conclusions

By using various MPNST cellular models and *Nf1* knockdown systems, data presented in this chapter have verified that NF1 regulates BMP2 expression in MPNST cell lines. Specifically, down-regulation of NF1 results in increases in mRNA, protein, and secreted levels of BMP2. Both low and high passage ST88-14($Nf1^{-/-}$) and T265($Nf1^{-/-}$) cells exhibit increased levels of *Bmp2* mRNA expression, active BMP2-SMAD1/5/8 and MEK1/2-ERK1/2 pathways, and increased secretion of BMP2 as compared to the STS26T $Nf1^{(+/-)}$ MPNST cells. Thereby, we can conclude that overexpression of BMP2 in MPNSTs is independent of cell culture passage effects. LP $Nf1^{(-/-)}$ MPNST cells were chosen to validate BMP2 expression and activity as they are a better physiological model of MPNSTs as compared to the HP $Nf1^{(-/-)}$ MPNST cell lines that were subjected to prolonged cell culturing. Concomitantly, data obtained from the LP $Nf1^{(-/-)}$ MPNST cells corroborates the gene expression profiling data of MPNST patient tissue samples by an independent group in which BMP2 is exclusively up-regulated in MPNSTs as compared to other benign forms of neurofibromas (Miller et al. 2009).

By using two independent *Nf1* knockdown cellular models, we validated the regulation of BMP2 by NF1, independent of genotypic variations that can be introduced by off-target effects of shRNAs and sites of lentivirus insertion. Both the pooled *Nf1* KD cells and the doxycycline-inducible *Nf1* KD cells have increased *Bmp2* mRNA expression and protein levels as compared to the control ($Nf1^{+/-}$) cells. Data obtained from both the pooled and the conditional *Nf1* KD cells demonstrated that the activation of the BMP2-SMAD pathway is dependent on the percentage of *Nf1* knockdown. The greater the decrease in NF1 levels, the higher the increase in levels of phosphorylated SMAD1/5/8

and secreted levels of BMP2. In summary, the increase in BMP2 expression and subsequent activation of the SMAD pathway is dependent on NF1 status in MPNST cells.

CHAPTER III: Therapeutic efficacy of combinatorial targeting of BMP2 and MEK1/2 in MPNSTs

3.1 Summary

The clinical management of MPNSTs is quite challenging due to its aggressive nature and limited therapeutic options. Surgical resection of the tumor with wide margins is often insufficient to remove all tumors cells and necessitates the use of chemotherapy to target the cancer cells left behind. Given that conventional chemotherapy has met with limited success in the management of MPNSTs, targeted therapy of aberrant signaling cascades involved in tumorigenesis is crucial for improving the clinical outcome of MPNST patients. The goal of this chapter is to test novel therapeutic strategies to target the viability, growth, proliferation, and invasiveness of MPNSTs by exploiting mechanisms of signal transduction downstream of the NF1 deficiency. In doing so, we will explore the functional significance of targeting BMP2 alone, and in combination with available therapeutic options targeting the constitutively active RAS-MEK1/2-ERK1/2 pathway. To determine the therapeutic efficacy of targeting of these signaling pathways in MPNSTs, a small molecule inhibitor of the BMP2 type I receptor (LDN-193189) and a MEK1/2 inhibitor (Selumetinib) was employed. Data presented in this chapter are an evaluation of the anti-cancer effects of mono-therapy or combinatorial therapy by these agents.

BMP2 is overexpressed in many different tumor types and has been associated with motility, invasiveness, and metastasis (Singh & Morris 2010); all of which are defining features of malignant spread of MPNSTs. Through inhibition of BMP2 signaling by LDN-193189, our lab has previously shown that LDN-193189 reduces cellular motility and invasiveness in various MPNST cell lines *in vitro* (Sun et al. 2013). Data presented in this

chapter validate these effects in physiologically relevant cellular models. Additionally, we demonstrate that selumetinib synergizes with LDN-193189 to decrease cellular viability, whereas combination treatment with both the candidate agents does not affect cellular migration and invasiveness of MPNST cells in comparison to treatment with LDN-193189.

3.2 Materials and Methods

3.2.1 Western blot analysis

MPNST cells were treated with specified concentrations of LDN-193189 and/or AZD6244 or with vehicle control (DMSO) for indicated time points. These were washed with ice cold PBS, scraped and lysed with RIPA buffer (150 mM NaCl; 1% Triton X-100; 0.5% deoxycholic acid, 0.1% SDS; 50 mM Tris-Cl; pH 8.0) supplemented with 1% protease inhibitor cocktail, 1% PMSF (from stock at 10 mg/ml in methanol), 1 mM Na_3VO_4, 1 mM $Na_4P_2O_7.10H_2O$, and 1 mM NaF. Sixty-five µg of whole cell lysate was loaded per well of 10% SDS-PAGE for subsequent detection of total and phosphorylated forms of SMAD1/5/8 and ERK1/2. α-Tubulin was used as the loading control. 0.45 µm nitrocellulose transfer membrane (Fisher Scientific, Waltham, MA, USA) was used for protein transfer.

Primary antibodies used in these experiments were rabbit monoclonal anti-phospho-SMAD1/5/8 1:600 (#9516S, Cell Signaling, Danvers, MA, USA), mouse monoclonal anti-phospho-ERK1/2 1:1000 (#9106S, Cell Signaling), rabbit polyclonal anti-SMAD1/5/8 1:400 (#9106S, Cell Signaling), rabbit monoclonal anti-ERK1/2 1:1000 (#4695S, Cell Signaling) and mouse monoclonal anti-α-tubulin (#T5168, Sigma-Aldrich, St. Louis, MO, USA). Secondary antibodies were conjugated to IRdye infrared dyes (Rockland Immunochemicals, Limerick, PA, USA). Signal was detected using the

Odyssey infrared imaging system and software (Licor Biosciences, Lincoln, NE, USA) and the protein bands were quantified using ImageJ software.

3.2.2 *In vitro* cytotoxicity assays

In vitro cytotoxicities of LDN-193189, and AZD6244, alone or in combination were measured by using 3-[4,5-dimethyl-thiazol-2-yl]-2,5-diphenyltetrazolium-bromide (MTT) (Sigma-Aldrich, St. Louis, MO, USA) in STS26T-V(*Nf1*$^{+/-}$), STS26T-*Nf1* KD, low and high passage ST88-14(*Nf1*$^{-/-}$), and low and high passage T265(*Nf1*$^{-/-}$) cells. Briefly, 1500-3000 cells were added to a 96-well plate and cultured in the presence of increasing drug concentrations for 48 hours. After 48 hours, MTT was added to a final concentration of 5 mg/mL. After four hours, formazan crystals were solubilized by addition of 0.1 N HCl in anyhydrous isopropanol. Crystals were allowed to dissolve for 15 minutes with gentle shaking, after which plates were read within an hour using a microplate reader at 570 nm, with a background subtraction of 690 nm. GI_{50} values were calculated as drug concentrations necessary to inhibit 50% growth compared to untreated control cells using GraphPad Prism 5 software (GraphPad Software, La Jolla, CA, USA). The anti-viability interaction of LDN-193189 and AZD6244 was determined by standard isobologram analyses and by evaluating combination index (CI) values, calculated using CompuSyn software (ComboSyn Inc., Paramus, NJ, USA), where CI < 1, CI = 1, and CI > 1 indicate synergistic, additive, and antagonistic effects, respectively.

3.2.3 Wound healing assay:

The effect of LDN-193189 and AZD6244 on motility was investigated by using CytoSelect™ Wound Healing Assay Kit (Cell Biolabs, Inc., San Diego, CA, USA). Cells were seeded at 4-5x10^4 cells/well in 24-well plates containing inserts aligned in the same

direction and incubated for 24 hours to allow the cells to adhere. After 24 hours, inserts were removed, and cells were washed twice with PBS to remove dead cells and debris. Next, the cells were treated with indicated concentrations of LDN-193189 and AZD6244 for another 48 hours. To better quantify the cell migration images by fluorescence, low and high passage T265(*Nf1*$^{-/-}$) and ST88-14(*Nf1*$^{-/-}$) cells were infected with the GFP expressing lentiviral plasmid. Migration into the wound field was determined by fluorescent images focused on the center of the wound field, photographed by Olympus IX71 fluorescent microscope, and area of the scratched region in pixels was quantified by ImagePro Software (Media Cybernetics, Rockville, MD, USA). This assay was independently repeated at least three times per cell line.

3.2.4 *In vitro* cell invasion assay:

The effects of LDN-193189 and AZD6244 alone, or in combination on MPNST cell invasion were determined using the CytoSelect™ 96-well cell invasion assay kit (Cell Biolabs Inc., San Diego, CA, USA) containing polycarbonate membrane inserts (8 µm pore size). Cells were pretreated overnight with indicated concentrations of LDN-193189, AZD6244, alone or in combination before seeding to the chambers. The day of seeding, the basement membrane layer was rehydrated by adding 100 µl of warm, serum-free medium to the inner compartment and incubated for 1 h in a cell culture incubator. A 100 µl cell suspension (1×10^5 cells/ml) for each cell line in serum-free medium with/without the indicated treatments was plated in duplicates on to the upper chamber wells containing the basement membrane after removal of the rehydration media. FBS was used at 10% as the chemoattractant of which 150 µl was added to the feeder tray. Duplicate controls of each cell suspension were plated in upper chambers adjoining

feeder wells without any chemoattractant. After 18 h of incubation, the medium in the membrane chamber was transferred to a new harvesting tray containing 150 µl of detachment solution for 30 min. The cells were dislodged completely from the underside of the membrane by gently tilting the membrane several times. Fifty microliters of 4x lysis buffer/CyQuant GR dye solution was added to all samples, which were then incubated for 20 min at room temperature. One hundred and fifty microliters of the lysate was transferred to a black walled plate with optical bottoms (Sigma-Aldrich, St. Louis, MO, USA) and fluorescence measurements were performed in a fluorescence plate reader Spectramax I3X (Molecular Devices, Sunnyvale, CA, USA) at 480 nm/520 nm. This assay was independently repeated three times.

3.2.5 Statistical analyses and synergy calculations:

All experiments presented were replicated a minimum of three times. Paired t-test or ANOVA was used to determine the significant differences at 95% confidence interval. Drug/drug synergy was evaluated by the Chou combination index (CI) using Compusyn software (http://www.combosyn.com). For these calculations, 8-point dose response curves for LDN-193189 in combination with selumetinib were constructed. Bliss Independence (BI) model was used to calculate the therapeutic interactions of the combination of candidate agents on migration and invasion as follows:

$$BI = ((F_a+F_b)-(F_a \times F_b))/F_{ab}$$

where:

F_a = fraction of effect of drug A

F_b = fraction of effect of drug B

$(F_a+F_b)-(F_a \times F_b)$ = predicted sum of the effects of combination treatment

F_{ab} = actual effect of combination therapy found experimentally

3.3 Results

To investigate the therapeutic efficacy and significance of targeting BMP2-SMAD1/5/8 alone and in combination with MEK1/2-ERK1/2 signaling, we evaluated the effects on cell viability, migration and invasion of MPNST cells upon single and dual targeting of the aforementioned pathways. First, we determined the optimal dose for inhibition of the targeted pathways by the candidate agents. This was followed by a comprehensive analysis of the effects on cell viability, migration and invasion of single agent treatment versus combination treatment. The experiments presented in the following sections have been conducted in both low and high passage *Nf1*$^{(-/-)}$ MPNST cell lines to minimize any cell line specific effects. Analysis of the data from the LP *Nf1*$^{(-/-)}$ MPNST cells provides physiologically relevant assessment of the anti-tumor interactions of the candidate agents.

3.3.1 LDN-193189 inhibits BMP2-SMAD1/5/8 signaling

BMP2 exerts its functional effects by binding to the BMP-activated Type I receptors, which then form a complex with Type II receptors with serine threonine kinase activity resulting in phosphorylation of SMAD1/5/8. The phosphorylated form of SMAD1/5/8 binds SMAD4 to translocate to the nucleus and thereby regulate gene expression (Chen et al. 2004a). To study the role of activated BMP2-SMAD1/5/8 signaling in MPNSTs, we utilized a small molecule inhibitor of BMP signaling, LDN-183189 [Fig. 3.1(A)]. Upon binding to the Type I receptors, LDN-193189 suppresses the hetero-oligomerization of the Type I and Type II serine/threonine kinase receptors leading to the inhibition of phosphorylation of the SMAD1/5/8 complex (Vogt et al. 2011) [Fig

3.1(B)]. For BMP2, receptor oligomerization is the critical step dictating the initiation of the SMAD1/5/8 signaling axis (Nohe et al. 2002). Thereby, inhibition of the BMP2-SMAD1/5/8 signaling by inhibition of the ligand binding to the Type I receptors by LDN-193189 allows us to investigate the therapeutic potential of targeting BMP2 in MPNSTs.

Currently, there are no FDA approved BMP2 receptor inhibitors. LDN-193189 is the most specific BMP2 activated Type I receptor inhibitor. It has at least a 100-fold selectivity for type I receptors (ALK2, ALK3 and ALK6) over other receptors of the TGF-β pathway (Engers et al. 2013). Results from animal studies demonstrate that LDN-193189 is readily available in plasma after intraperitoneal injection or oral administration with a plasma half-life of 1.6 – 4.3 hours depending on the mode of delivery (Hong & Yu 2009; Cuny et al. 2008). Most importantly, LDN-193189 administered at biochemically relevant concentrations does not induce weight loss, growth retardation, skeletal, hematopoietic or developmental abnormalities, when administered for more than two months to newborn or adult mice (Yu et al. 2008).

We evaluated the inhibition efficacy of LDN-193189 at different concentrations and time intervals in MPNST cells to optimize the drug application. We found that treatment of ST88-14(*Nf1*$^{-/-}$) cells with 0.01 μM LDN-193189 for 1 hour resulting in nearly complete inhibition of phospho-SMAD1/5/8 [Fig. 3.1(C)]. Upon increasing concentrations of LDN-193189 particularly 0.03 μM to 0.3 μM, total SMAD levels increase. We further evaluated the effects of using LDN-193189 on the MEK1/2-ERK1/2 pathway. We did not find any changes in the activation of ERK1/2 at 0.01 μM LDN-193189 or at a 30-fold higher concentration of 0.3 μM LDN-193189. All MPNST cell lines used in the study exhibited the same response to treatment with LDN-193189. From these data we concluded that

a dosage between 0.01 µM and 0.3 µM of LDN193189 effectively inhibits BMP2 signaling by preventing phosphorylation of SMAD1/5/8 without any effects on MEK1/2-ERK1/2 signaling in MPNST cells.

3.3.2 Selumetinib inhibits MEK1/2 signaling in MPNST cells

Kinases of the MAPK pathway are significant targets for cancer therapy. MEK1/2 phosphorylates ERK1/2 on the tyrosine and threonine residues in the activation loop leading to promotion of cell survival, growth and proliferation [Fig. 3.2(B)]. Selumetinib is a specific ATP-uncompetitive inhibitor of the MEK1/2 [Fig. 3.2(A)] which is in clinical trials for various types of cancers specifically those that are dependent on increased MAPK signaling. It was recently approved by the U.S. FDA for treatment of uveal melanomas, in which *GNAQ* and *GNA11* mutations drive the activation of the MAPK pathway (Van Raamsdonk et al. 2010; Van Raamsdonk et al. 2009). Selumetinib has also been clinically evaluated as a single and a combinatorial drug in a variety of cancers including melanoma, pancreatic, biliary tract, colorectal, and lung cancers (Haass et al. 2008; Bennouna et al. 2011; Hainsworth et al. 2010; Bekaii-Saab et al. 2011). Most importantly, selumetinib has proven patient tolerance in clinical trials, however, its effects as a single drug seem to be limited (Adjei et al. 2008). Selumetinib is currently in Phase II clinical trial for young adults with NF1 and inoperable plexiform neurofibromas [NCT02407405]. Preliminary data from the Phase I study on plexiform neurofibromas in NF1 patients shows that selumetinib has a mean terminal plasma half-life of 7.6-7.7 hours, depending on level of dosage in NF1 patients. Notably, all patients with >1 MRI restaging had a median decrease of 24% in the volume of plexiform neurofibromas, with reversible toxicities (Widemann et al., 2014).

The chemical name of selumetinib is AZD6244, which is used in the figures of this chapter. To test the efficacy of selumetinib, we treated MPNST cells with indicated concentrations of selumetinib to optimize the drug application [Fig. 3.2(C)]. We found that the treatment of ST88-14(*Nf1*$^{-/-}$) cells with 0.03 μM selumetinib for 1 hour inhibits phosphorylation of ERK1/2 nearly completely. We further evaluated the effect of using 0.03 μM selumetinib on the BMP2-SMAD1/5/8 pathway, in which we did not find any changes in SMAD1/5/8 signaling dependent at the concentration of selumetinib up to 3.0μM. Dose response for selumetinib treatment was similar in all MPNST cell lines used in this study.

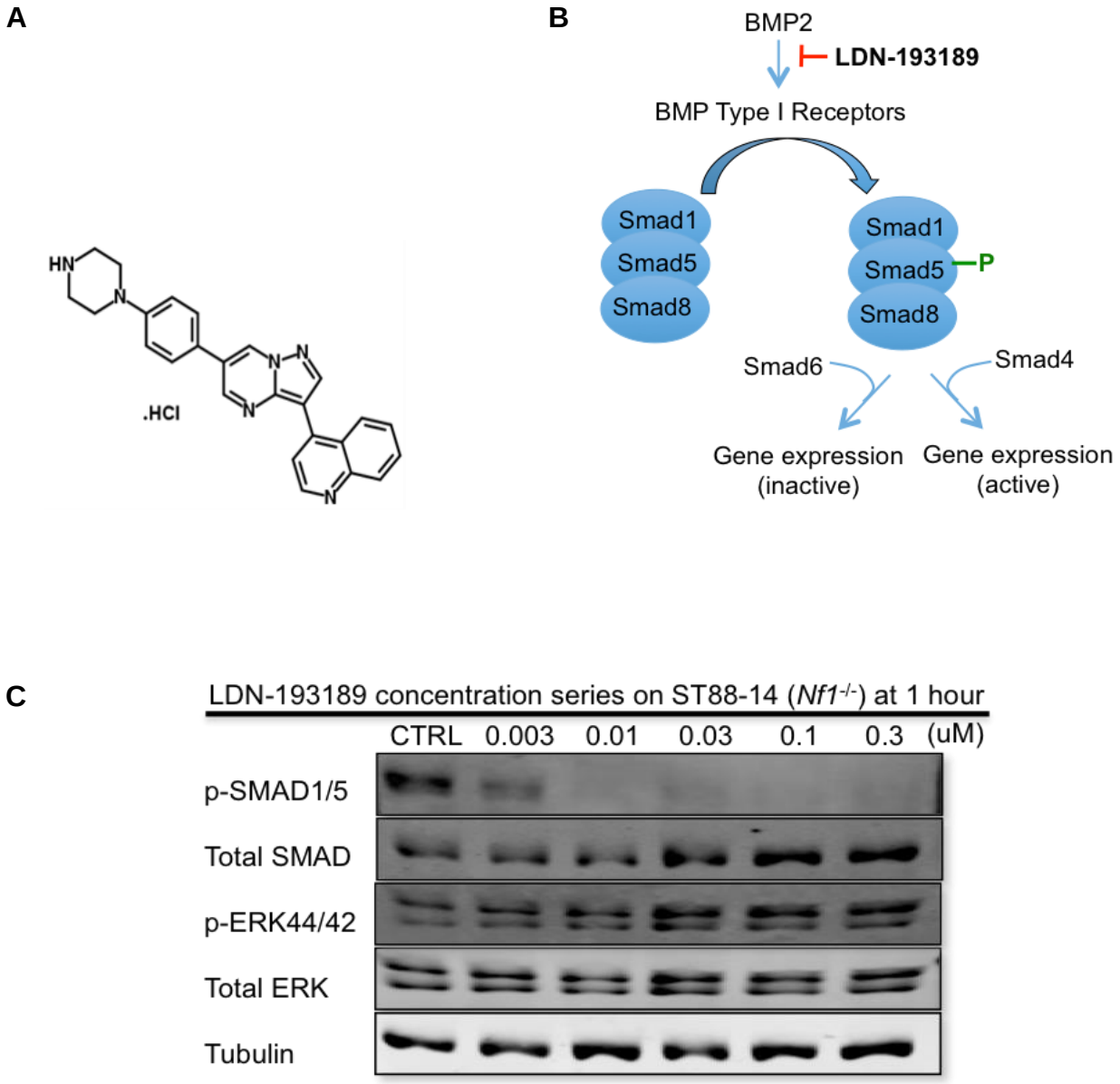

Figure 3.1: Efficacy of LDN-193189 in inhibiting BMP2-SMAD1/5/8 signaling. A: The chemical structure of LDN-193189 (Engers et al. 2013). **B:** Schematic of the BMP2-SMAD1/5/8 signaling pathway and inhibition by LDN-193189. **C:** Representative western blot of titration of LDN-193189 in MPNST cells to determine optimal dose of inhibition. LDN-193189 inhibits phospho-SMAD signaling at 0.003 µM and more efficiently at 0.01 µM, without any effects on the ERK signaling pathway in the ST88-14(*Nf1*$^{-/-}$ cells). Cells were treated with the indicated concentrations for 1 hour and whole cell lysate was fractionated on SDS-PAGE followed by immunoblotting for indicated proteins.

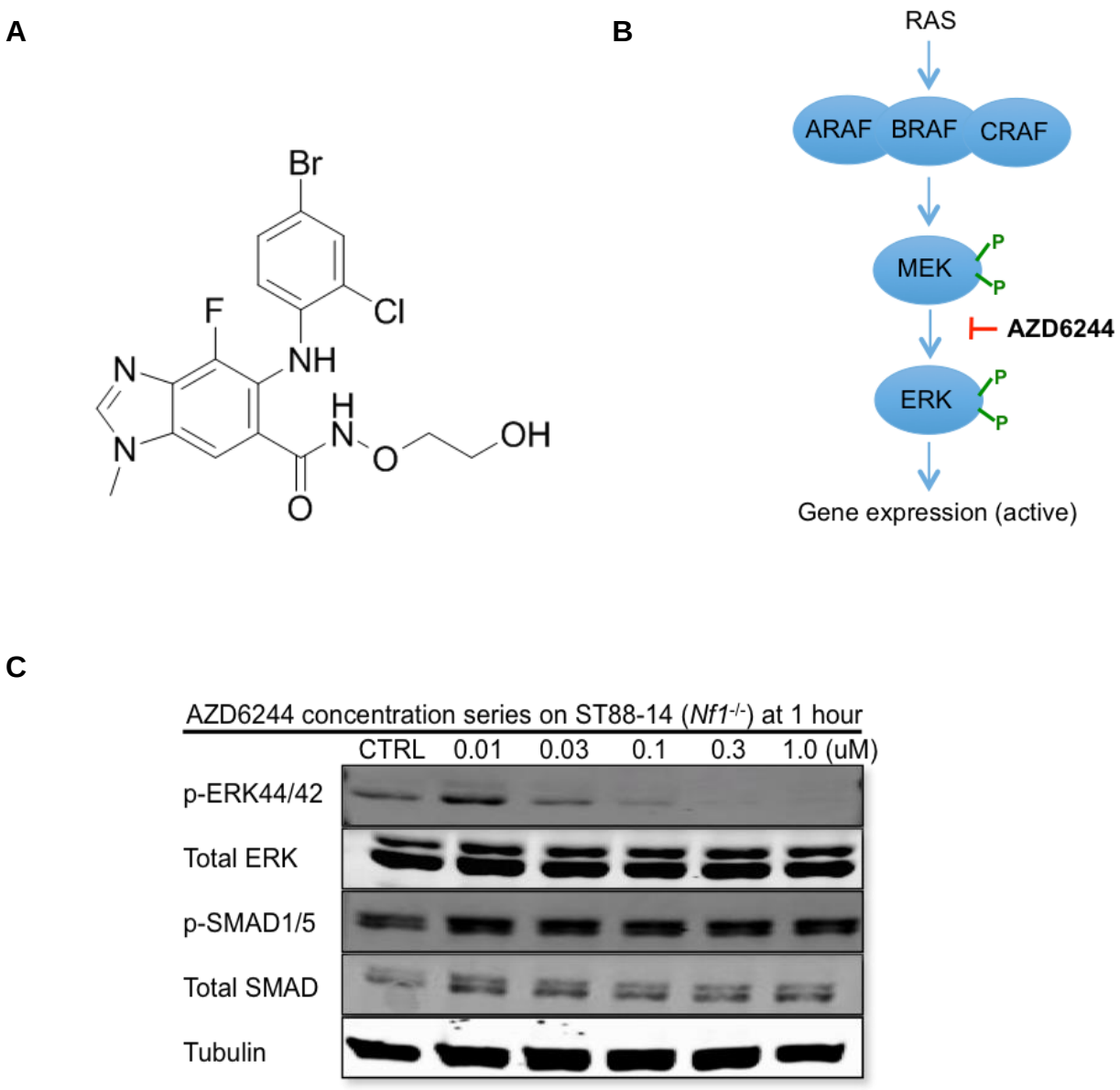

Figure 3.2: Efficacy of selumetinib (AZD6244) in inhibition of MEK1/2-ERK1/2 signaling. A: The chemical structure of AZD6244 (Yeh et al. 2007). **B:** Schematic of the AZD6244 inhibition of MEK1/2 leading to inhibition of ERK1/2. **C:** Representative western blot of titration of AZD6244 in MPNST cells to determine optimal dose of inhibition. AZD6244 inhibits phospho-ERK1/2 at 0.03 μM and continues to inhibit the MEK1/2-ERK1/2 pathway without any effects on the SMAD1/5/8 pathways. Cells were treated with the indicated concentrations for 1 hour and whole cell lysate was fractionated on SDS-PAGE followed by immunoblotting for indicated proteins.

3.3.3 Selumetinib synergizes with LDN-193189 to decrease viability of MPNST cells

In order to investigate the effects of BMP2 or MEK1/2 inhibition on cell viability in MPNSTs, a standard 48-hour MTT assay was employed. Concentration ranges were initially chosen based on results from the western blot analysis, corresponding with the length of the MTT assay [Fig. 3.3]. LDN-193189 as a single agent has a cell viability GI_{50} range of ~1.0-2.0 µM as a single agent in various MPNST cell lines [Figs. 3.4(A), 3.5(A), 3.6(A)]. The GI_{50} of LDN-193189 at which it affects cellular viability is at least 10-fold higher than the dose required to inhibit SMAD1/5/8 signaling in 48 hours as seen by western blotting [Fig. 3.3(A)]. Therefore, the effects on cellular viability and proliferation of MPNST cell lines by LDN-193189 are potentially off-target effects of a higher dose.

Next, we determined the cell viability GI_{50} of selumetinib in MPNST cell lines. STS26T-V(*Nf1*$^{+/}$) and STS26T-*Nf1* KD cells have a cell viability GI_{50} of ~10 µM [Fig. 3.4(B)], HP ST88-14(*Nf1*$^{-/-}$) and HP T265(*Nf1*$^{-/-}$) cells have GI_{50}s between 7-9 µM [Figs. 3.5(B), 3.6(B)], respectively. LP ST88-14(*Nf1*$^{-/-}$) and LP T265(*Nf1*$^{-/-}$) cells are more sensitive to selumetinib treatment with a cell viability GI_{50} range of ~3-4 µM as compared to their HP counterparts [Figs. 3.5(B), 3.6(B)]. Interestingly, selumetinib also requires a much higher concentration to affect cellular viability than the concentration required to inhibit its target in 48 hours [Fig. 3.3]. The cell viability GI_{50}s obtained for the single agent treatments were used for determination of appropriate concentration ranges of these agents in combinatorial cell viability studies.

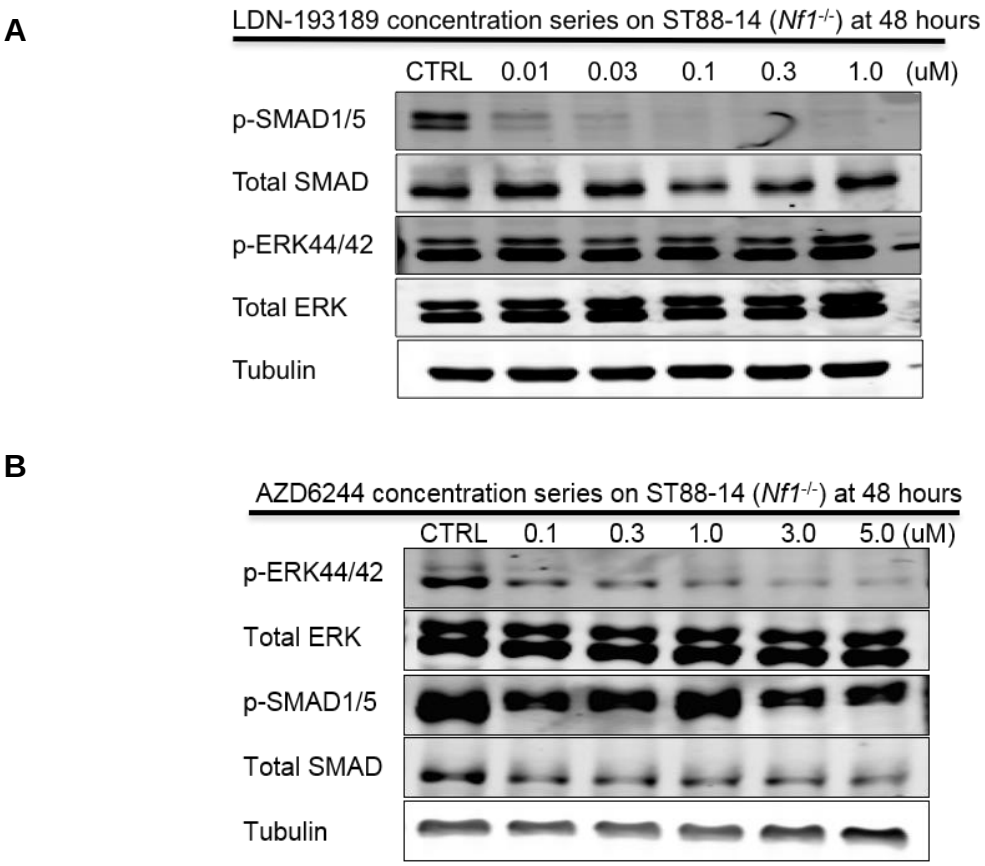

Figure 3.3: Analysis of inhibition of BMP2 by LDN-193189 and MEK1/2 by selumetinib (AZD6244) upon 48 hours of drug treatments. A: LDN-193189 continues to inhibit phospho-SMAD1/5/8 at the low concentration of 0.01 µM in 48 hours, however, it requires between 0.03 and 0.1 µM for complete inhibition of the target in 48 hours. None of the tested concentrations of LDN-193189 up to 1.0 µM had any effects on MEK1/2-ERK1/2 signaling. Similar dose responses were obtained for all tested MPNST cell lines. **B:** AZD6244 inhibits phospho-ERK1/2 in a concentration dependent manner, in which increasing the concentration of the drug leads to a further decrease in phospho-ERK1/2 levels. Cells were treated with the indicated concentrations for 48 hours, and whole cell lysate was fractionated on SDS-PAGE followed by immunoblotting for indicated proteins.

After identification of the proper concentration range for each of the drugs on cell viability, the effects of the combination of LDN-193189 and selumetinib were determined by a 48 hour MTT assay. Standard isobolograms and combination indices (CIs) were used to compare the combinatorial effects of both agents. Isobolograms take into account the GI_{50} of each drug and allow for a quick evaluation of the nature of the drug interaction. Each axis is representative of the concentration of the indicated drug. Any combination that lies below the line connecting the points representing GI_{50}s of single drug treatments is considered to be synergistic, those on the line are considered additive, and those above the line are considered antagonistic interactions. We used four concentrations of selumetinib ranging from 0.1 µM to 3.0 µM, based on the biochemically relevant inhibition of the MEK1/2-ERK1/2 pathway at 48 hours, in combination with seven increasing doses of LDN-193189 corresponding with its cell viability GI_{50} in each of the cell lines. Selumetinib and LDN-193189 synergistically inhibited cell viability in the STS26T-V(*Nf1*$^{+/-}$) and STS26T-*Nf1* KD cells with CI values ranging from 0.55-0.74 [Figs. 3.4(C) and (D)]. The combinatorial drug treatment has a strong to moderate synergistic effect on cell viability in the HP ST88-14(*Nf1*$^{-/-}$) cells [Fig. 3.5(D)]. While combinatorial treatment of HP T265(*Nf1*$^{-/-}$) cells trends towards additivity at low concentrations of selumetinib, it appears to synergize at the higher doses [Fig 3.6(D)]. Dual treatment with LDN-193189 and selumetinib show a strong synergistic interaction inhibiting cell viability of both LP ST88-14(*Nf1*$^{-/-}$) and T265(*Nf1*$^{-/-}$) cells [Figs. 3.5(C), and 3.6(C)]. Table 3.1 displays the average CI values obtained from combination treatments of the tested MPNST cell lines.

From the cell viability studies of LDN-193189 as a single agent or in combination with selumetinib, we conclude that these drugs synergize to inhibit cellular viability in

MPNST cells. The strongest synergistic interaction of both agents is seen in the low passage MPNST cells with the combination of LDN-193189 and lower concentrations of selumetinib. However, the inhibitory effects on cell viability by LDN-193189 and selumetinib are potentially off-target effects as the individual GI_{50}s of the candidate agents are higher than the effective dose at which these agents inhibit their targets.

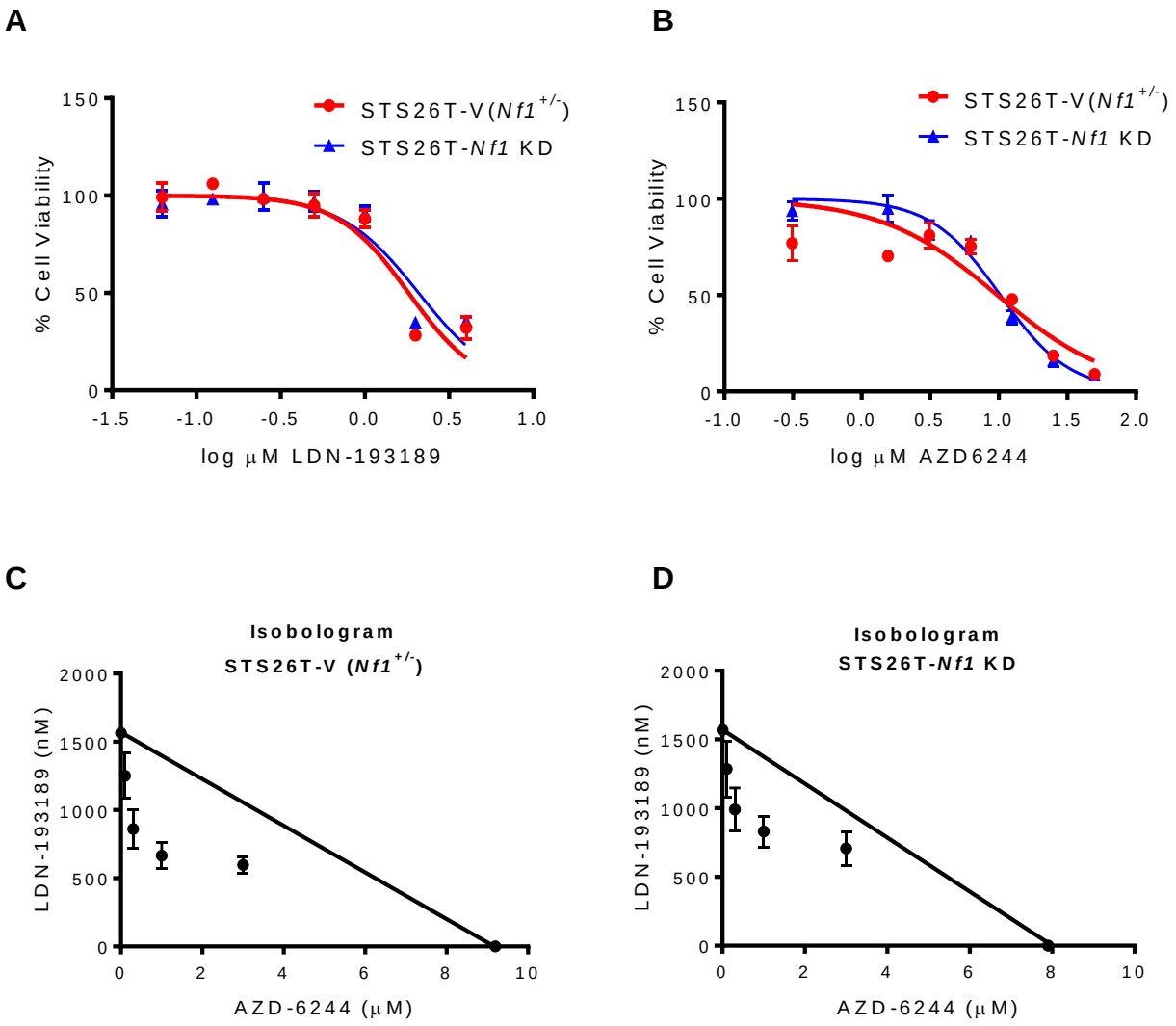

Figure 3.4: The combinatorial effects of LDN-193189 and selumetinib (AZD6244) on cell viability in STS26T-V(*Nf1*$^{+/-}$) and STS26T-*Nf1* KD cells. A and B: The GI_{50}s for single agent treatments are plotted on a semi-logarithmic scale in which x-axis (log_{10} scale) indicates drug concentration and y-axis represents % effect on cell viability as measured by 48-hour MTT assays. Data were analyzed by non-linear regression analysis to generate sigmoidal dose response curves and each point represents mean value from three independent experiments ± SD. **A:** The effects of single treatment by LDN-193189 on the percent of viable STS26T-V(*Nf1*$^{+/-}$), GI_{50}: 1.8 ± 0.2 and STS26T-*Nf1* Kd cells, GI_{50}: 2.1 ± 0.1. **B:** The effects of single treatment by AZD6244 on the percent of viable STS26T-V, GI_{50}: 9.8 ± 0.8, and STS26T-*Nf1* KD cells, GI_{50}: 10.2 ± 0.3. **C and D:** Standard isobologram analyses of the interactions between LDN-193189 and AZD6244 on cell viability. Each axis represents the GI_{50} concentration of the indicated drug. All drug combinations in both cell lines show a synergistic effect. Data points represent the average value from three independent experiments ± SD.

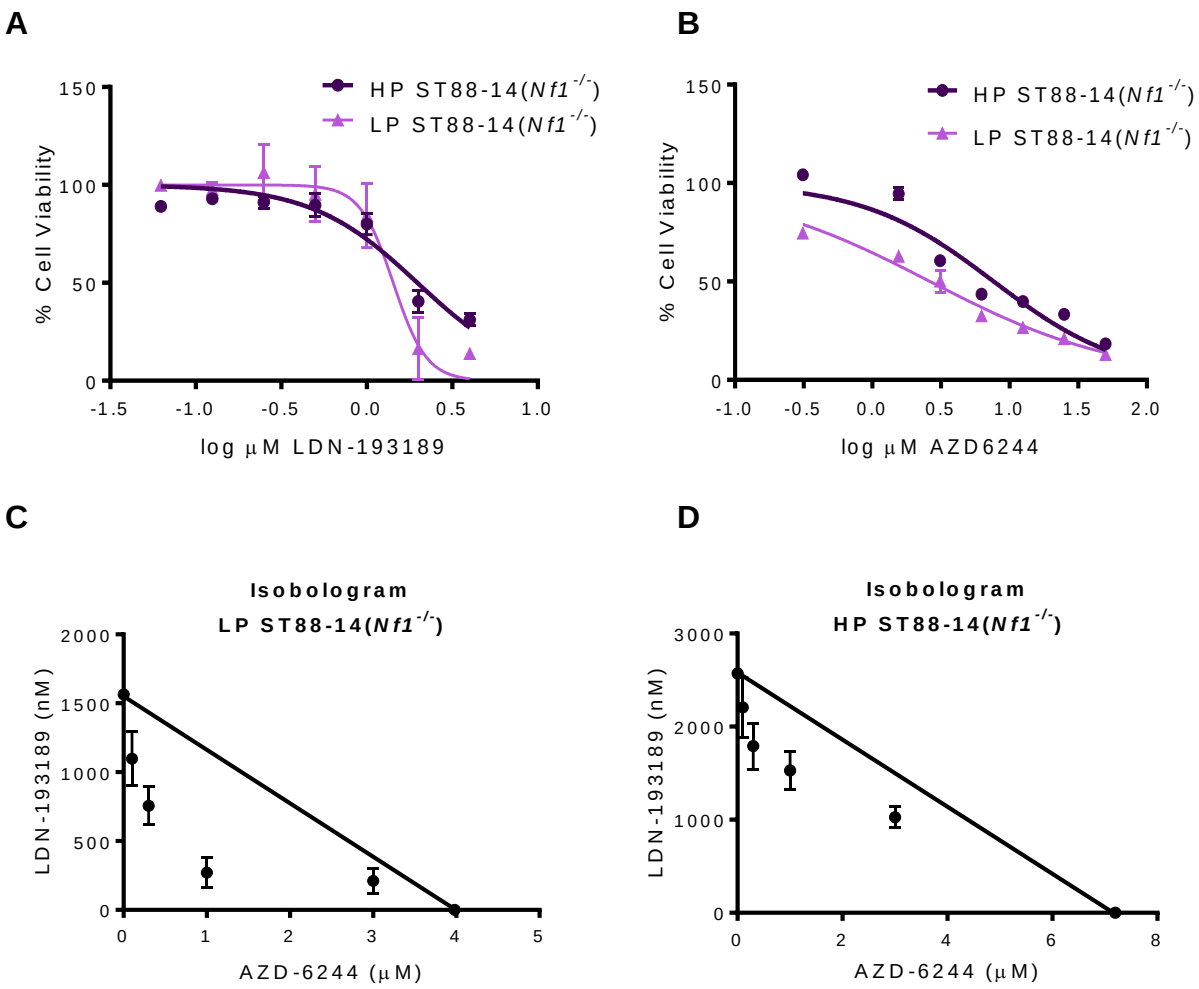

Figure 3.5: The combinatorial effects of LDN-193189 and selumetinib (AZD6244) on cell viability in low and high passage ST88-14(*Nf1*$^{-/-}$) cells. A and B: The GI_{50}s for single agent treatments are plotted on a semi-logarithmic scale in which x-axis (log_{10} scale) indicates drug concentrations and y-axis represents % effect on cell viability as measured by 48-hour MTT assays. Data were analyzed by non-linear regression analysis to generate sigmoidal dose response curves, and point represents mean value from three independent experiments ± SD. **A:** The effects of single treatment by LDN-193189 on the percent of viable LP ST88-14(*Nf1*$^{-/-}$), GI_{50}: 1.3 ± 0.3 and HP ST88-14(*Nf1*$^{-/-}$), GI_{50}: 2.0 ± 0.1. **B:** The effects of single treatment by AZD6244 on the percent of viable LP ST88-14 (*Nf1*$^{-/-}$), GI_{50}: 2.7 ± 0.2, and HP ST88-14 (*Nf1*$^{-/-}$), GI_{50}: 7.6 ± 0.3. **C and D:** Standard isobologram analyses of the interactions between LDN-193189 and AZD6244 on cell viability. Each axis represents the indicated drug concentrations. All drug combinations exhibit a synergistic effect in both low and high passage cells with increased synergy in the LP ST88-14(*Nf1*$^{-/-}$) cells. Data points represent the average value from three independent experiments ± SD.

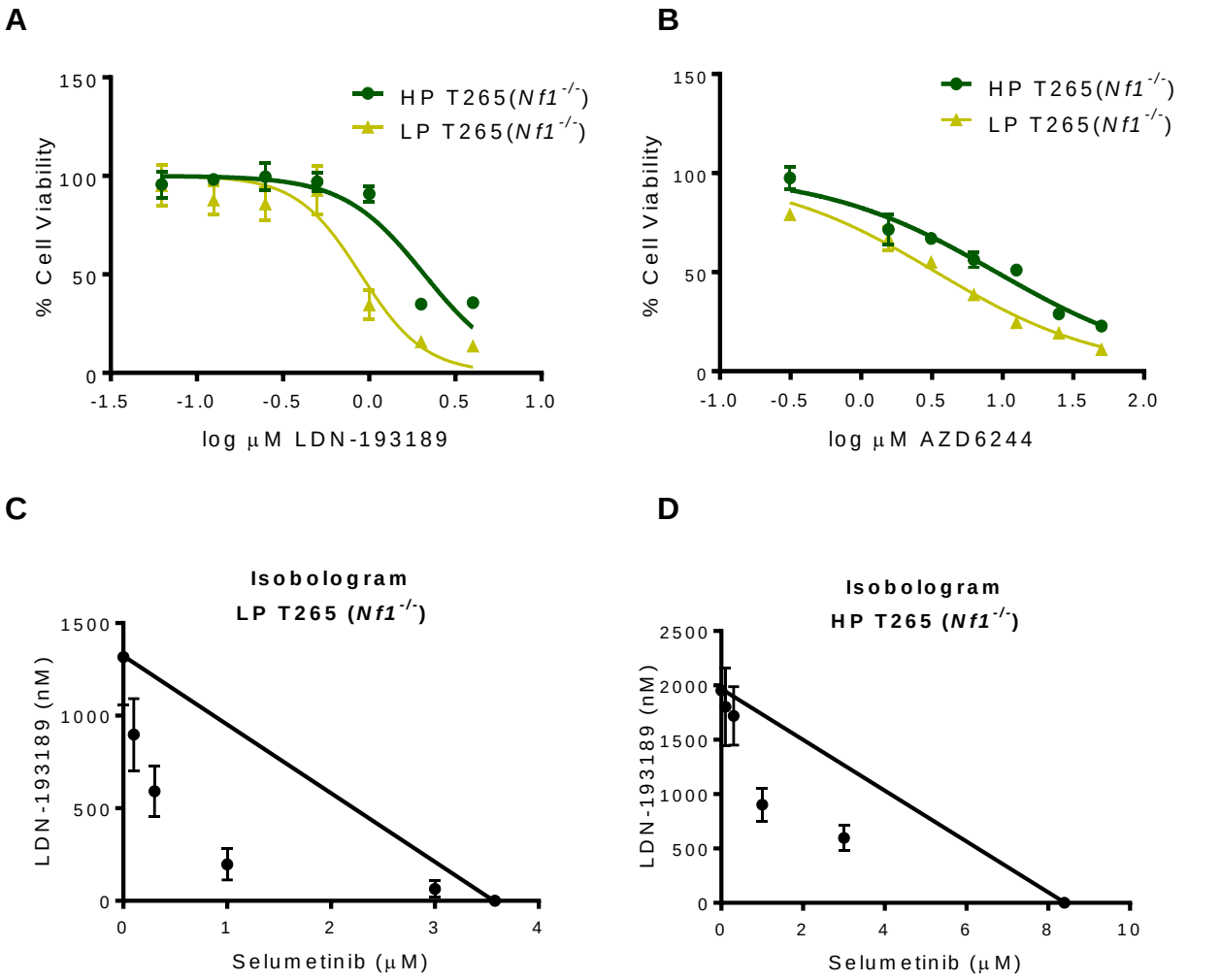

Figure 3.6: The combinatorial effects on cell viability of LDN-193189 and selumetinib (AZD6244) in low and high passage T265(*Nf1*$^{-/-}$) cells. A and B: The GI_{50} for single agent treatments are plotted on a semi-logarithmic scale in which x-axis (log_{10} scale) indicates drug concentrations and y-axis represents % effect on cell viability as measured by 48-hour MTT assays. Data were analyzed by non-linear regression analysis to generate sigmoidal dose response curves. Data points represent mean values from three independent experiments ± SD. **A:** The effects of single treatment by LDN-193189 on the percent of viable LP T65(*Nf1*$^{-/-}$) cells, GI_{50}: 0.1 ± 0.4 and HP T65(*Nf1*$^{-/-}$) cells, GI_{50} 2.1 ± 0.1. **B:** The effects of single treatment by AZD6244 on the percent of viable LP T65(*Nf1*$^{-/-}$), GI_{50}: 3.5 ± 0.2, and HP T65(*Nf1*$^{-/-}$) cells, GI_{50}: 9.1 ± 0.4, as measured by 48 hour MTT assay. **C and D:** Standard isobologram analyses of the interactions between LDN-193189 and AZD6244 on cell viability. All drug combinations exhibit a synergistic effect in both low and high passage cells with increased synergy reported in the LP T265(*Nf1*$^{-/-}$) cells. Each axis represents the indicated concentrations of that drug. Data points represent the average value from three independent experiments ± SD.

CI values						
Combination Drug Treatments	**MPNST cell lines**					
	STS26T-V (*Nf1*$^{+/-}$)	STS26T-*Nf1* KD	LP ST88-14 (*Nf1*$^{-/-}$)	HP ST88-14 (*Nf1*$^{-/-}$)	LP T265 (*Nf1*$^{-/-}$)	HP T265 (*Nf1*$^{-/-}$)
LDN-193189 +0.1μM AZD	0.73	0.65	0.58	0.85	0.62	0.99
LDN-193189 +0.3μM AZD	0.64	0.61	0.39	0.86	0.48	0.99
LDN-193189 +1.0μM AZD	0.55	0.74	0.32	0.91	0.37	0.71
LDN-193189 +3.0μM AZD	0.68	0.67	0.92	0.84	0.78	0.65

Table 2: CI values for combination treatment of MPNST cells. CalcuSyn software was used to calculate the combination index (CI), according to the median-effect method of Chou-Talay. CI values less than 1, 1, and greater than 1, represent synergism, additivity, and antagonism, respectively. The combinatorial treatment has a synergistic effect on cell viability in the STS26T-V(*Nf1*$^{+/-}$) and STS26T-*Nf1* KD cell lines. HP ST88-14(*Nf1*$^{-/-}$), and HP T265(*Nf1*$^{-/-}$) trend towards additivity at lower concentrations of AZD6244, however, increasing the dose of AZD6244 increases synergy in these cell lines. Both LP ST88-14(*Nf1*$^{-/-}$) and T265(*Nf1*$^{-/-}$) cells exhibit a strong synergistic interaction at lower doses of AZD6244 combined with LDN-193189. The CI values shown are averages of CI values of three independent experiments per cell line and treatment conditions.

3.3.4 The effects of combinatorial targeting of BMP2 and MEK1/2 signaling pathways on cellular migration and invasion in MPNSTs μM

Metastases of MPNSTs occurs in about 39% of patients (Panigrahi et al. 2013) with the most frequent metastatic sites being lungs, lymph nodes, and liver (Wong et al. 1998). As expression of *Bmp2* positively correlates with malignancy in neurofibromas (Miller et al. 2009), increased expression of BMP2 in MPNSTs may promote metastatic characteristics such as cell migration and invasion. To investigate the effects of BMP2 on migration and invasion of MPNST cell lines upon treatment with LDN-193189 and/or selumetinib, we employed an *in vitro* wound healing assay and a basement membrane invasion assay.

To determine the nature of the therapeutic interaction of LDN-193189 and selumetinib on migration and invasion of MPNST cells, Bliss Independence (BI) model was used. BI model assumes different, independent, mutually nonexclusive sites of action for the candidate agents (Geary 2013; Foucquier & Guedj 2015), which is the case in this study. Based on the western blot analyses [Figs. 3.1(C), 3.2(C)], the concentrations used in the migration and invasion assays for LDN-193189 (0.01 μM, 0.1 μM) do not affect phosphorylation of ERK1/2, and treatment with 0.03 μM and 0.3 μM selumetinib has no effect on the phosphorylation of SMAD1/5/8 in the MPNST cell lines.

3.3.4.1 Combinatorial treatment with LDN-193189 and selumetinib does not affect cellular migration as compared to single treatment with LDN-193189 in MPNST cells

For the wound healing assay, cell lines were treated with two concentrations of LDN-193189 (0.01 and 0.1 μM) and selumetinib (0.03 and 0.3 μM), which result in biochemical inhibition of their respective targets as per the length of the wound healing

assay. It is important to note that cell viability and growth, as tested by the MTT assay, is unaffected by the concentration of the drugs used for the migration and invasion studies [see results section 3.3.3]. For the wound healing assay, cells were plated in 24-well plates on either side of the wound area made by inserts. After 24 hours of plating, the inserts were removed, and cells were washed and treated with the indicated concentration of the drugs. As the vehicle control treated cells were unable to close the gap of the wound area within 24 hours of treatment, the wound healing assay was extended to 48 hours with a daily dose of the indicated drugs. Fluorescent images were captured prior to the drug treatments (pre-treatment), 24 hours, and 48 hours post-treatment and quantified by the wound healing module of the Image Pro software. Representative images of the analysis with wound areas highlighted in blue are shown for one of the treatment conditions for each cell line. The boundaries of the wound field created by the cells are based on the selected thresholds for each image and background fluorescence intensity is subtracted per image. Cell migration to the wound field at 24 h and 48 h time intervals is normalized to the area of the wound in pre-treatment conditions.

Treatment with 0.01 µM and 0.1 µM LDN-193189 effectively reduces the cell migration field of LP ST88-14(*Nf1*$^{-/-}$) and LP T265(*Nf1*$^{-/-}$) cells [Figs. 3.7, 3.8]. Selumetinib (0.03 µM) has no effect on migration in any of the tested cell lines as compared to the control. However, increasing the dose of selumetinib to 0.3 µM inhibits migration significantly in both the low passage cell lines. Even though the combination treatment in the low passage cells reduces migration, this effect is insignificant as compared to single treatment with LDN-193189. Based on the BI calculations, the combinatorial effects of these drugs trend from additivity to antagonism, with the exception of LP ST88-

14 which shows a weak synergistic interaction of the drug combination when treated with 0.01 µM LDN-193189 and 0.03 µM selumetinib. Similarly, the migratory ability of both HP ST88-14(*Nf1*$^{-/-}$) and HP T265(*Nf1*$^{-/-}$) cells is greatly reduced by LDN-193189. However, addition of selumetinib lowers the inhibitory effect on migration by single treatment with LDN-193189, resulting in a strong antagonistic effect [Figs. 3.9, 3.10].

Results from the wound healing assays suggest that the addition of selumetinib to LDN-193189 does not significantly affect cellular migration as compared to single treatment with LDN-193189, which has a strong effect on cellular migration by itself in MPNST cells. Interestingly, low passage *Nf1*$^{(-/-)}$ MPNST cells are more sensitive to selumetinib in regards to their migratory potential as compared to the high passage *Nf1*$^{(-/-)}$ MPNST cells. We had also found the low passage *Nf1*$^{(-/-)}$ MPNST cells to be more sensitive to selumetinib in cell viability assays [see results section 3.3.3].

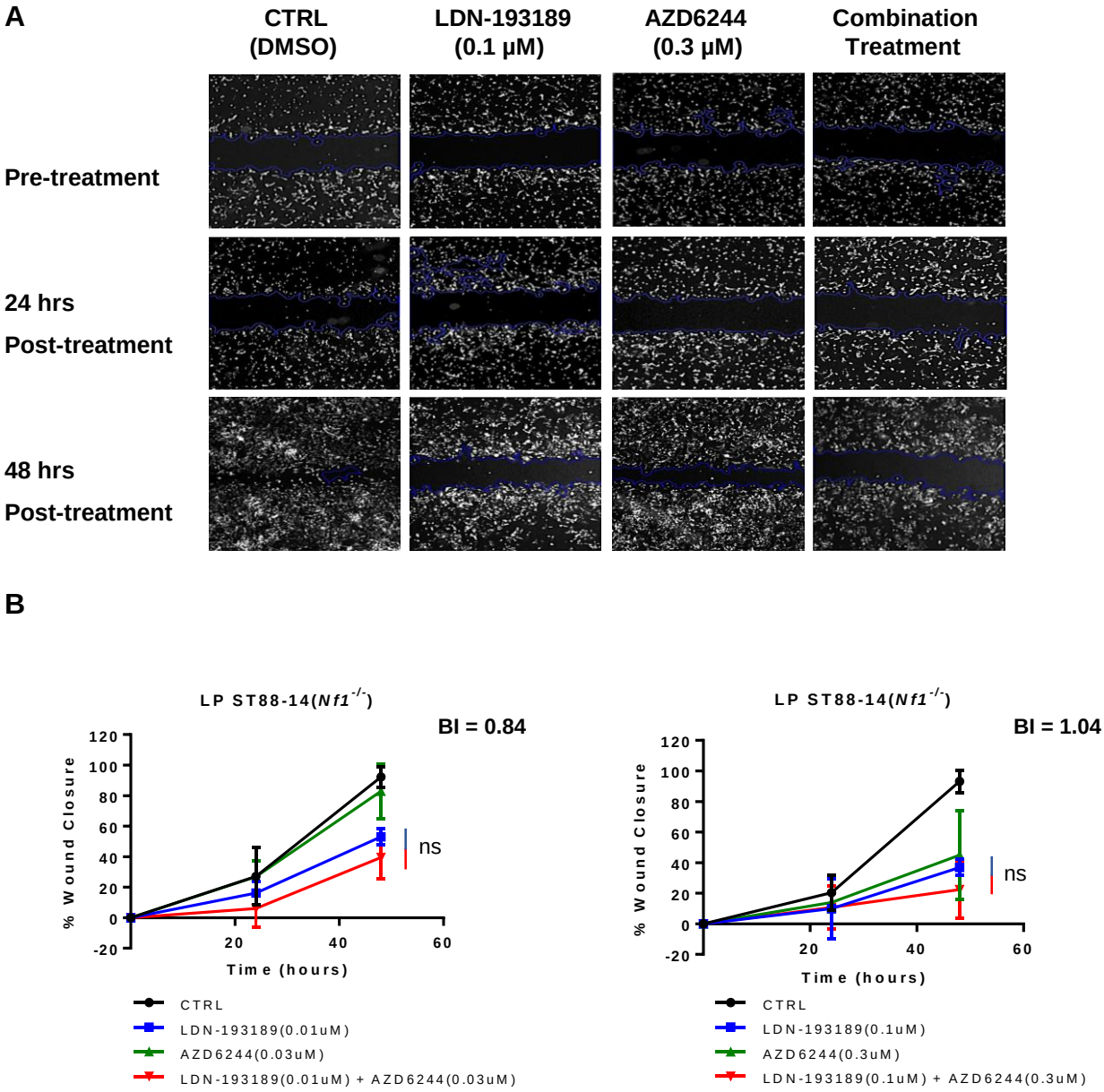

Figure 3.7: The combinatorial treatment with LDN-193189 and selumetinib (AZD6244) does not affect cellular motility in LP ST88-14(*Nf1*$^{-/-}$) cells. A: Representative images of the analyzed cellular wound area of LP ST88-14(*Nf1*$^{-/-}$) cells taken at different time points during the course of the migration assay. The highlighted blue lines represent the analyzed wound area. **B:** The percent quantification of the wound area was normalized to the pre-treatment wound area for each condition. LDN-193189 (0.01 µM, 0.1 µM) reduces the motility of LP ST88-14 cells (P<0.001). AZD6244 affects motility only at a higher concentration of 0.3 µM (P<0.001). The combination of both the drugs results in an insignificant decrease in motility, as compared to single treatment with LDN-193189. BI values represent a low synergistic to additive effects of the drug combinations. Data presented are the mean average of quantification of the wound areas of at least three independent experiments ± S.D (n=3, One-way ANOVA for single treatments as compared to control, Two-way ANOVA for combination treatments compared to LDN-193189 followed by Tukey's test for multiple comparisons).

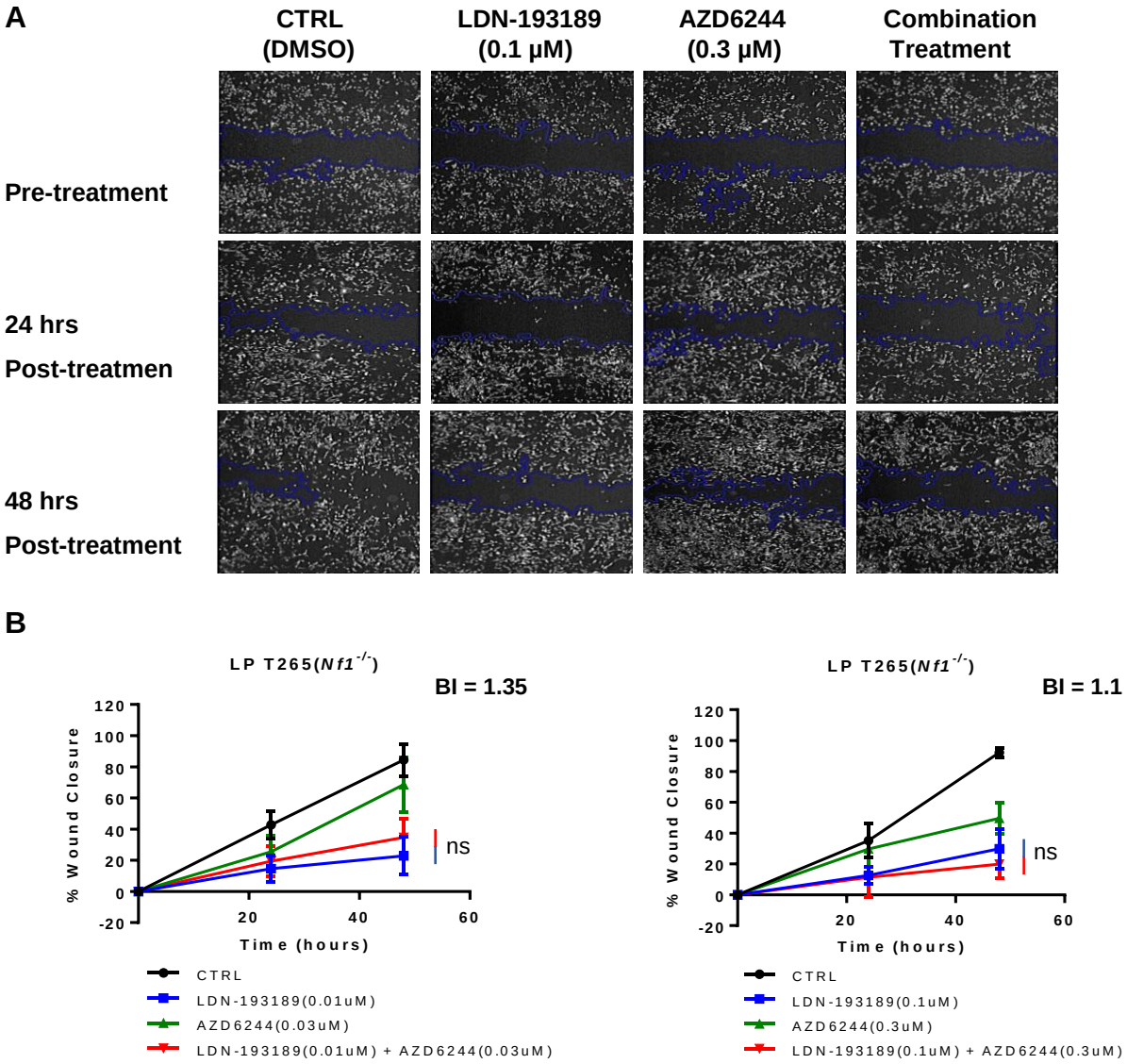

Figure 3.8: The combinatorial treatment with LDN-193189 and selumetinib (AZD6244) does not affect cellular motility in LP-T265 (*Nf1*$^{-/-}$) cells. A: Representative images of the analyzed cellular wound area of LP T265(*Nf1*$^{-/-}$) cells taken at different time points during the course of the migration assay. The highlighted blue lines represent the analyzed wound area. **B:** The percent quantification of the wound area was normalized to the pre-treatment wound area for each condition. LDN-193189 (0.01 µM, 0.1 µM) reduces the motility of LP T265 cells as compared to the control (P<0.0001). AZD6244 affects motility only at a higher concentration of 0.3 µM (P<0.001). The addition of AZD6244 to LDN-193189 does not significantly affect motility as compared to single treatment with LDN-193189. BI values represent an antagonistic effect of drug combinations on motility. Data presented are the average of quantification of the wound areas of at least three independent experiments ± S.D (n=3, One-way ANOVA for single agent treatments as compared to control, Two-way ANOVA for combination treatments compared to single treatment with LDN-193189 followed by Tukey's test for multiple comparisons).

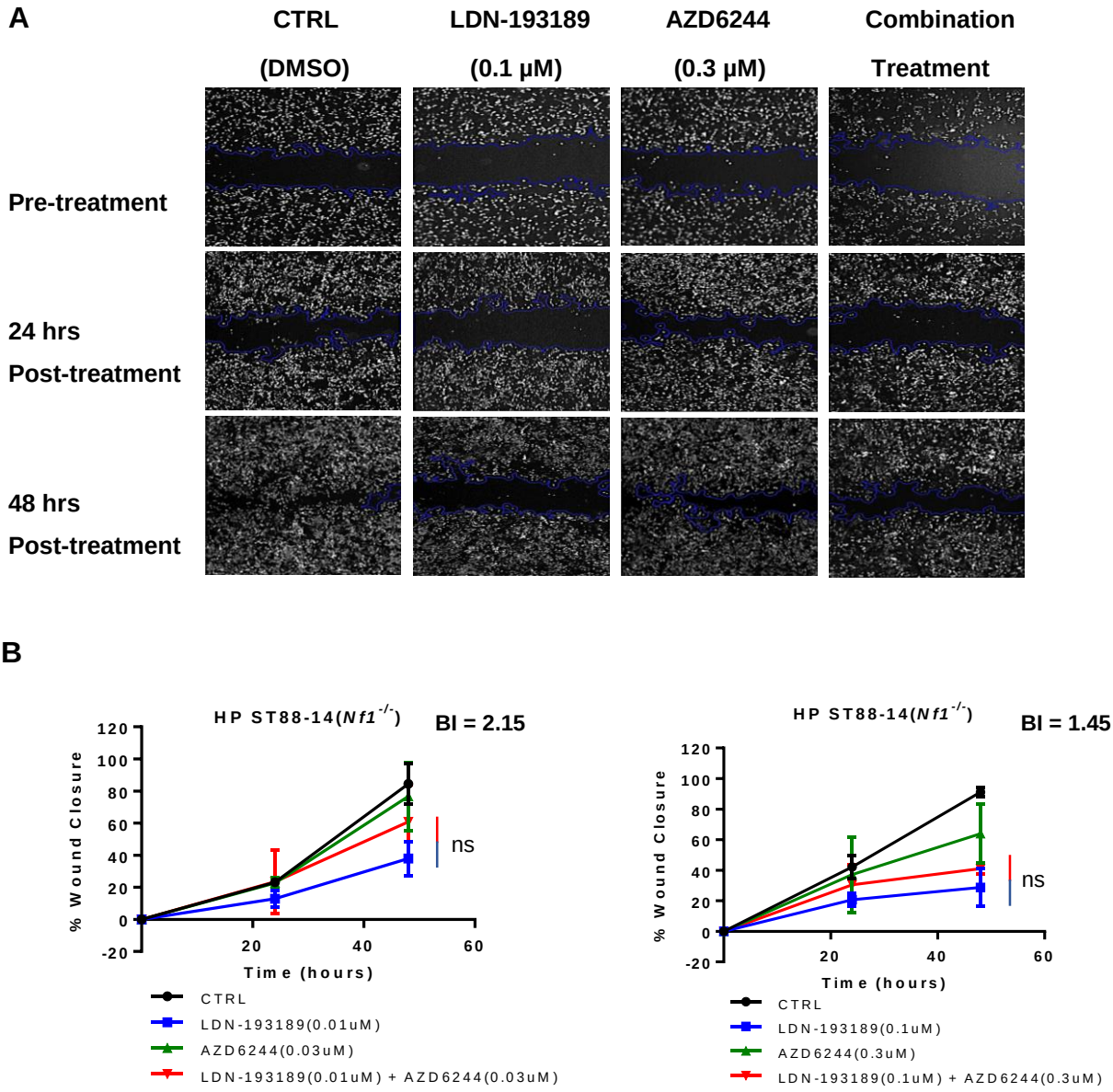

Figure 3.9: The combinatorial treatment with LDN-193189 and selumetinib (AZD6244) does not affect cellular motility in HP ST88-14(*Nf1*$^{-/-}$) cells. A: Representative analyzed images of the cellular wound area of HP ST88-14(*Nf1*$^{-/-}$) cells taken at different time points during the course of the migration assay. The highlighted blue lines represent the analyzed wound area. **B:** The percent quantification of the wound area was normalized to the pre-treatment wound area for each condition. LDN-193189 (0.01 μM, 0.1 μM) reduces the motility of HP ST88-14 cells in a concentration dependent manner respectively (P<0.01, P<0.001). 0.03 μM AZD6244 does not affect motility, however 0.3 μM inhibits motility (P<0.05). The combination treatment does not affect migration in HP ST88-14 as compared to single treatment with LDN-193189. BI values represent an antagonistic effect of drug combinations on motility. Data presented are the average of quantification of the wound areas of at least three independent experiments ± S.D (n=3, One-way ANOVA for single agent treatments as compared to control, Two-way ANOVA for combination treatments compared to single treatment with LDN-193189 followed by Tukey's test for multiple comparisons).

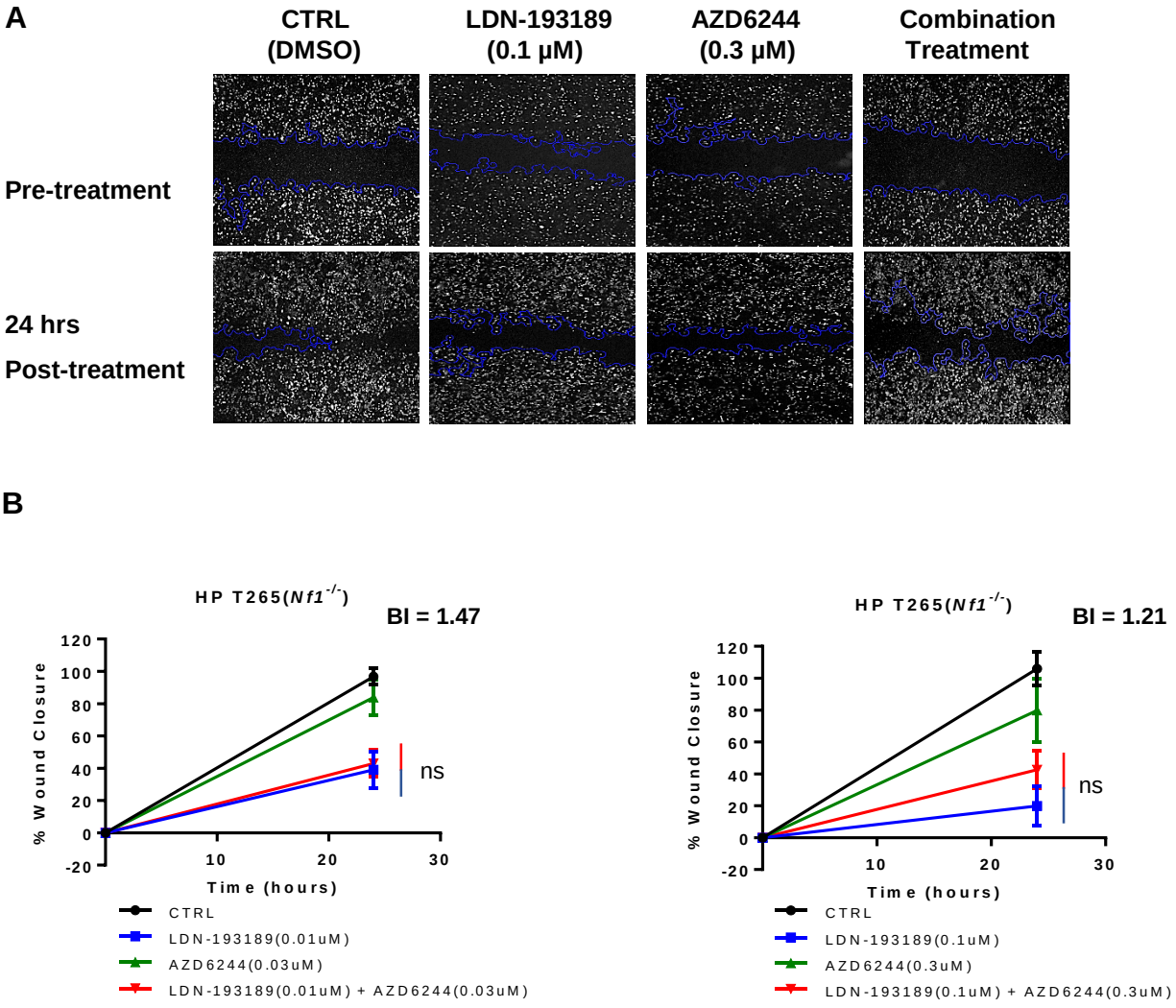

Figure 3.10: The combinatorial treatment with LDN-193189 and selumetinib (AZD6244) does not affect cellular motility in HP T265(*Nf1*$^{-/-}$) cells. **A:** Representative of the analyzed cellular wound area of HP T265(*Nf1*$^{-/-}$) cells taken at different time points during the course of the migration assay. The highlighted blue lines represent the analyzed wound area. Wound healing assay for HP T265 cells was terminated at 24 hours post-treatment because the wound area of the vehicle treatment condition had almost closed. **B:** The percent quantification of the wound area was normalized to the pre-treatment wound area for each condition. LDN-193189 (0.01 µM, 0.1 µM) reduces the motility of HP T265 cells (P<0.0001). Only the high concentration of AZD6244 at 0.3 µM affects motility in the HP T265 cells (P<0.05). The addition of AZD6244 to LDN-193189 in combination treatment does not affect the migratory potential of HP T265 cells as shown by insignificant differences in percent wound closure. BI values represent an antagonistic effect of drug combinations on motility. Data presented are the average of quantification of the wound areas of at least three independent experiments ± S.D (n=3, One-way ANOVA for single agent treatments as compared to control, Two-way ANOVA for combination treatments compared to single treatment with LDN-193189 followed by Tukey's test for multiple comparisons).

3.3.4.2 Combinatorial treatment with LDN-193189 and selumetinib does not affect cellular invasion as compared to single treatment with LDN-193189

The effect of BMP2 and MEK1/2 signaling pathways on the invasive properties of MPNST cells was measured by a basement membrane invasion assay. The invasion assay was performed in 96-well plates, the upper chamber of which was coated with extracellular matrix (ECM) gel and the cells that digested and invaded through the ECM were quantified by a fluorescence plate reader. FBS was used at 10% in media as the chemoattractant in the bottom chamber. Fluorescence readings of duplicate wells without any chemoattractant per cell line were subtracted from all experimental conditions. Next, wells with variable treatments were normalized to vehicle-controls of the respective treatment. To certify that the effects on invasion by LDN-193189 are specific to BMP2, recombinant BMP2 protein with or without LDN-193189 was added to the serum free media of the suspended cells. The effects of LDN-193189 and selumetinib on cell invasion of MPNST cells were assessed by single doses and combination doses of these agents.

The invasive capability of the tested MPNST cell lines is significantly increased by 200 ng/ml BMP2 stimulation, and the addition of LDN-193189 completely blocks the effects induced by BMP2 on MPNST cell invasion [Fig. 3.11]. Both LP and HP *Nf1*($^{-/-}$) cells responded to LDN-193189 treatment with a significant decrease in invasion [Fig 3.12(A) and (B)]. As seen in the migration analyses, single treatment with 0.3 μM selumetinib significantly affects invasion of the LP MPNST cells, however this effect is not as pronounced as that of LDN-193189. Upon combination treatment with LDN-193189 and selumetinib, the invasive capability of both LP ST88-14(*Nf1*$^{-/-}$) and LP T265(*Nf1*$^{-/-}$)

cell lines is reduced, however the effect is statistically insignificant [Fig. 3.12(A), Fig. 3.12(B)]. The combinatorial effect on invasion of both the drugs in the LP MPNST cells trends from a weak synergistic effect to an additive effect. In the HP ST88-14(*Nf1*$^{-/-}$) and HP T265(*Nf1*$^{-/-}$), LDN-193189 significantly inhibits invasion, whereas addition of selumetinib has no effect on the invasive capability as compared to treatment with LDN-193189 alone [Fig. 3.12(C), 3.12(D)].

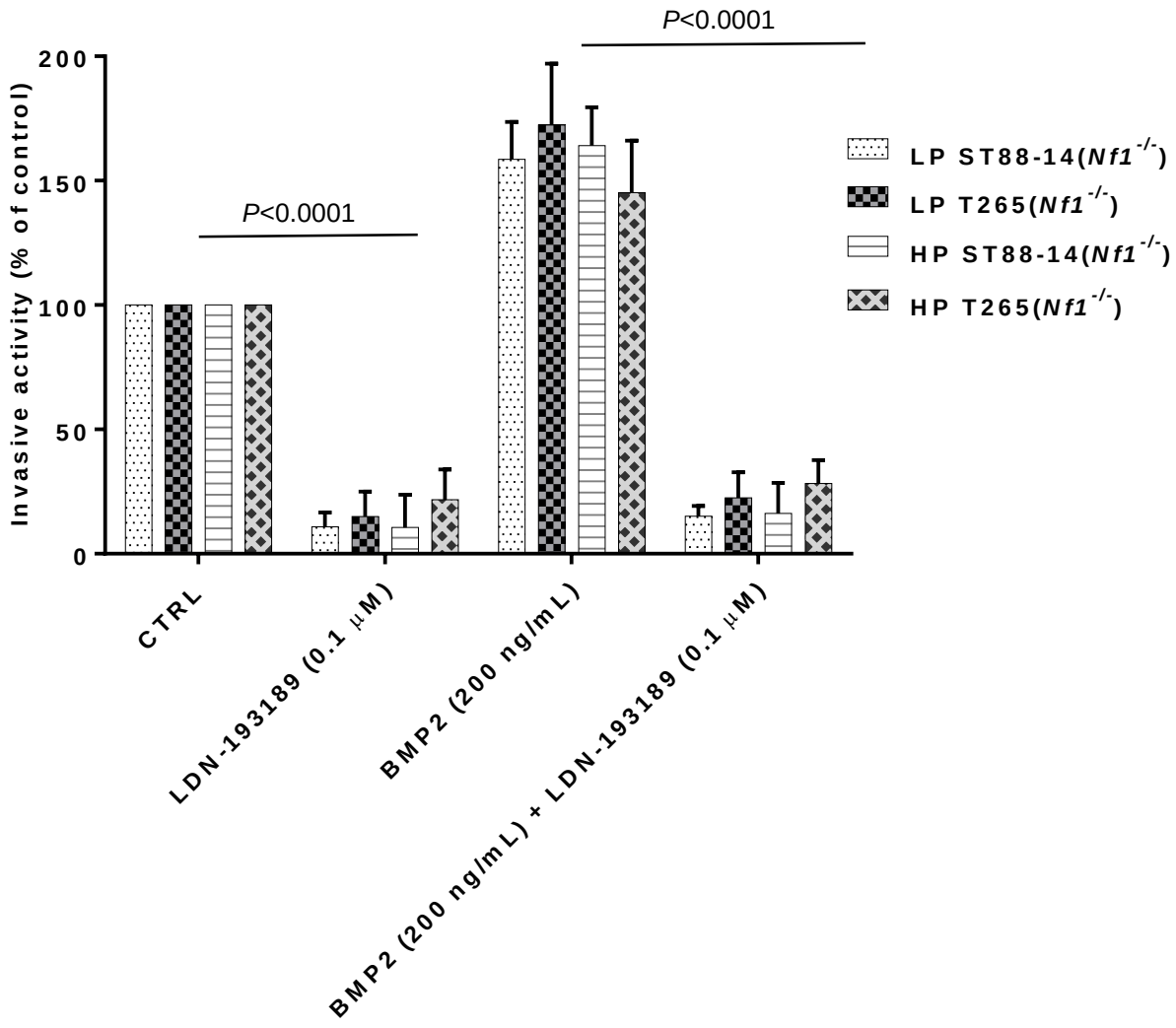

Figure 3.11: LDN-193189 rescues the effects of BMP2 on cellular invasion in MPNST cell lines. Graphical representations of the quantified fluorescence of the cells that invaded through the ECM, normalized to invasive activity without any chemoattractant and the vehicle control. LDN-193189 inhibits cellular invasion as compared to the vehicle treated control in LP and HP *Nf1*$^{(-/-)}$ MPNST cells. Addition of 200ng/mL BMP2 promoted invasion in these cells (*P*<0.01), which is blocked by the addition of LDN-193189 in all the tested MPNST cells. Cells were stained with CyQuant/GR dye and the number of invaded cells was quantified by a fluorescence plate reader. Data presented are mean average of three independent experiments ± S.D with the corresponding *P*-values (n=3, One-way ANOVA followed by Tukey's test for multiple comparisons).

A

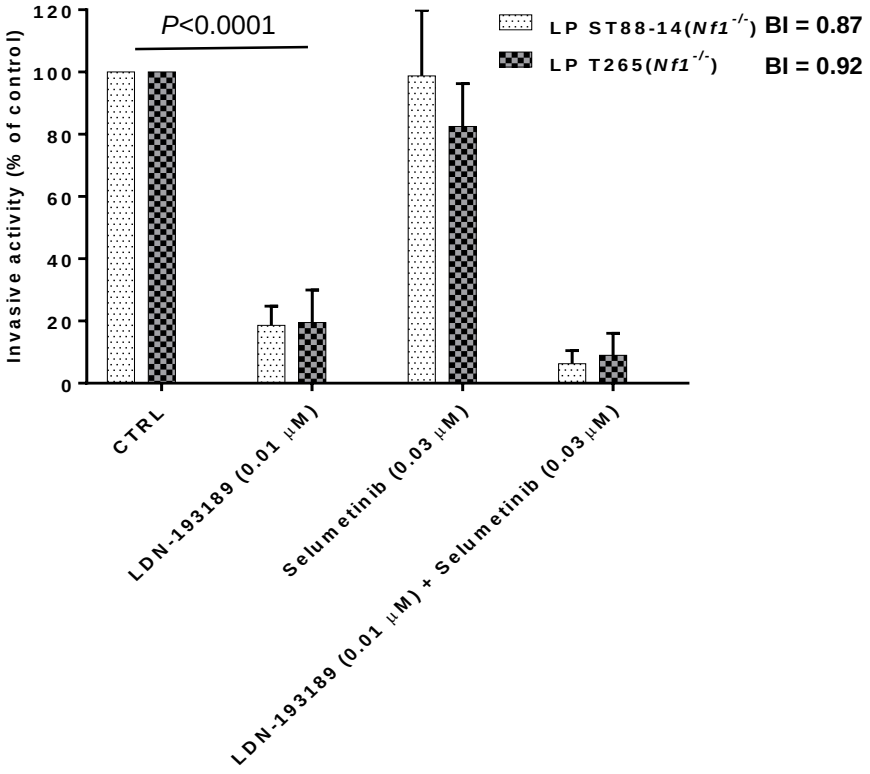

B

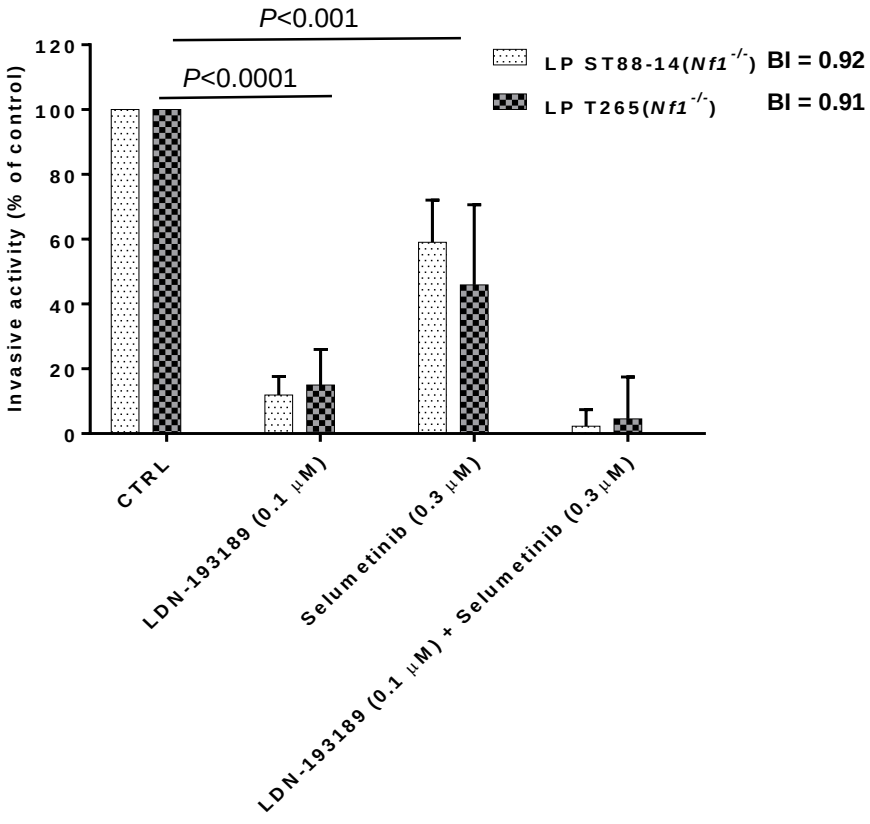

C

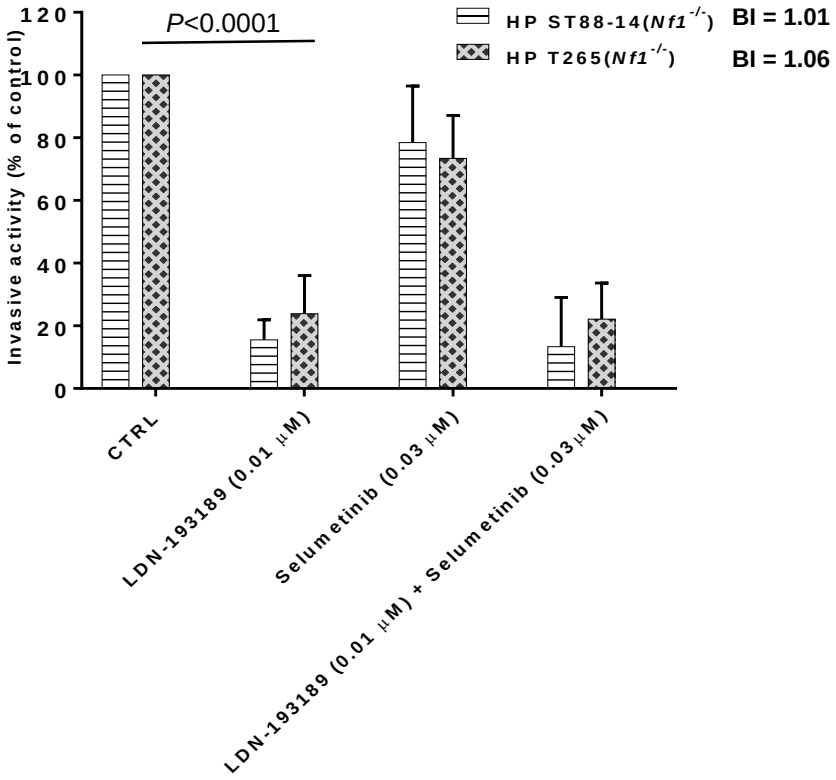

D

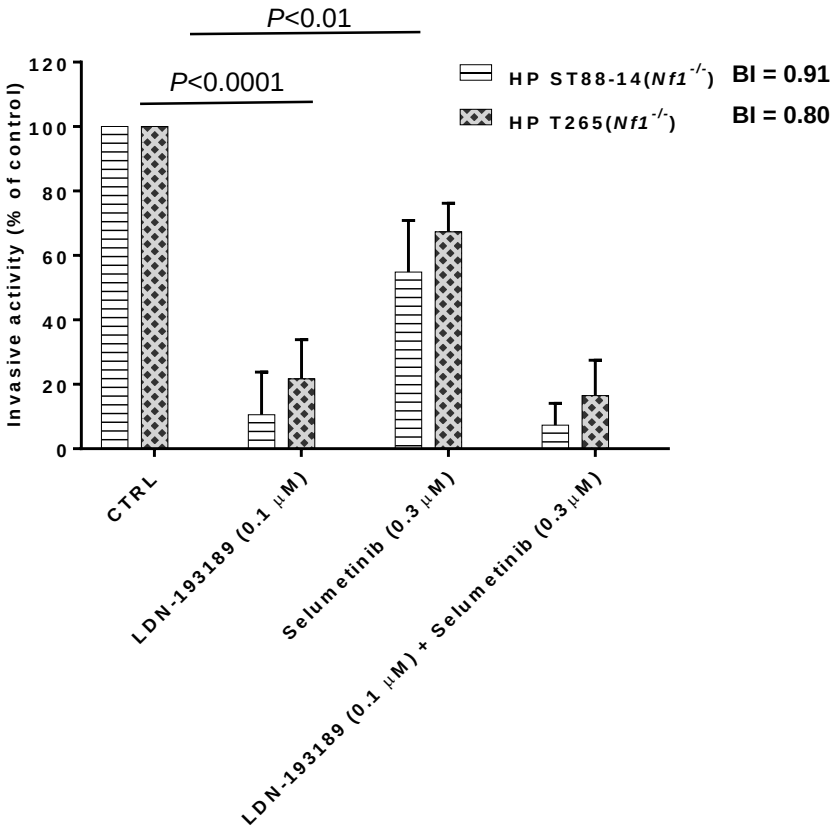

Figure 3.12: The effects of combination treatment with LDN-193189 and selumetinib (AZD6244) on the invasion of *Nf1(-/-)* MPNST cells. Graphical representations of the quantified fluorescence of the cells that invaded through the ECM, normalized to invasive activity without any chemoattractant and the vehicle control. **A and B:** The percentage of low passage cells invading through the ECM using LDN-193189 and selumetinib. The invasive ability of LP cells is greatly reduced by LDN-193189 (0.01 µM, 0.1 µM), whereas selumetinib only affects cellular invasion at 0.3 µM. The combinatorial treatment does not result in an enhancement of the inhibitory effect of LDN-193189 on invasion. Based on the BI model, the therapeutic interaction of the combination treatment on invasion is weakly synergistic. **C and D:** The percentage of high passage cells invading through the ECM using LDN-193189 and selumetinib. The invasive ability of HP cells is greatly reduced by LDN-193189 (0.01 µM, 0.1 µM), whereas selumetinib only affects cellular invasion at 0.3 µM. BI values indicate a weakly synergistic to an additive interaction of the combination treatment on invasion. Data presented are the mean average of three independent experiments ± S.D. with appropriate *P*-values shown on the graph, (n=3, One-way ANOVA for single agent treatments as compared to the controls followed by Tukey's test for multiple comparisons, Two-way ANOVA for combination treatments as compared to single agent treatments with LDN-193189, followed by Tukey's test for multiple comparisons).

3.4 Conclusions

The data presented in this chapter have established the functional significance of targeting BMP2 in MPNST cells. Inhibition of BMP2 by LDN-193189, not only decreases cell migration and invasion but also cell viability in MPNST cell lines. Inhibition of cell viability by LDN-193189 is an off-target effect in the MPNST cells, given that the cell viability GI_{50}s are at least 10-fold higher than the biochemically effective dose required to inhibit SMAD1/5/8 signaling. Interestingly, an independent study of the effects of LDN-193189 on viability of three pancreatic cancer cell lines corroborates our results as LDN-193189 decreases viability of pancreatic cancer cell lines within the concentration ranges used in our MTT experiments (Voorneveld et al. 2013). These off-target effects of LDN-193189 may be modulated by targeting of receptors or kinases other than BMP Type I receptors. In fact, a study of kinase specificity of LDN-193189 determined that at 1.0 µM concentration (within cell viability GI_{50} range in MPNST cells), LDN-193189 affects 24 kinases notably RIPK2, GCK, FGF-R1, etc, independent of its effects on the phosphorylation of SMAD1/5/8 complex (Vogt et al. 2011). Kinases involved in the MAPK pathway were unaffected by 1.0 µM LDN-193189 in the same study, and results from our western blots conclude that treatment with up to 1.0 µM LDN-193189 does not affect MEK1/2 in MPNST cell lines. Conclusively, LDN-193189 and selumetinib via off-target effects, synergize to decrease cellular viability in various MPNST cell lines. We cannot speculate on the mode of decrease in cellular viability at this time as inhibition of viability by apoptosis, necrosis, or cytostatic effects cannot be distinguished by the MTT assay employed in this study.

Given that BMP2-SMAD1/5/8 pathway is involved in cellular migration and

invasion, inhibition of these malignant characteristics by LDN-193189 in MPNST cells was expected. Results presented in this chapter corroborate the decrease in motility and invasiveness by LDN-193189 in MPNST cells previously tested in the HP *Nf1*$^{(-/-)}$ MPNST cells by our lab (Sun et al. 2013). However, we did not expect changes in the migratory and invasive potential of the tested cell lines upon treatment with selumetinib. Selumetinib is a specific inhibitor of MEK1/2 signaling that is primarily involved in the regulation of cell viability, growth and proliferation. Results from the *in vitro* migration and invasion studies indicate that selumetinib, in addition to suppressing the growth of MPNSTs, may also provide a significant benefit by inhibiting the invasiveness of such tumors. However, the combination treatment with both the candidate agents does not result in a significant change in the motility and invasiveness of MPNST cell lines as compared to single treatment with LDN-193189. In fact, the combinatorial effect on migration is antagonistic in nature. Interestingly, even though the combination treatment does not significantly affect invasion of MPNST cells as compared to treatment with LDN-193189 alone, the nature of the combinatorial interaction is weakly synergistic and additive. This is because the BI model takes into account the effects of single treatment with both the candidate agents, whereas for statistical analyses combinatorial treatment was only compared to single treatment with LDN-193189. Accordingly, in comparing the effects of combination treatment versus selumetinib alone, the combination significantly decreases invasion (P<0.01) in all the tested MPNST cells. However, the purpose of these experiments was to assess the feasibility of combination treatment versus single treatment with LDN-193189. Therefore, due to insignificant differences between combination treatments and single treatment with LDN-193189, the addition of

selumetinib to LDN-193189 does not affect cellular migration and invasion of MPNST cells.

CHAPTER IV: Mechanistic studies of BMP2 regulation by NF1 in MPNSTs

4.1 Summary

The importance of targeting the BMP2-SMAD1/5/8 signaling pathway in MPNSTs is highlighted by the reversal of invasiveness and migration of MPNST cells as presented in Chapter III. Even though small molecule inhibitors such as LDN-193189 are effective at inhibiting BMP2-SMAD1/5/8 signaling, the potential off-target effects of protein targeting molecules limit the efficacy of pharmacological inhibition. The unintended inhibition of receptors/kinases other than the targeted protein may be harmless or toxic depending on the affected cells and the signaling pathways involved. Gene therapy provides us with an alternative methodology to pharmacological inhibition, in which the specificity of targeting the gene of interest minimizes off-target effects. Our goal in this chapter is to identify a genetic target of increased *Bmp2* expression by *Nf1* deficiency in MPNSTs; for which, an understanding of the regulatory mechanisms by which NF1 deficiency results in activation of BMP2-SMAD1/5/8 pathway, is warranted.

To understand the molecular mechanisms underlying *Bmp2* expression patterns in MPNSTs, it is important to identify the transcriptional regulatory elements associated with *Bmp2* upon down-regulation of *Nf1*. Data presented in this chapter identified regulatory elements that control *Bmp2* expression in MPNSTs, by transcriptional and post-transcriptional analyses of *Bmp2* in $Nf1^{(+/-)}$ and *Nf1* knockdown conditions. Multiple levels of genetic regulation of *Bmp2* by *Nf1* were explored via *Bmp2* promoter analysis, determination of mRNA half-life, and studies of the *Bmp2* 3'UTR. These mechanism-based studies enabled the identification of genetic targets of *Bmp2* up-regulation that can be targeted to reduce the migration and invasion of MPNSTs.

4.2 Materials and Methods

4.2.1 Construction of plasmids

For the *Bmp2* promoter assay, eight fragments of the human *Bmp2* promoter including the distal and proximal TSSs spanning 1786 nucleotides were cloned into the SacI and XhoI restriction sites of the pGL3 luciferase promoter vector (Promega, Madison, WI, USA). Cloning was performed using the InFusion® HD cloning kit (Clontech, Mountainview, CA, USA). To investigate the human *Bmp2* 3'UTR, full length human *Bmp2* 3'UTR was isolated using standard PCR from CRL-2522 cells. The isolated 3'UTR fragments were cloned into the DraI and XbaI restriction sites of the pmiRGLO luciferase reporter expression constructs (Promega, Madison, WI, USA). InFusion® HD cloning system was used for cloning the 3'UTR fragment placed between the luciferase gene and the polyadenylation site of the pmiRglo vector. All constructs were analyzed by restriction mapping and DNA sequencing.

4.2.2 Promoter assays and transient transfections

Promoter reporter experiments were performed in STS26T-V(*Nf1*$^{+/-}$), and STS26T-*Nf1* KD. Cells were seeded on 96-well plates, and were transiently transfected with the prepared luciferase vectors and the control pGL3 promoter vector (Promega, Madison, WI, USA). DNA transfection was carried out using Xtremegene 9 (Roche life sciences, Indianapolis, IN, USA). For each well, 0.05 µg of the luciferase vector was mixed with 0.02ng of pRL–SV40 renilla luciferase control expression vector (Promega, Madison, WI, USA). The DNA concentration for transfection was optimized by titration prior to the actual experiments. The mixture was then added to 0.15 µl of the transfection reagent, in 5 µl of OptiMem reduced serum media (Life Technologies, Grand Island, NY, USA).

The mixture was incubated for 30 min at room temperature. The reagent mixture was combined with 100 µl of the complete culture medium, and subsequently added to the washed cell monolayer in each well. The transfected cells were cultured for 36-48 hours and then lysed in 25 µl of the reporter lysis buffer per well (Promega, Madison, WI, USA). Twenty microliters of lysate was transferred to opaque white polystyrene 96-well plates (Sigma-Aldrich, St. Louis, MO, USA). Luciferase activity was assayed on GloMax® 96 Microplate Luminometer using a Dual-Glo luciferase assay system (Promega, Madison, WI, USA). Each condition had 8 replicates and all transfection experiments were repeated a minimum of 3 times.

4.2.3 *Bmp2* 3'UTR analysis and transient transfections

Analysis of the human *Bmp2* 3'UTR was performed on the STS26T-V(*Nf1*$^{+/-}$), STS26T-*Nf1* KD, Cond KD#1 (+/- dox), Cond KD#2 (+/- dox), and Cond KD#3 (+/- doxycycline) cells. For a detailed explanation of the conditional KD cell lines, refer to Chapter II. Cells were plated on 96-well plates, and were transiently transfected with the prepared luciferase vectors and the control pmirGLO vector (Promega, Madison, WI, USA). DNA transfection was carried out using Xtremegene 9 (Roche life sciences, Indianapolis, IN, USA). For each well, 0.05 µg of the luciferase vector was mixed with 0.15µl of the transfection reagent, in 5 µl of OptiMem reduced serum media (Life Technologies, Grand Island, NY, USA). The mixture was incubated for 30 min at room temperature. The reagent mixture was combined with 100 µl of the complete culture medium, and subsequently added to the washed cell monolayer in each well. Renilla luciferase vector was not added in these experiments as the pmirGLO vector contains an internal renilla (hRluc-neo fusion) expression construct. The transfected cells were

cultured for 24-36 hours and then lysed in 25 µl of the reporter lysis buffer per well (Promega, Madison, WI, USA). Twenty microliters of each lysate was transferred to opaque white polystyrene 96-well plates (Sigma-Aldrich, St. Louis, MO, USA). Luciferase activity was assayed on GloMax® 96 Microplate Luminometer using a Dual-Glo luciferase assay system (Promega, Madison, WI. USA). Each condition had 8 replicates and all transfection experiments were repeated a minimum of 3 times.

4.2.4 RNA extraction and quantitative real time PCR

RNA was extracted from 10 mm plates of 70-85% confluent cells using the RNeasy Mini Kit (#74106, Qiagen, Valencia, CA, USA). Three batches of total RNA (2.0 µg) for each cell line were reverse transcribed by SuperScript® II First-Strand Synthesis System (Invitrogen, Waltham, MA, USA). Q-RT-PCR was performed using Power SYBR Green MasterMix (Applied Biosystems, Carlsbad, CA, USA) and analyzed on the ABI 5700 Sequence Detection System (Applied Biosystems, Carlsbad, CA, USA). Primers for each gene analyzed are listed in Table 4.1. For mRNA half-life experiments, 18S was used as the reference gene due to its prolonged half-life and stability. The relative fold change was calculated using the CT method as follows: $2^{-\Delta\Delta CT}$, where, $\Delta\Delta CT = (CT_{Bmp2} - CT_{18S})$ experimental time - $(CT_{Bmp2} - CT_{18S})$ 0 time point. Statistical significance was determined through student's t-test and a *p-value* of less than 0.05 was considered significant.

Table 3: Primer sequences used to determine *Bmp2* half-life by qRT-PCR

Gene	Forward	Reverse
Bmp2	GACACTGAGACGCTGTTCC	CCATGGTCGACCTTTAGG
18S	GTAACCCGTTGAACCCCATT	CCATCCAATCGGTAGTAGCG

4.3 Results

Transcriptional regulation is a dynamic web of tightly controlled processes, which spatially and temporally dictate gene expression. Most notably, the expression of a given gene is regulated by initiation of transcription via gene-specific promoters, pre-mRNA processing, and mRNA stability. To identify the mechanism of increased *Bmp2* transcript levels by down-regulation of NF1, we investigated the transcriptional regulation of *Bmp2* by the initiation of transcription through *Bmp2* promoter analysis, and post-transcriptional regulation by *Bmp2* mRNA stability and 3'UTR activity upon knockdown of *Nf1* in MPNSTs. The experiments presented in this chapter were performed in two independent *Nf1* knockdown cell models detailed in Chapter II. Comparison of the mechanistic data between the stable knockdown of *Nf1* and the inducible *Nf1* knockdown system serves to minimize cell line or knockdown vector-specific variations.

4.3.1 NF1 does not regulate *Bmp2* promoter activity in MPNST cells

The promoter region of a gene is located in the distal 5' end of a given gene, which is composed of specific sequences of regulatory elements that control the initiation of transcription of that gene. The combinatorial input of various elements within the promoter region such as TSSs, TF-binding sites, and interaction of *cis*- and *trans*-regulatory elements i.e. enhancers or repressors, determine the steady-state levels of transcription of a given gene (Maston et al. 2006). *Bmp2* is regulated by highly guanine/cytosine (GC)-rich distal and proximal promoter regions (Jiang et al. 2010), with greater activity reported in the proximal promoter TSS (Helvering et al. 2000; Ghosh-Choudhury et al. 2001). The GC-rich promoter regions of *Bmp2* are characteristic of transcriptionally repressed genes. Thereby, *Bmp2* transcription requires a balancing of

activating factors with the repressive factors to initiate *Bmp2* transcription (Jiang et al. 2010). To understand the regulatory elements governing the activation of *Bmp2* by *Nf1*, we conducted an analysis of the promoter activity of *Bmp2* upon *Nf1* knockdown.

Based on published human *Bmp2* promoter sequences (Helvering et al. 2000; Jiang et al. 2010), eight promoter constructs spanning ~1.8 kb of the *Bmp2* gene containing the distal and proximal promoter TSSs were cloned into a pGL3 promoter luciferase reporter vector [Fig. 4.1(A) and 4.1(B)]. These vectors were transiently transfected into the STS26T-V($Nf1^{+/-}$) and STS26T-*Nf1* KD cells in which the intensity of the luciferase signal is proportional to the activity of the *Bmp2* promoter regions. Analysis of the luciferase activity comparing the *Bmp2* promoter activity in the STS26T-V($Nf1^{+/-}$) and STS26T-*Nf1* KD cells did not show any significant changes in the vector control and *Nf1* KD cells [Fig. 4.1(C)]. The full-length promoter construct (-1000 to +786 nt) shows the least luciferase activity, whereas the region spanning (+494 to +675 nt) has the highest luciferase activity. Therefore, 181 nucleotides of the promoter region between +494 and +675 consist of activating *Bmp2* elements in the sporadic MPNST cell line. Due to the inability to find any difference in *Bmp2* promoter activity upon *Nf1* knockdown between the STS26T-V($Nf1^{+/-}$), STS26T-*Nf1* KD, I concluded that the *Bmp2* promoter was not the region of the genome regulating Nf1 regulation of BMP2 expression in MPNSTs.

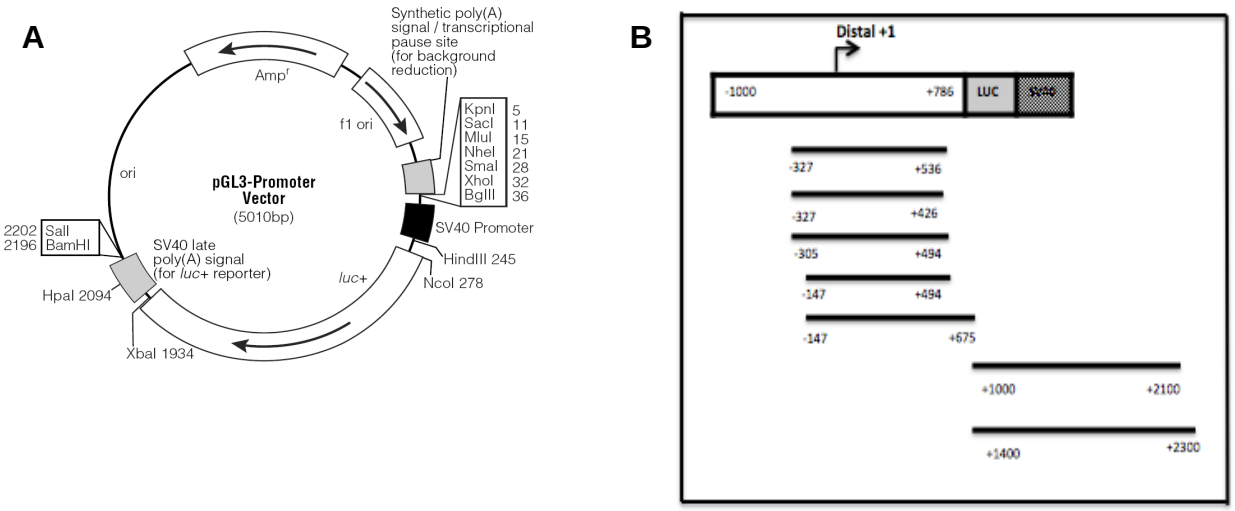

C

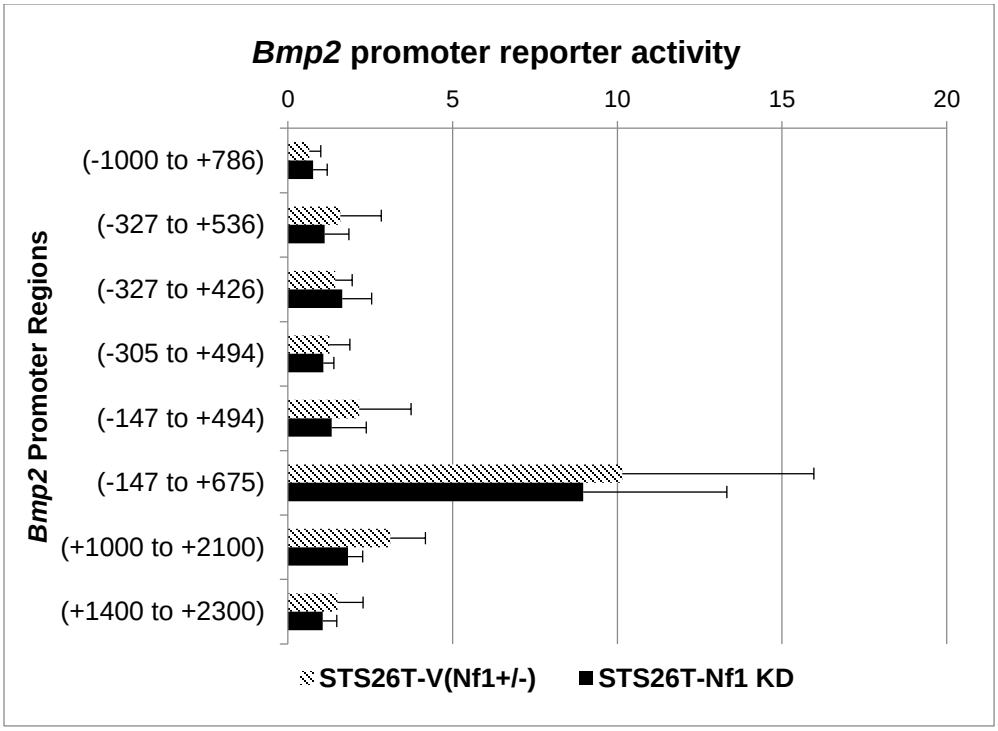

Figure 4.1: NF1 does not regulate activity of the *Bmp2* promoter in MPNSTs. A: The pGL3-promoter luciferase reporter vector construct used for cloning fragments of the *Bmp2* promoter. **B:** Schematic of the *Bmp2* promoter fragments cloned upstream of the luciferase gene in the promoter vector. C: Representative analysis of the luciferase activity, normalized to renilla in the STS26T-V(*Nf1*$^{+/-}$) and STS26T-*Nf1* KD cells shows no significant change in activity of the *Bmp2* promoter upon *Nf1* knockdown conditions. Paired t-test, n=8, ns. Data presented are mean of three independent experiments with average of eight replicates per condition ± S.D.

4.3.2 The post-transcriptional regulation of *Bmp2* by NF1

Because I did not find any changes in the activity of *Bmp2* promoter based on NF1 status, I investigated the post-transcriptional regulation of *Bmp2* upon knockdown of *Nf1*. There are multiple levels of post transcriptional regulatory mechanisms such as mRNA processing, splicing, polyadenylation, editing, transport, and stability (Day & Tuite 1998). Among which, the expression of 5-10% of human genes is controlled by mRNA stability (Bolognani & Perrone-Bizzozero 2008). Analysis of the post-transcriptional regulation of *Bmp2* was conducted by determining the differences in the rate of *Bmp2* mRNA turnover, followed by analysis of the *Bmp2* 3'UTR between *Nf1*$^{(+/-)}$ and *Nf1* knockdown conditions.

4.3.2.1 NF1 regulates *Bmp2* mRNA stability

Stability of a given mRNA is a major determinant of its expression. Regulation of mRNA turnover controls the abundance of cellular transcripts, hence the levels of protein expression (Wilusz et al. 2001). Each mRNA has an intrinsic half-life, however intracellular and extracellular stimuli can modulate the half-life of a given mRNA (Chen et al. 2008). *In vitro* analyses of *Bmp2* mRNA decay rates has shown that half-life of *Bmp2* mRNA correlate with the endogenous mRNA levels of *Bmp2* in human, mouse, and zebrafish cells (Fritz et al. 2004).

To investigate the changes in the rate of *Bmp2* mRNA turnover between *Nf1*$^{(+/-)}$ and *Nf1* knockdown conditions, I determined the half-life of *Bmp2* mRNA under both conditions. Determination of the *Bmp2* mRNA half-life was performed by using actinomycin D to inhibit global transcription within the cells, followed by quantification of the *Bmp2* mRNA levels by qRT-PCR at various time points under the *Nf1*$^{(+/-)}$ and *Nf1* knockdown conditions. Actinomycin D is a widely used transcriptional inhibitor that

inhibits DNA-dependent RNA synthesis. Actinomycin D intercalates into single stranded DNA (ssDNA) and prevents the annealing of the newly synthesized (-) ssDNA to the acceptor RNA, specifically RNA polymerase I (Jeeninga et al. 1998; Sobell 1985), which leads to inhibition of transcription. Cells were treated with actinomycin D (5 µM), after which RNA was extracted at intervals of 0, 1, 3, 6, 9, 12 and 24 hours. qRT-PCR was used to determine the expression of *Bmp2* at these intervals to determine the mRNA half-life of *Bmp2* over the course of 24 hours. The *18S* ribosomal RNA gene was used as the reference gene due to its increased stability and prolonged half-life. The fold changes in *Bmp2* transcript levels were normalized to *Bmp2* levels at the 0 time point per cell line. RNA extracted at the 24 hour time point for each cell line was excluded from data analyses due to high Ct values that may skew the final determination of half-lives. The half-lives of the *Bmp2* transcripts were calculated by determination of the decay rate constant (k_{decay}) per experiment, which is proportional to the rate of disappearance of the mRNA concentration at a given time point. Fold changes were plotted on a semi-logarithmic scale, and non-linear regression analysis was used to determine the slope of the best-fit line, which represents k_{decay}. mRNA half-life ($t_{1/2}$) is then calculated by the following equation: $t_{1/2} = \ln 2/k_{decay}$ (Chen et al. 2008).

As shown in Figure 4.2(A) and Table 4, mRNA half-life in the STS26T-*Nf1* KD cells is almost double, 4.4 hours, as compared to the half-life of STS26T-V($Nf1^{+/-}$) cells at 2.3 hours. This doubling of *Bmp2* mRNA half-life correlates with the steady state *Bmp2* mRNA levels upon *Nf1* KD as measured in Fig 2.4, where *Bmp2* mRNA levels increase almost two-fold in the STS26T-*Nf1* KD cells as compared to the STS26T-V($Nf1^{+/-}$) cells.

To validate the changes in *Bmp2* mRNA half-life depending on the status of *Nf1*, three inducible *Nf1* knockdown cell lines were used. This approach provides a tight and rapid genetic switch to control levels of NF1 within cells, therefore any resulting changes in *Bmp2* transcription can be ascertained to changes in the NF1 status within the same cell population. The inducible *Nf1* KD clones were treated with doxycycline (2 µg/ml) to induce the *Nf1* shRNA 18 hours prior to treatment with actinomycin D. All of the inducible *Nf1* KD cell lines show a decrease in the degradation of *Bmp2* transcript upon treatment with actinomycin D [Fig 4.2 (B), (C), and (D)], and a 1.5-2.0 fold increase in *Bmp2* mRNA half-life upon down-regulation of *Nf1*. These increases in *Bmp2* half-life upon knockdown of *Nf1* are comparatively similar to the increases in steady state *Bmp2* transcript levels under the same conditions, as shown in Fig. 2.8. For example, the steady state *Bmp2* mRNA levels in the Cond KD#3 increase ~1.8 fold upon induction of the *Nf1* shRNA [Fig. 2.8] and the *Bmp2* mRNA half increases by 1.9 fold [Table 4].

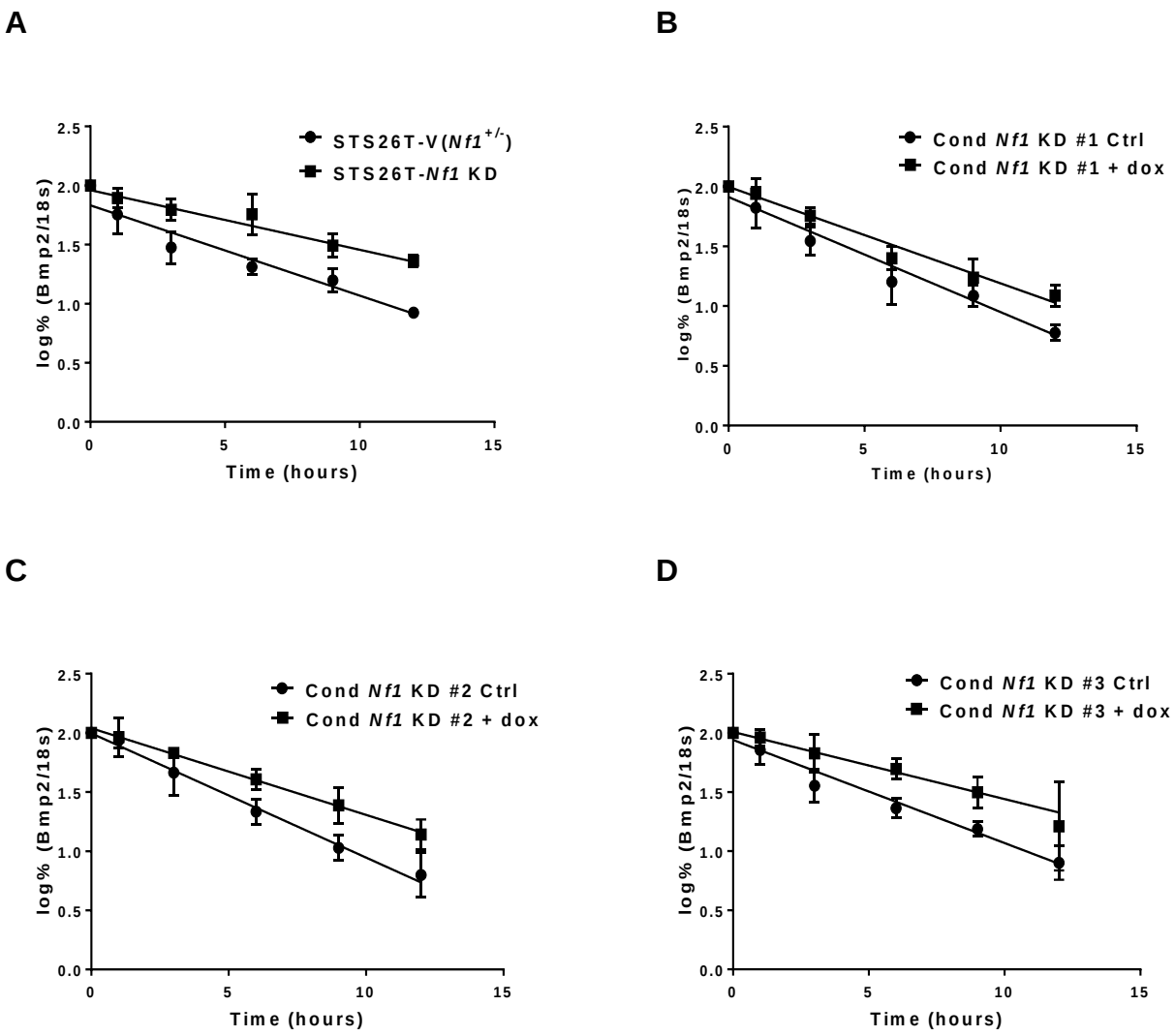

Figure 4.2: The rate of *Bmp2* mRNA decay decreases upon NF1 downregulation in MPNST cells. Changes in *Bmp2* mRNA levels are plotted on a semi-logarithmic scale and non-linear regression analysis is used to draw a straight line through the data points. **A:** *Bmp2* transcripts in the STS26-T *Nf1* KD cells degrade slower than those in the STS26T-V($Nf1^{+/-}$) cells upon treatment with actinomycin D. Paired t-test, n=3, $P<.05$. Data presented are mean of three independent experiments ± S.D. **B, C, and D:** Induction of the *Nf1* shRNA by treatment with doxycycline induces an increase in *Bmp2* transcripts over the course of 12 hours in three independent conditional *Nf1* knockdown cells. Data presented are mean of at least three independent experiments ± S.D.

$t_{1/2}$ (hours)			
Cell lines	**Vector Ctrl (*Nf1*$^{+/-}$)**	***Nf1* KD**	***P-value***
STS26T (*Nf1*$^{+/-}$)	2.3 ± 0.2	4.4 ± 0.5	0.02
Cond KD #1	1.8 ± 0.2	2.9 ± 0.8	0.07
Cond KD #2	2.4 ± 0.1	4.3 ± 0.4	0.01
Cond KD #3	2.1 ± 0.3	4.0 ± 0.6	0.03

Table 4: Comparison of *Bmp2* mRNA half-lives between *Nf1*$^{(+/-)}$ and *Nf1* KD cells. Mean *Bmp2* mRNA half-life in MPNST cells as calculated by the method described in the results section ($t_{1/2} = \ln 2/k_{decay}$). Upon down-regulation of *Nf1* *Bmp2* mRNA half-life almost doubles in all of the tested cell lines. The doubling of half-life correlates with steady state *Bmp2* expression levels per cell line. $t_{1/2}$ shown is the average of half-life calculations from three independent experiments.

4.3.2.2 NF1 regulates *Bmp2* 3'UTR

The stability of mRNA is controlled by its 3'-untranslated region (3'-UTR), which consists of regulatory sequences that post-transcriptionally influence gene expression. Remarkably, regulatory elements within the *Bmp2* 3'UTR are well-conserved across species (Fritz et al. 2004) and more conserved than its coding region (Abrams et al. 2004), which is indicative of its important role in the regulation of *Bmp2* expression. The 3'UTRs of the human and mouse *Bmp2* transcripts are 83% identical over 1,088 nucleotides, and high degree of conservation of *Bmp2* 3'UTR is reported between several mammalian orders (Fritz et al. 2004).

To further explore the regulation of *Bmp2* stability upon knockdown of *Nf1*, I assessed the activity of *Bmp2* 3'UTR under $Nf1^{(+/-)}$ and *Nf1* knockdown conditions. Full-length human *Bmp2* 3'UTR (3530 nucleotides) was isolated from normal human fibroblasts and cloned into a pmirGLO luciferase reporter vector [Fig. 4.3(A)] between the luciferase gene and the polyadenylation site of the vector. All cell lines were transfected with the control vector and the vector containing the *Bmp2* 3'UTR sequence. The intensity of the luciferase signal is proportional to the activity or stability induced by the *Bmp2* 3'UTR. Luciferase activity for each *Nf1*-KD cell line is normalized to its control ($Nf1^{+/-}$). Figure 4.3(B) shows that *Bmp2* 3'UTR activity in the STS26T-*Nf1* KD cells is approximately 4.5 fold higher in the STS26T-*Nf1* KD cells as compared to the vector control. For the inducible *Nf1* knockdown cell models, *Nf1* shRNA was induced by doxycycline (2 µg/ml) 10 hours post-transfection to limit any effects of doxycycline on transfection conditions. All three inducible *Nf1* KD cells exhibit increased *Bmp2* 3'UTR activity [Fig. 4.3(C)], with highest relative activity reported in the Cond KD#3 which also

has the highest fold change in steady-state expression levels and mRNA half-life. The increase in *Bmp2* 3'UTR activity in the inducible *Nf1* knockdown cells is not as pronounced as that of the STS26T-*Nf1* KD cells. The average 1.8-2.4 fold increase in *Bmp2* 3'UTR activity in dox-treated cells, after subtraction of the luciferase signal from untreated cells is similar to the steady state *Bmp2* mRNA levels and its half-life upon knockdown of *Nf1*. The increased activity (~4.5 fold) of the *Bmp2* 3'UTR in the STS26T-*Nf1* KD compared to the STS26T-V($Nf1^{+/-}$) cells can be attributed to analysis of the 3'UTR activity in two different cell populations. The inducible knockdown system represents a better, more specific model to study the direct effects of NF1 on the *Bmp2* 3'UTR as analysis is conducted within the same cell population.

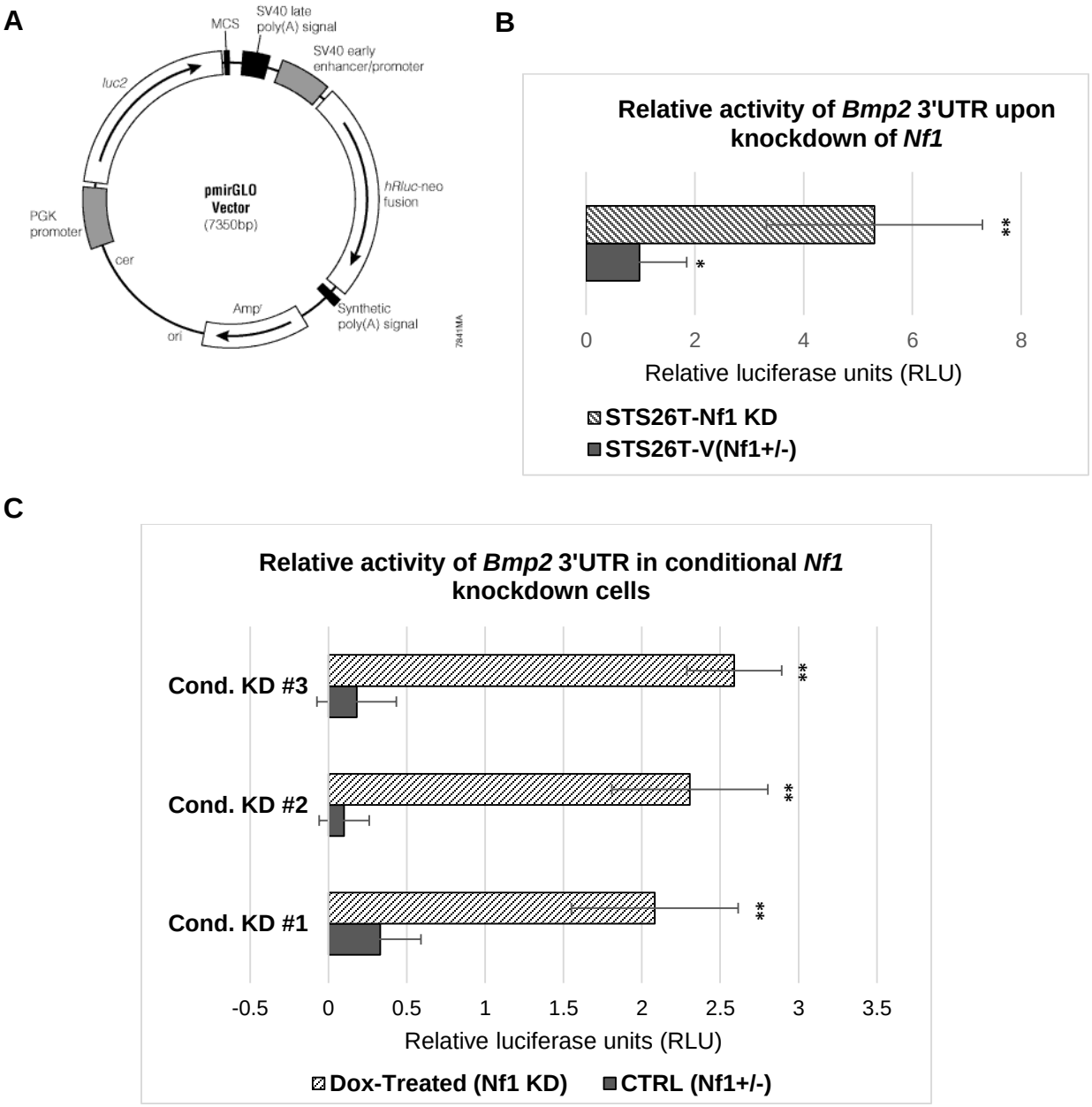

Figure 4.3: Activity of the *Bmp2* 3'UTR upon *Nf1* down-regulation. **A:** Schematic of the pmirGLO vector used for testing *Bmp2* 3'UTR activity. **B:** Luciferase activity of the *Bmp2* 3'UTR measured in STS26T-V($Nf1^{+/-}$), and STS26T-*Nf1* KD cells normalized to luciferase activity of the control vector. Paired t-test, n=3, **P*<.05, ***P*<.01. Data presented are mean of 3 independent experiments with 8 replicates per condition in each experiment ± S.D. **C:** Luciferase activity of the *Bmp2* 3'UTR normalized to activity of control vector in conditional *Nf1* KD cells. All conditional *Nf1* KD cells show an increase in the *Bmp2* 3'UTR activity upon induction of *Nf1* shRNA by doxycycline (2 µg/mL). Paired t-test, n=3, ***P*<.01. Data presented are mean average of 3 independent experiments with 8 replicates per condition in each experiment ± S.D.

4.4 Conclusions

From the mechanism-based experiments, we concluded that *Nf1* regulates *Bmp2* post-transcriptionally via regulation of the *Bmp2* 3'UTR, which results in an increase in the cytoplasmic half-life of *Bmp2* mRNA in MPNSTs. A further investigation into the regulatory elements of the *Bmp2* 3'UTR will reveal the regulatory factors responsible for stabilizing *Bmp2* mRNA upon *Nf1* deficiency. Thereby, we propose two notable post-transcriptional mechanisms of mRNA stability, i.e. adenylate-uridylate (AU)-rich elements (ARE) and miR-response elements in the 3'UTR, which may be involved in regulation of *Bmp2* expression in *Nf1*-null MPNSTs.

Stability of the mRNA can be modulated by ARE and miR-response elements in the 3'UTR (Cheneval et al. 2010). RNA-binding proteins bind the AU-rich motifs in the 3'UTR and stabilize or aid in degradation of the transcript. The importance of ARE sites is underscored by studies which have established that loss of ARE-mediated control of a given gene leads to severe pathologies such as developmental abnormalities and tumorigenesis (Hodson et al. 2010; Ghosh et al. 2009; Hao & Baltimore 2009). The 3'UTR of human *Bmp2* is ARE-rich, containing thirteen classical AUUUA pentamer motifs along with several non-canonical AU motifs [Fig 4.4(A)]. The heavy presence of ARE sites in the *Bmp2* 3'UTR, which are well-conserved across species, is indicative of the role of this region in controlling *Bmp2* expression. Additional inquiry of the *Bmp2* 3'UTR by localizing the specific region of *Bmp2* 3'UTR that is responsive to changes in the NF1 status will identify ARE sites alongside RNA-binding proteins, involved in regulating *Bmp2* expression in *Nf1*-null MPNSTs.

Regulation by microRNAs (miRs) is another possible post-transcriptional regulatory mechanism by which *Nf1* regulates *Bmp2* expression in MPNSTs. miRs are 20-24 nucleotides long noncoding RNAs that post-transcriptionally regulate gene expression by mRNA degradation and/or translational repression. More than 50% of mammalian RNAs are predicted to be controlled by miR-mediated regulation (Fabian et al. 2010). Although the exact mechanism of post-transcriptional inhibition by miRs is not well understood, the proposed model suggests that miRs bind target mRNAs via base-pairing to miR-response elements in the 3'UTR and induce deadenylation, which results in degradation of the transcript (Filipowicz et al. 2008). The 3'UTR of *Bmp2* contains many miR response elements with the highly conserved miR sites displayed in Figure [4.4(B)]. We studied activities of miR-response elements of miR-17, miR-140, miR-214, miR-374, and miR-378 on targeting of the *Bmp2* 3'UTR upon *Nf1* knockdown. The aforementioned miR-response elements were selected on the basis of degree of conservation and published literature. However, due to variable results between experimental repeats we could not identify a miR or subset of miRs regulating changes in *Bmp2* expression upon *Nf1* deficiency. We also studied alternative splicing of *Bmp2* 3'UTR between *Nf1*-KD and $Nf1^{(+/-)}$ conditions. Analysis of the poly(A) sites in the *Bmp2* 3'UTR by PCR of the poly(A)-associated regions in the cDNAs of STS26T-V($Nf1^{+/-}$) and STS26T-*Nf1* KD cells did not reveal any alternative splicing.

This is the first report of the mRNA half-life regulation by *Nf1* in MPNSTs. However, the exact mechanism, RNA-binding proteins or miRs, by which *Nf1* deficiency leads to up-regulation of BMP2 need be investigated. Many groups have shown the

A

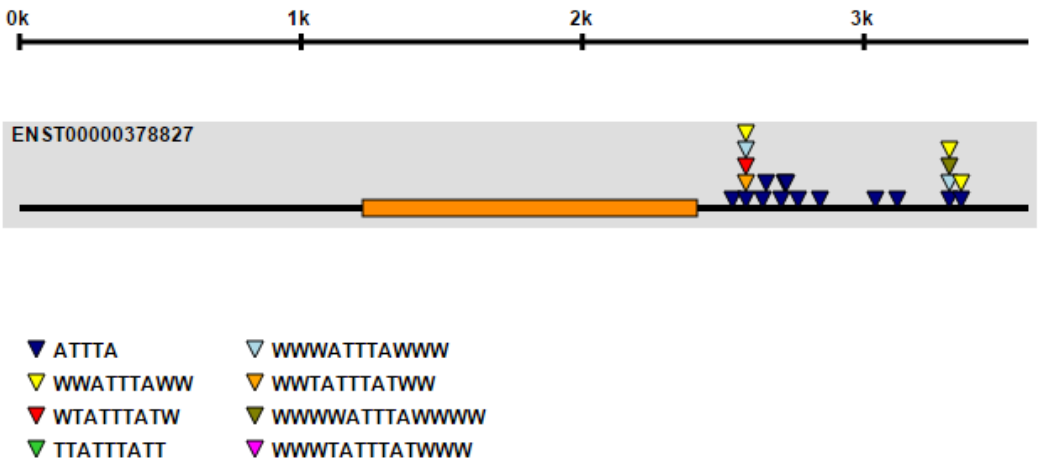

B

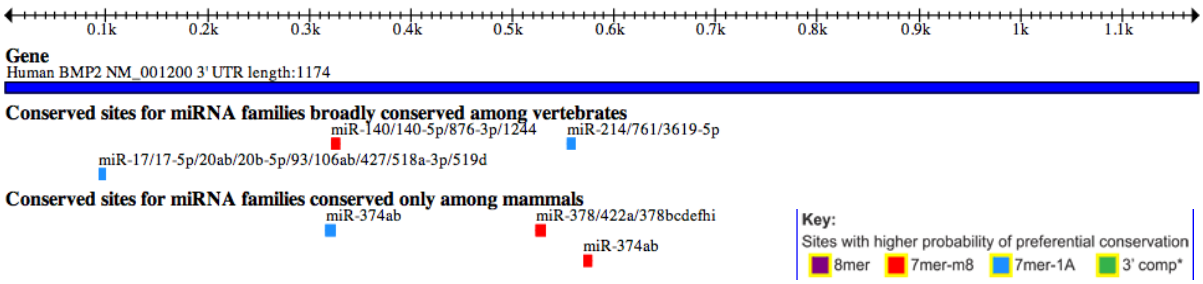

Figure 4.4: Human *Bmp2* 3'UTR with associated ARE and miR-response elements. **A:** Schematic of the analysis of the *Bmp2* 3'UTR by courtesy of AREsite. Colored triangles represent ARE sites, with their locations shown in the *Bmp2* 3'UTR. There are thirteen canonical ARE sites (AUUUA) in the *Bmp2* 3'UTR, nine of which are conserved in mice. **B:** Simplified schematic of the five broadly conserved families of miRs, with miR-response elements in the *Bmp2* 3'UTR. The color key indicates the extent of base complementarity of the given miR to the miR-response elements in the *Bmp2* 3'UTR. Red color denotes 7mer-m8, which is an exact match to positions 2-8 of the mature miRNA (the seed + position 8). Blue color denotes 7mer-1A which is an exact match to positions 2-7 of the mature miRNA (the seed) followed by an 'A'. Diagram is made by computational analysis of miR sites in the *Bmp2* 3'UTR via TargetScan 6.0.

deregulation of miRs and pertinent effects in NF1 and non-NF1 related MPNSTs (Subramanian et al. 2010; Sedani et al. 2012; Masliah-Planchon et al. 2013). Overexpression of miR-204 via its effects on the Ras pathway reduces proliferation, invasion and migration in the ST88-14(*Nf1*$^{-/-}$) and T265(*Nf1*$^{-/-}$) cells *in vitro*, and reduces growth and malignancy of the STS26T(*Nf1*$^{+/-}$) cells *in vivo* (Gong et al. 2012). Inhibition of expression of miR-214 and miR-10b in NF1-related MPNSTs decreases cell proliferation and migration (Subramanian et al. 2010). Therefore, additional investigation of the RNA-binding proteins and the associated ARE sites of the *Bmp2* 3'UTR combined with a microRNAome profiling of *Nf1*$^{(+/-)}$ and *Nf1*-KD cells MPNST cells will not only provide a comprehensive view of the mechanism of *Bmp2* regulation by NF1, but will also aid in identification of a genetic target of enhanced BMP2 signaling promoting migration, invasion, and survival of MPNSTs.

CHAPTER V: Discussion

MPNST is a rare form of cancer that comprises approximately 2% of all sarcomas (Ng et al. 2013). Approximately half of all MPNST cases occur in association with NF1 disease (King et al. 2000), where the biallelic loss of *Nf1* in Schwann cells is thought to be responsible for transformation of neurofibromas to MPNSTs (Zhu et al. 2002). Given that neurofibromas affect almost all NF1 patients (Compston 1994b; Huson 1989b) but only 8-13% of these patients develop MPNSTs (Anghileri et al. 2006), the molecular path from neurofibromas to MPNST formation is unclear. Mutations in the *Nf1* RAS-GRD and subsequent hyperactivation of downstream signaling pathways of RAF-MEK1/2-ERK1/2 and PI3K-AKT-mTOR are necessary but not sufficient to drive the transformation of neurofibromas to MPNSTs (Cichowski et al. 1999; Zhu et al. 2002).

The genomic complexity of MPNSTs, in which multiple signaling pathways cooperate to promote tumorigenesis, has limited treatment options for MPNST patients. The failure of conventional chemotherapy by doxorubicin and ifosfamide (Zehou et al. 2013) and anti-RAS agents (Kim et al. 2013) has stimulated interest in rationally developed targeted therapy for clinical management of MPNSTs. Thus far, targeted therapies aimed at downstream signaling pathways of RAS have fared poorly in clinical trials, although redesigned agents targeting the same pathways are currently under investigation (Farid et al. 2014). To improve clinical outcomes for MPNST patients, a comprehensive understanding of the biological events and gene expression changes independent of Ras signaling, in the setting of NF1 is imperative.

The goal of this study was to utilize gene expression profiling followed by molecular and biochemical studies, to identify a novel target of *Nf1* regulation independent of RAS-

GRD, understand gene regulation, and therapeutic utility of multiple targeted pathways to improve clinical outcomes for NF1-related MPNSTs. To this end, we have identified BMP2-SMAD1/5/8 pathway, independent of the RAS-MEK1/2-ERK1/2 axis (Sun et al. 2013) to be associated with invasion, migration and metastatic properties of MPNST cell lines. I identified a novel regulatory mechanism of mRNA stabilization by NF1. Most importantly, I developed a combinatorial therapeutic approach that reduces the cellular viability of MPNST cells by targeting BMP2 and MEK1/2 with LDN-193189 and selumetinib, respectively.

Anti-tumor interactions of LDN-193189 and selumetinib were evaluated in multiple MPNST cell lines including physiologically relevant low passage NF1-null MPNST cells. Unsurprisingly, single treatment with LDN-193189 resulted in reversal of migratory and invasive properties of MPNST cells regardless of passage number. The efficacy of combinatorial treatment with LDN-193189 and selumetinib on cell viability was enhanced in the low passage cells as compared to the high passage cells. However, combination treatment did not result in a significant decrease in cellular migration or invasion of these cells. This can be due to the strong inhibitory effect of LDN-193189 on migration and invasion of MPNST cells, therefore addition of selumetinib does not result in a significant change in the migratory and invasive potential of these cells. Decreasing the concentration of LDN-193189 in the combinatorial treatments may provide a better assessment of the combinatorial effects of these drugs on cellular migration and invasion of MPNSTs.

I found that the combination of LDN-193189 and selumetinib synergistically inhibited cell viability in all of the tested MPNST cell lines through possible off-target

effects, independent of passage number or NF1 status. The cell viability GI_{50} for LDN-193189 was at least 10-20 times higher than the biochemically relevant concentration required to inhibit BMP2-SMAD1/5/8 signaling. With the demonstrated lack of adverse side effects of LDN-193189 in animal studies (Yu et al. 2008), the inhibition of cell viability by LDN-193189 at higher doses may provide an additional therapeutic benefit in treatment of MPNSTs. The decrease in viability of MPNST cells was associated with increased cleavage of Poly(ADP- ribose) polymerase (PARP), a marker of cell death, detected by western blots in combination treatment as compared to single treatments with LDN-193189 or selumetinib (data not shown). The presence of cleaved PARP fragments (~89 kDa) is indicative of cytotoxicity induced by these agents. Nonetheless, we cannot delineate the precise mechanism of cytotoxicity (apoptosis, autophagy or necrosis) without additional assessment of caspase activity, and/or annexin V staining. Likewise, cytostatic effects of the combinatorial treatment cannot be ruled out as we did not test for any markers associated with cytostasis upon treatment of MPNST cells.

In our pharmacology studies, I also assessed the efficacy of targeting the PI3K/AKT/mTOR pathway regulated by RAS in MPNSTs. Additionally, BMP2-SMAD1/5/8 pathway has been reported to interact with the PI3K/AKT/mTOR pathway to induce invasiveness in cancer subtypes (Kang et al. 2010). Treatment with a dual PI3K/mTOR inhibitor VS-5584 (0.3µM) for 3 hours promoted cell death by presence of cleaved PARP fragments in ST88-14(*Nf1*$^{-/-}$) cells; however, addition of LDN-193189 and/or selumetinib to VS-5584 treated cells did not significantly increase cell death (data not shown). These therapeutic studies suggest that targeting of BMP2-SMAD1/5/8 pathway by LDN-193189 in combination with inhibition of MEK1/2-ERK1/2 signaling by

selumetinib provides an effective strategy to reduce the cell viability of MPNSTs, however further analysis of the combinatorial interaction of both the agents on migration and invasion is warranted.

To explore the mechanism by which NF1 deficiency leads to increased expression of *Bmp2*, we analyzed the transcriptional regulation of *Bmp2* by promoter, 3'UTR, and transcript half-life studies. I identified a post-transcriptional regulatory mechanism by which NF1 regulates the 3'UTR of *Bmp2*. The 3'UTR of *Bmp2* exhibits increased activity upon knockdown of *Nf1* leading to increased half-life and stability of *Bmp2* mRNA. I determined that *Bmp2* mRNA half-life in *Nf1* heterozygous conditions is approximately 2 hours, which virtually doubles upon knockdown of *Nf1*. mRNAs with short half-lives such as *Bmp2*, have fast induction and repression rates (Bolognani & Perrone-Bizzozero 2008) and are known to respond to changes in transcription more rapidly than those with longer half-lives (Ross 1995). Importantly, stabilization of mRNAs with short half-lives can result in dramatic changes in gene expression, hence protein levels (Hargrove & Schmidt 1989). Accordingly, the increased stability of the *Bmp2* mRNA upon *Nf1* knockdown may permit a prolonged translational window, leading to increases in BMP2 protein levels and its functional effects on migration and invasion. I noticed a strong association between the increase in *Bmp2* mRNA half-life and steady-state mRNA levels. These findings agree with a previous report where human *Bmp2* mRNA decay rate correlates with endogenous *Bmp2* mRNA levels (Fritz et al. 2004). The unusually high degree of conservation of the *Bmp2* 3'UTR (Fritz et al. 2004) coupled with the ample presence of ARE sites and miR-response elements within this region, is suggestive of a strictly regulated region which is instrumental in controlling *Bmp2* expression levels. The regulation of transcript stability

by NF1 is a novel concept that need be further explored. Although there is an overall down-regulation of genes in MPNST tissue samples as compared to the benign forms of neurofibromas (Miller et al. 2009), our gene expression profiling study identified overexpression of several candidate genes upon NF1 deficiency such as SOX9, STAG1, POU5F1, VEGFC, EDN1, CXCL3, etc. mRNA stabilization may be the mechanism of increased expression of other genes up-regulated by knockdown of *Nf1* in MPNST cells. Analysis of the transcript half-lives and 3'UTR regions of these up-regulated genes may potentially identify common *cis*- and *trans*-acting elements regulated by NF1 that can be therapeutically targeted in MPNSTs.

Overall, this study has shown the feasibility of targeting BMP2-SMAD1/5/8 signaling in combination with MEK1/2-ERK1/2 inhibition in MPNSTs. Additionally, targeting of post-transcriptional regulatory elements involved in regulation of *Bmp2* 3'UTR by NF1 provides an alternative genetic target to precisely inhibit BMP2 expression and its functional effects on cell migration and invasion in MPNSTs. A model diagram of the proposed combinatorial targeting approach presented in this study with the goal of improving clinical outcomes for MPNST patients is presented in Fig 5.1.

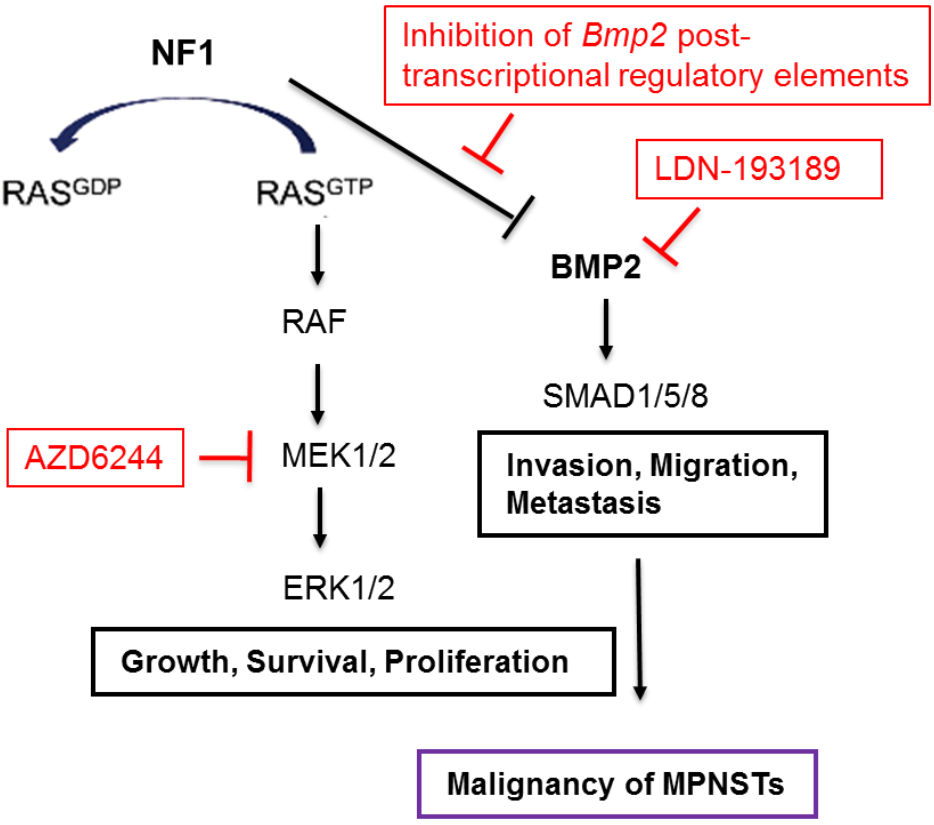

Figure 5.1: Diagram summarizing the proposed combinatorial targeted therapeutic approach for treatment of MPNSTs. NF1 attenuates RAS and associated downstream signaling cascades by accelerating hydrolysis of RAS-GTP to RAS-GDP. NF1 post-transcriptionally regulates *Bmp2* leading to suppression of BMP2-SMAD1/5/8 signaling pathway. NF1 deficiency leads to constitutive activation of RAS-MEK1/2-ERK1/2, and BMP2-SMAD1/5/8 signaling pathways, enhancing the tumorigenic properties of MPNSTs. Combinatorial targeting of MEK1/2 by selumetinib (AZD6244) and BMP2 by LDN-193189 or inhibition of *Bmp2* post-transcriptional regulatory elements reduces the increased survival of MPNSTs, however does not affect the migratory and invasive characteristics of malignant MPNSTs.

REFERENCES

Abrams, K.L. et al., 2004. An evolutionary and molecular analysis of Bmp2 expression. *The Journal of biological chemistry*, 279(16), pp.15916–15928.

Adjei, A.A. et al., 2008. Phase I pharmacokinetic and pharmacodynamic study of the oral, small-molecule mitogen-activated protein kinase kinase 1/2 inhibitor AZD6244 (ARRY-142886) in patients with advanced cancers. *Journal of clinical oncology : official journal of the American Society of Clinical Oncology*, 26(13), pp.2139–2146.

Akhurst, R.J. & Hata, A., 2012. Targeting the TGF[beta] signalling pathway in disease. *Nat Rev Drug Discov*, 11(10), pp.790–811. Available at: http://dx.doi.org/10.1038/nrd3810.

Anghileri, M. et al., 2006. Malignant peripheral nerve sheath tumors: Prognostic factors and survival in a series of patients treated at a single institution. *Cancer*, 107(5), pp.1065–1074.

Bajenaru, M.L. et al., 2002. Astrocyte-specific inactivation of the neurofibromatosis 1 gene (NF1) is insufficient for astrocytoma formation. *Molecular and cellular biology*, 22(14), pp.5100–5113.

Balboni, a. L. et al., 2015. p53 and Np63 Coregulate the Transcriptional and Cellular Response to TGF and BMP Signals. *Molecular Cancer Research*, 13(4), pp.732–742. Available at: http://mcr.aacrjournals.org/cgi/doi/10.1158/1541-7786.MCR-14-0152-T.

Balboni, A.L. et al., 2013. Δnp63A-Mediated Activation of Bone Morphogenetic Protein Signaling Governs Stem Cell Activity and Plasticity in Normal and Malignant

Mammary Epithelial Cells. *Cancer Research*, 73(2), pp.1020–1030.

Basso, A.D., Kirschmeier, P. & Bishop, W.R., 2006. Lipid posttranslational modifications. Farnesyl transferase inhibitors. *Journal of lipid research*, 47(1), pp.15–31.

Bates, J.E. et al., 2014. Malignant peripheral nerve sheath tumors (MPNST): a SEER analysis of incidence across the age spectrum and therapeutic interventions in the pediatric population. *Pediatric blood & cancer*, 61(11), pp.1955–1960.

Bekaii-Saab, T. et al., 2011. Multi-institutional phase II study of selumetinib in patients with metastatic biliary cancers. *Journal of clinical oncology : official journal of the American Society of Clinical Oncology*, 29(17), pp.2357–2363.

Bennouna, J. et al., 2011. A Phase II, open-label, randomised study to assess the efficacy and safety of the MEK1/2 inhibitor AZD6244 (ARRY-142886) versus capecitabine monotherapy in patients with colorectal cancer who have failed one or two prior chemotherapeutic regimens. *Investigational new drugs*, 29(5), pp.1021–1028.

Bernards, A. et al., 1992. Complete human NF1 cDNA sequence: two alternatively spliced mRNAs and absence of expression in a neuroblastoma line. *DNA and cell biology*, 11(10), pp.727–734.

Bernards, A. et al., 1993. Mouse neurofibromatosis type 1 cDNA sequence reveals high degree of conservation of both coding and non-coding mRNA segments. *Human molecular genetics*, 2(6), pp.645–650.

Bhola, P. et al., 2010. Preclinical in vivo evaluation of rapamycin in human malignant

peripheral nerve sheath explant xenograft. *International journal of cancer. Journal international du cancer*, 126(2), pp.563–571.

Bieniasz, M. et al., 2015. The positive correlation between gene expression of the two angiogenic factors: VEGF and BMP-2 in lung cancer patients. *Lung Cancer*, 66(3), pp.319–326. Available at: http://dx.doi.org/10.1016/j.lungcan.2009.02.020.

Bolognani, F. & Perrone-Bizzozero, N.I., 2008. RNA-protein interactions and control of mRNA stability in neurons. *Journal of neuroscience research*, 86(3), pp.481–489.

Bottillo, I. et al., 2009. Germline and somatic NF1 mutations in sporadic and NF1-associated malignant peripheral nerve sheath tumours. *The Journal of pathology*, 217(5), pp.693–701.

Boyanapalli, M. et al., 2006. Neurofibromin binds to caveolin-1 and regulates ras, FAK, and Akt. *Biochemical and Biophysical Research Communications*, 340(4), pp.1200–1208.

Bradtmoller, M. et al., 2012. Impaired Pten expression in human malignant peripheral nerve sheath tumours. *PloS one*, 7(11), p.e47595.

Brems, H. et al., 2009. Glomus tumors in neurofibromatosis type 1: Genetic, functional, and clinical evidence of a novel association. *Cancer Research*, 69(18), pp.7393–7401.

Carragee, E.J. et al., 2013. Cancer risk after use of recombinant bone morphogenetic protein-2 for spinal arthrodesis. *The Journal of bone and joint surgery. American volume*, 95(17), pp.1537–1545.

Chandler, R.L. et al., 2007. Bmp2 transcription in osteoblast progenitors is regulated by a distant 3' enhancer located 156.3 kilobases from the promoter. *Molecular and cellular biology*, 27(8), pp.2934–2951.

Chen, A. et al., 2012. Inhibitory effect of BMP-2 on the proliferation of breast cancer cells. *Molecular medicine reports*, 6(3), pp.615–620.

Chen, C.Y. a, Ezzeddine, N. & Shyu, A. Bin, 2008. *Chapter 17 Messenger RNA Half-Life Measurements in Mammalian Cells* 1st ed., Elsevier Inc. Available at: http://dx.doi.org/10.1016/S0076-6879(08)02617-7.

Chen, D., Zhao, M. & Mundy, G.R., 2004a. Bone morphogenetic proteins. *Growth factors (Chur, Switzerland)*, 22(4), pp.233–241.

Chen, D., Zhao, M. & Mundy, G.R., 2004b. Bone morphogenetic proteins. *Growth factors (Chur, Switzerland)*, 22(4), pp.233–241.

Cheneval, D. et al., 2010. A review of methods to monitor the modulation of mRNA stability: a novel approach to drug discovery and therapeutic intervention. *Journal of biomolecular screening : the official journal of the Society for Biomolecular Screening*, 15(6), pp.609–622.

Chu, H. et al., 2014. Silencing BMP-2 expression inhibits A549 and H460 cell proliferation and migration. *Diagnostic Pathology*, 9(1), p.123. Available at: http://www.diagnosticpathology.org/content/9/1/123.

Cichowski, K. et al., 1999. Mouse models of tumor development in neurofibromatosis type 1. *Science (New York, N.Y.)*, 286(5447), pp.2172–2176.

Compston, A., 1994a. The Neurofibromatoses. A pathogenetic and clinical overview. *Journal of Neurology, Neurosurgery, and Psychiatry*, 57(10), p.1301. Available at: http://www.ncbi.nlm.nih.gov/pmc/articles/PMC485524/.

Compston, A., 1994b. The Neurofibromatoses. A pathogenetic and clinical overview. *Journal of Neurology, Neurosurgery, and Psychiatry*, 57(10), p.1301.

Cuny, G.D. et al., 2008. Structure-activity relationship study of bone morphogenetic protein (BMP) signaling inhibitors. *Bioorganic & medicinal chemistry letters*, 18(15), pp.4388–4392.

Daginakatte, G.C. & Gutmann, D.H., 2007. Neurofibromatosis-1 (Nf1) heterozygous brain microglia elaborate paracrine factors that promote Nf1-deficient astrocyte and glioma growth. *Human molecular genetics*, 16(9), pp.1098–1112.

Dai, J. et al., 2008. Prostate cancer induces bone metastasis through Wnt-induced bone morphogenetic protein-dependent and independent mechanisms. *Cancer research*, 68(14), pp.5785–5794.

Dasgupta, B., Dugan, L.L. & Gutmann, D.H., 2003. The neurofibromatosis 1 gene product neurofibromin regulates pituitary adenylate cyclase-activating polypeptide-mediated signaling in astrocytes. *The Journal of neuroscience : the official journal of the Society for Neuroscience*, 23(26), pp.8949–8954.

Daston, M.M. & Ratner, N., 1992. Neurofibromin, a predominantly neuronal GTPase activating protein in the adult, is ubiquitously expressed during development. *Developmental dynamics : an official publication of the American Association of Anatomists*, 195(3), pp.216–226.

Day, D.A. & Tuite, M.F., 1998. Post-transcriptional gene regulatory mechanisms in eukaryotes: an overview. *The Journal of endocrinology*, 157(3), pp.361–371.

Devlin, R.D. et al., 2003. Skeletal overexpression of noggin results in osteopenia and reduced bone formation. *Endocrinology*, 144(5), pp.1972–1978.

Dilworth, J.T. et al., 2006. Molecular targets for emerging anti-tumor therapies for neurofibromatosis type 1. *Biochemical pharmacology*, 72(11), pp.1485–1492.

Dimauro, T. & David, G., 2010. Ras-induced senescence and its physiological relevance in cancer. *Current cancer drug targets*, 10(8), pp.869–876.

Dore, J.J. et al., 2009. Multiple signaling pathways converge to regulate bone-morphogenetic-protein-dependent glial gene expression. *Developmental neuroscience*, 31(6), pp.473–486.

Dore, J.J., Crotty, K.L. & Birren, S.J., 2005. Inhibition of glial maturation by bone morphogenetic protein 2 in a neural crest-derived cell line. *Developmental neuroscience*, 27(1), pp.37–48.

Ducatman, B., 1986a. Malignant peripheral nerve sheath tumors. A clinicopathological study of 120 cases. *Cancer*, 57, pp.2006–2021. Available at: http://www.ncbi.nlm.nih.gov/pubmed/23318430.

Ducatman, B., 1986b. Malignant peripheral nerve sheath tumors. A clinicopathological study of 120 cases. *Cancer*, 57, pp.2006–2021.

Engers, D.W. et al., 2013. Synthesis and structure-activity relationships of a novel and selective bone morphogenetic protein receptor (BMP) inhibitor derived from the

pyrazolo[1.5-a]pyrimidine scaffold of Dorsomorphin: The discovery of ML347 as an ALK2 versus ALK3 selective MLPCN . *Bioorganic and Medicinal Chemistry Letters*, 23(11), pp.3248–3252.

Evans, D.G.R. et al., 2002. Malignant peripheral nerve sheath tumours in neurofibromatosis 1. *Journal of medical genetics*, 39(5), pp.311–314.

Evans, D.G.R. et al., 2011. Mortality in neurofibromatosis 1: in North West England: an assessment of actuarial survival in a region of the UK since 1989. *European Journal of Human Genetics*, 19(11), pp.1187–1191.

Evans, D.G.R., Huson, S.M. & Birch, J.M., 2012. Malignant peripheral nerve sheath tumours in inherited disease. *Clinical Sarcoma Research*, 2(1), p.17. Available at: Clinical Sarcoma Research.

Fabian, M.R., Sonenberg, N. & Filipowicz, W., 2010. Regulation of mRNA translation and stability by microRNAs. *Annual review of biochemistry*, 79, pp.351–379.

Farid, M. et al., 2014. Malignant Peripheral Nerve Sheath Tumors. *The Oncologist* , 19 (2), pp.193–201. Available at: http://theoncologist.alphamedpress.org/content/19/2/193.abstract.

Fei, Z.-H. et al., 2013. Serum BMP-2 up-regulation as an indicator of poor survival in advanced non-small cell lung cancer patients. *Asian Pacific journal of cancer prevention : APJCP*, 14(9), pp.5293–9. Available at: http://www.ncbi.nlm.nih.gov/pubmed/24175816.

Feng, J.Q. et al., 2003. NF-kappaB specifically activates BMP-2 gene expression in growth plate chondrocytes in vivo and in a chondrocyte cell line in vitro. *The*

Journal of biological chemistry, 278(31), pp.29130–29135.

Filipowicz, W., Bhattacharyya, S.N. & Sonenberg, N., 2008. Mechanisms of post-transcriptional regulation by microRNAs: are the answers in sight? *Nature reviews. Genetics*, 9(2), pp.102–114.

Fotinos, A. et al., 2014. Bone Morphogenetic Protein-focused Strategies to Induce Cytotoxicity in Lung Cancer Cells. *Anticancer research*, 34(5), pp.2095–104. Available at: http://www.ncbi.nlm.nih.gov/pubmed/24778011.

Foucquier, J. & Guedj, M., 2015. Analysis of drug combinations: current methodological landscape. *Pharmacology Research & Perspectives*, 3(3), p.e00149. Available at: http://www.ncbi.nlm.nih.gov/pmc/articles/PMC4492765/.

Friedman, J.M., 1999. Epidemiology of neurofibromatosis type 1. *American journal of medical genetics*, 89(1), pp.1–6.

Friedman, J.M., 2002. Neurofibromatosis 1: clinical manifestations and diagnostic criteria. *Journal of child neurology*, 17(8), pp.542–548,646–651.

Fritz, D.T. et al., 2004. Conservation of Bmp2 post-transcriptional regulatory mechanisms. *Journal of Biological Chemistry*, 279(47), pp.48950–48958.

Fukui, N. et al., 2006. Pro-inflammatory cytokine tumor necrosis factor-?? induces bone morphogenetic protein-2 in chondrocytes via mRNA stabilization and transcriptional up-regulation. *Journal of Biological Chemistry*, 281(37), pp.27229–27241.

Fukui, N. et al., 2003. Stimulation of BMP-2 expression by pro-inflammatory cytokines IL-1 and TNF-alpha in normal and osteoarthritic chondrocytes. *The Journal of bone*

and joint surgery. American volume, 85-A Suppl, pp.59–66.

Garber, J.E. & Offit, K., 2005. Hereditary cancer predisposition syndromes. *Journal of Clinical Oncology*, 23(2), pp.276–292.

Geary, N., 2013. Understanding synergy. *American journal of physiology. Endocrinology and metabolism*, 304(3), pp.E237–53.

Gerber, P. a et al., 2009. Neurofibromatosis. *Euopean journal of medical research*, March 17, pp.102–105.

Ghosh, M. et al., 2009. Essential role of the RNA-binding protein HuR in progenitor cell survival in mice. *The Journal of clinical investigation*, 119(12), pp.3530–3543.

Ghosh-Choudhury, N. et al., 2001. Autoregulation of Mouse BMP-2 Gene Transcription Is Directed by the Proximal Promoter Element. *Biochemical and Biophysical Research Communications*, 286(1), pp.101–108. Available at: http://www.sciencedirect.com/science/article/pii/S0006291X01953513.

Giancotti, F.G., 2015. HHS Public Access. , 155(4), pp.750–764. Available at: http://www.ncbi.nlm.nih.gov/pmc/articles/PMC4354734/pdf/nihms666054.pdf.

Gilman, A.G., 1987. G PR . OTEINS : TRANSDUCERS OF RECEPTOR-GENERATED SIGNALS.

Gong, M. et al., 2012. MicroRNA-204 critically regulates carcinogenesis in malignant peripheral nerve sheath tumors. *Neuro-Oncology*, 14(8), pp.1007–1017.

Gregory PE1, Gutmann DH, Mitchell A, Park S, Boguski M, Jacks T, Wood DL, Jove R, C.F., 1993. Neurofibromatosis type 1 gene product (neurofibromin) associates with

microtubules. *Somat Cell Mol Genet.*, 19(3), pp.265–74.

Guo, H.F. et al., 1997. Requirement of Drosophila NF1 for activation of adenylyl cyclase by PACAP38-like neuropeptides. *Science (New York, N.Y.)*, 276(5313), pp.795–798.

Guo, M. et al., 2014. miR-656 inhibits glioma tumorigenesis through repression of BMPR1A. *Carcinogenesis*, 35(8), pp.1698–1706.

Guo, X. & Wang, X.-F., 2009. Signaling cross-talk between TGF-beta/BMP and other pathways. *Cell research*, 19(1), pp.71–88.

Gutmann, D.H. et al., 2002. Mouse glioma gene expression profiling identifies novel human glioma-associated genes. *Annals of neurology*, 51(3), pp.393–405.

Gutmann, D.H., Cole, J.L. & Collins, F.S., 1995. Expression of the neurofibromatosis type 1 (NF1) gene during mouse embryonic development. *Progress in brain research*, 105, pp.327–335.

Haass, N.K. et al., 2008. The mitogen-activated protein/extracellular signal-regulated kinase kinase inhibitor AZD6244 (ARRY-142886) induces growth arrest in melanoma cells and tumor regression when combined with docetaxel. *Clinical cancer research : an official journal of the American Association for Cancer Research*, 14(1), pp.230–239.

Hainsworth, J.D. et al., 2010. A phase II, open-label, randomized study to assess the efficacy and safety of AZD6244 (ARRY-142886) versus pemetrexed in patients with non-small cell lung cancer who have failed one or two prior chemotherapeutic regimens. *Journal of thoracic oncology : official publication of the International*

Association for the Study of Lung Cancer, 5(10), pp.1630–1636.

Hao, S. & Baltimore, D., 2009. The stability of mRNA influences the temporal order of the induction of genes encoding inflammatory molecules. *Nature immunology*, 10(3), pp.281–288.

Hargrove, J.L. & Schmidt, F.H., 1989. The role of mRNA and protein stability in gene expression. *FASEB journal : official publication of the Federation of American Societies for Experimental Biology*, 3(12), pp.2360–2370.

Harrisingh, M.Ct. et al., 2004. Ras/Raf/ERK signalling pathway drives Schwann cell dedifferentiation. *The EMBO journal*, 23(15), pp.3061–3071.

Hatori, M. et al., 2006. Osteosarcoma in a patient with neurofibromatosis type 1: a case report and review of the literature. *The Tohoku journal of experimental medicine*, 208(4), pp.343–348.

Hegedus, B. et al., 2007. Neurofibromatosis-1 regulates neuronal and glial cell differentiation from neuroglial progenitors in vivo by both cAMP- and Ras-dependent mechanisms. *Cell stem cell*, 1(4), pp.443–457.

Helvering, L.M. et al., 2000. Regulation of the promoters for the human bone morphogenetic protein 2 and 4 genes. *Gene*, 256(1-2), pp.123–138.

Hiatt, K.K. et al., 2001. Neurofibromin GTPase-activating protein-related domains restore normal growth in Nf1-/- cells. *The Journal of biological chemistry*, 276(10), pp.7240–7245.

Hirbe, A.C. & Gutmann, D.H., 2014. Neurofibromatosis type 1: a multidisciplinary

approach to care. *Lancet neurology*, 13(8), pp.834–843. Available at: http://www.sciencedirect.com/science/article/pii/S1474442214700638.

Hodgson, S., 2008. Mechanisms of inherited cancer susceptibility. *Journal of Zhejiang University. Science. B*, 9(1), pp.1–4.

Hodson, D.J. et al., 2010. Deletion of the RNA-binding proteins Zfp36l1 and Zfp36l2 leads to perturbed thymic development and T-lymphoblastic leukaemia. *Nature immunology*, 11(8), pp.717–724. Available at: http://www.ncbi.nlm.nih.gov/pmc/articles/PMC2953641/.

Holtkamp, N. et al., 2007. MMP-13 and p53 in the Progression of Malignant Peripheral Nerve Sheath Tumors. *Neoplasia (New York, N.Y.)*, 9(8), pp.671–677. Available at: http://www.ncbi.nlm.nih.gov/pmc/articles/PMC1950437/.

Hong, C.C. & Yu, P.B., 2009. Applications of small molecule BMP inhibitors in physiology and disease. *Cytokine & growth factor reviews*, 20(5-6), p.409. Available at: http://www.ncbi.nlm.nih.gov/pmc/articles/PMC2813719/.

Hsu, M.-Y. et al., 2005. Bone morphogenetic proteins in melanoma: angel or devil? *Cancer metastasis reviews*, 24(2), pp.251–263.

Hsueh, Y.P. et al., 2001. Bipartite interaction between neurofibromatosis type I protein (neurofibromin) and syndecan transmembrane heparan sulfate proteoglycans. *The Journal of neuroscience : the official journal of the Society for Neuroscience*, 21(11), pp.3764–3770.

Huson, S.M., 1989a. Recent developments in the diagnosis and management of neurofibromatosis. *Archives of Disease in Childhood*, 64(5), pp.745–749. Available

at: http://www.ncbi.nlm.nih.gov/pmc/articles/PMC1792032/.

Huson, S.M., 1989b. Recent developments in the diagnosis and management of neurofibromatosis. *Archives of Disease in Childhood*, 64(5), pp.745–749.

Ide, H. et al., 1997. Cloning of human bone morphogenetic protein type IB receptor (BMPR-IB) and its expression in prostate cancer in comparison with other BMPRs. *Oncogene*, 14(11), pp.1377–1382.

Imamura, T. et al., 1997. Smad6 inhibits signalling by the TGF-beta superfamily. *Nature*, 389(6651), pp.622–626.

Ishida, W. et al., 2000. Smad6 is a Smad1/5-induced smad inhibitor. Characterization of bone morphogenetic protein-responsive element in the mouse Smad6 promoter. *The Journal of biological chemistry*, 275(9), pp.6075–6079.

Ismat, F.A. et al., 2006. The neurofibromin GAP-related domain rescues endothelial but not neural crest development in Nf1 mice. *The Journal of clinical investigation*, 116(9), pp.2378–2384.

Jacks, T. et al., 1994. Tumour predisposition in mice heterozygous for a targeted mutation in Nf1. *Nature genetics*, 7(3), pp.353–361.

Jeeninga, R.E. et al., 1998. The mechanism of actinomycin D-mediated inhibition of HIV-1 reverse transcription. *Nucleic Acids Research* , 26 (23), pp.5472–5479. Available at: http://nar.oxfordjournals.org/content/26/23/5472.abstract.

Jett, K. & Friedman, J.M., 2010. Clinical and genetic aspects of neurofibromatosis 1. *Genetics in medicine : official journal of the American College of Medical Genetics*,

12(1), pp.1–11.

Jiang, S. et al., 2010. Repressive BMP2 gene regulatory elements near the BMP2 promoter. *Biochemical and biophysical research communications*, 392(2), pp.124–128.

Johannessen, C.M. et al., 2005. The NF1 tumor suppressor critically regulates TSC2 and mTOR. *Proceedings of the National Academy of Sciences of the United States of America*, 102(24), pp.8573–8578.

Kang, M.H. et al., 2010. BMP2 accelerates the motility and invasiveness of gastric cancer cells via activation of the phosphatidylinositol 3-kinase (PI3K)/Akt pathway. *Experimental cell research*, 316(1), pp.24–37.

Katsuno, Y. et al., 2008. Bone morphogenetic protein signaling enhances invasion and bone metastasis of breast cancer cells through Smad pathway. *Oncogene*, 27(49), pp.6322–6333.

Kim, A. et al., 2013. Phase I trial and pharmacokinetic study of sorafenib in children with neurofibromatosis type I and plexiform neurofibromas. *Pediatric blood & cancer*, 60(3), pp.396–401.

King, A.A. et al., 2000. Malignant peripheral nerve sheath tumors in neurofibromatosis 1. *American journal of medical genetics*, 93(5), pp.388–392.

Kleber, M. et al., 2005. Neural crest stem cell maintenance by combinatorial Wnt and BMP signaling. *The Journal of cell biology*, 169(2), pp.309–320.

Kleeff, J. et al., 1999. Bone morphogenetic protein 2 exerts diverse effects on cell

growth in vitro and is expressed in human pancreatic cancer in vivo. *Gastroenterology*, 116(5), pp.1202–1216.

Klose, A. et al., 1998. Selective disactivation of neurofibromin GAP activity in neurofibromatosis type 1. *Human molecular genetics*, 7(8), pp.1261–1268.

Kluwe, L., Friedrich, R.E. & Mautner, V.F., 1999. Allelic loss of the NF1 gene in NF1-associated plexiform neurofibromas. *Cancer genetics and cytogenetics*, 113(1), pp.65–69.

Knudson, a G., 1971. Mutation and cancer: statistical study of retinoblastoma. *Proceedings of the National Academy of Sciences of the United States of America*, 68(4), pp.820–823.

Koenig, B.B. et al., 1994. Characterization and cloning of a receptor for BMP-2 and BMP-4 from NIH 3T3 cells. *Molecular and cellular biology*, 14(9), pp.5961–5974.

Kolberg⇓, M. et al., 2013. Survival meta-analyses for> 1800 malignant peripheral nerve sheath tumor patients with and without neurofibromatosis type 1. *Neuro-Oncology*, 15(2), pp.135–147. Available at: http://neuro-oncology.oxfordjournals.org/content/15/2/135.short\nhttp://www.pubmedcentral.nih.gov/articlerender.fcgi?artid=3548581&tool=pmcentrez&rendertype=abstract.

Krause, C., Guzman, A. & Knaus, P., 2011. Noggin. *The international journal of biochemistry & cell biology*, 43(4), pp.478–481.

Kroep, J.R. et al., 2011. First-line chemotherapy for malignant peripheral nerve sheath tumor (MPNST) versus other histological soft tissue sarcoma subtypes and as a prognostic factor for MPNST: an EORTC soft tissue and bone sarcoma group

study. *Annals of oncology : official journal of the European Society for Medical Oncology / ESMO*, 22(1), pp.207–214.

LaFemina, J. et al., 2013. Oncologic outcomes of sporadic, neurofibromatosis-associated, and radiation-induced malignant peripheral nerve sheath tumors. *Annals of surgical oncology*, 20(1), pp.66–72.

Langenfeld, E.M., Kong, Y. & Langenfeld, J., 2006. Bone morphogenetic protein 2 stimulation of tumor growth involves the activation of Smad-1/5. *Oncogene*, 25(5), pp.685–692.

Langenfeld, E.M., Kong, Y. & Langenfeld, J., 2005. Bone morphogenetic protein-2-induced transformation involves the activation of mammalian target of rapamycin. *Molecular cancer research : MCR*, 3(12), pp.679–684.

Larribere, L. et al., 2015. NF1 loss induces senescence during human melanocyte differentiation in an iPSC-based model. *Pigment Cell & Melanoma Research*, p.n/a–n/a. Available at: http://doi.wiley.com/10.1111/pcmr.12369.

Le, L.Q. et al., 2011. Susceptible stages in Schwann cells for NF1-associated plexiform neurofibroma development. *Cancer Research*, 71(13), pp.4686–4695.

Leondaritis, G., Petrikkos, L. & Mangoura, D., 2009. Regulation of the Ras-GTPase activating protein neurofibromin by C-tail phosphorylation: Implications for protein kinase C/Ras/extracellular signal-regulated kinase 1/2 pathway signaling and neuronal differentiation. *Journal of Neurochemistry*, 109(2), pp.573–583.

Lerner, E.C. et al., 1997. Inhibition of the prenylation of K-Ras, but not H- or N-Ras, is highly resistant to CAAX peptidomimetics and requires both a farnesyltransferase

and a geranylgeranyltransferase I inhibitor in human tumor cell lines. *Oncogene*, 15(11), pp.1283–1288.

Li, Y. et al., 1995. Genomic organization of the neurofibromatosis 1 gene (NF1). *Genomics*, 25(1), pp.9–18.

Lin, H.-K. et al., 2003. Suppression Versus Induction of Androgen Receptor Functions by the Phosphatidylinositol 3-Kinase/Akt Pathway in Prostate Cancer LNCaP Cells with Different Passage Numbers. *Journal of Biological Chemistry* , 278 (51), pp.50902–50907. Available at: http://www.jbc.org/content/278/51/50902.abstract.

Liu, A. & Niswander, L.A., 2005. Bone morphogenetic protein signalling and vertebrate nervous system development. *Nature reviews. Neuroscience*, 6(12), pp.945–954.

Lubelski, D. et al., 2015. Adverse Events With the Use of rhBMP-2 in Thoracolumbar and Lumbar Spine Fusions: A 9-Year Institutional Analysis. *Journal of spinal disorders & techniques*, 28(5), pp.E277–83.

Masliah-Planchon, J. et al., 2013. MicroRNAome profiling in benign and malignant neurofibromatosis type 1-associated nerve sheath tumors: evidences of PTEN pathway alterations in early NF1 tumorigenesis. *BMC genomics*, 14, p.473. Available at: http://www.pubmedcentral.nih.gov/articlerender.fcgi?artid=3744175&tool=pmcentrez&rendertype=abstract.

Maston, G. a, Evans, S.K. & Green, M.R., 2006. Transcriptional regulatory elements in the human genome. *Annual review of genomics and human genetics*, 7, pp.29–59.

Mattingly, R.R. et al., 2006. The mitogen-activated protein kinase/extracellular signal-

regulated kinase kinase inhibitor PD184352 (CI-1040) selectively induces apoptosis in malignant schwannoma cell lines. *The Journal of pharmacology and experimental therapeutics*, 316(1), pp.456–465.

Mautner, V.-F. et al., 2008. Assessment of benign tumor burden by whole-body MRI in patients with neurofibromatosis 1. *Neuro-oncology*, 10(4), pp.593–598.

Midgley, R.S. & Kerr, D.J., 2002. Ras as a target in cancer therapy. *Critical Reviews in Oncology/Hematology*, 44(2), pp.109–120.

Miller, S.J. et al., 2009. Integrative genomic analyses of neurofibromatosis tumours identify SOX9 as a biomarker and survival gene. *EMBO Molecular Medicine*, 1(4), pp.236–248.

Monteiro, J. & Fodde, R., 2015. Cancer stemness and metastasis: Therapeutic consequences and perspectives. *European Journal of Cancer*, 46(7), pp.1198–1203. Available at: http://dx.doi.org/10.1016/j.ejca.2010.02.030.

Moustakas, A. et al., 2002. Mechanisms of TGF-beta signaling in regulation of cell growth and differentiation. *Immunology letters*, 82(1-2), pp.85–91.

Munchhof, A.M. et al., 2006. Neurofibroma-associated growth factors activate a distinct signaling network to alter the function of neurofibromin-deficient endothelial cells. *Human Molecular Genetics*, 15(11), pp.1858–1869.

Nauth, A. et al., 2009. Bone morphogenetic proteins in open fractures: past, present, and future. *Injury*, 40 Suppl 3, pp.S27–31.

Ng, V.Y. et al., 2013. Incidence and survival in sarcoma in the United States: a focus on

musculoskeletal lesions. *Anticancer research*, 33(6), pp.2597–2604.

Nguyen, R. et al., 2011. Plexiform neurofibromas in children with neurofibromatosis type 1: Frequency and associated clinical deficits. *Journal of Pediatrics*, 159(4), pp.652–655.e2. Available at: http://dx.doi.org/10.1016/j.jpeds.2011.04.008.

Nikumbh, D.B. et al., 2013. Giant Sporadic Low Grade Malignant Peripheral Nerve Sheath (MPNST) of Left Thigh. *Journal of Clinical and Diagnostic Research : JCDR*, 7(6), pp.1155–1158. Available at: http://www.ncbi.nlm.nih.gov/pmc/articles/PMC3708222/.

Niswander, L. & Martin, G.R., 1993. FGF-4 and BMP-2 have opposite effects on limb growth. *Nature*, 361(6407), pp.68–71.

Nohe, A. et al., 2002. The mode of bone morphogenetic protein (BMP) receptor oligomerization determines different BMP-2 signaling pathways. *The Journal of biological chemistry*, 277(7), pp.5330–5338.

Ozawa, T. et al., 2005. The neurofibromatosis type 1 gene product neurofibromin enhances cell motility by regulating actin filament dynamics via the Rho-ROCK-LIMK2-cofilin pathway. *Journal of Biological Chemistry*, 280(47), pp.39524–39533.

Le Page, C. et al., 2009. BMP-2 signaling in ovarian cancer and its association with poor prognosis. *Journal of ovarian research*, 2, p.4.

Panigrahi, S. et al., 2013. Primary malignant peripheral nerve sheath tumor at unusual location. *Journal of Neurosciences in Rural Practice*, 4(Suppl 1), pp.S83–S86. Available at: http://www.ncbi.nlm.nih.gov/pmc/articles/PMC3808069/.

Park, S.-J. et al., 2013. Serum biomarkers for neurofibromatosis type 1 and early detection of malignant peripheral nerve-sheath tumors. *BMC medicine*, 11, p.109. Available at: http://www.pubmedcentral.nih.gov/articlerender.fcgi?artid=3648455&tool=pmcentrez&rendertype=abstract.

Patmore, D.M. et al., 2012. In vivo regulation of TGF-β by R-Ras2 revealed through loss of the RasGap protein NF1. *Cancer Research*, 72(20), pp.5317–5327.

Peart, T.M. et al., 2012. BMP signalling controls the malignant potential of ascites-derived human epithelial ovarian cancer spheroids via AKT kinase activation. *Clinical and Experimental Metastasis*, 29(4), pp.293–313.

Persano, L. et al., 2012. BMP2 sensitizes glioblastoma stem-like cells to Temozolomide by affecting HIF-1alpha stability and MGMT expression. *Cell death & disease*, 3, p.e412.

Pregizer, S. & Mortlock, D.P., 2009. Control of BMP gene expression by long-range regulatory elements. *Cytokine and Growth Factor Reviews*, 20(5-6), pp.509–515.

Van Raamsdonk, C.D. et al., 2009. Frequent somatic mutations of GNAQ in uveal melanoma and blue naevi. *Nature*, 457(7229), pp.599–602.

Van Raamsdonk, C.D. et al., 2010. Mutations in GNA11 in uveal melanoma. *The New England journal of medicine*, 363(23), pp.2191–2199.

De Raedt, T. et al., 2003. Elevated risk for MPNST in NF1 microdeletion patients. *American journal of human genetics*, 72(5), pp.1288–1292.

Rahrmann, E.P. et al., 2013. Forward genetic screen for malignant peripheral nerve sheath tumor formation identifies new genes and pathways driving tumorigenesis. *Nature Genetics*, 45(7), pp.756–766. Available at: http://eutils.ncbi.nlm.nih.gov/entrez/eutils/elink.fcgi?dbfrom=pubmed&id=23685747&retmode=ref&cmd=prlinks\npapers3://publication/doi/10.1038/ng.2641.

Rao, V. V et al., 1992. The gene for bone morphogenetic protein 2A (BMP2A) is localized to human chromosome 20p12 by radioactive and nonradioactive in situ hybridization. *Human genetics*, 90(3), pp.299–302.

Riccardi, V.M., 1993. Molecular biology of the neurofibromatoses. *Seminars in dermatology*, 12(3), pp.266–273.

Rogers, M.B. et al., 1992. Bone morphogenetic proteins-2 and -4 are involved in the retinoic acid-induced differentiation of embryonal carcinoma cells. *Molecular Biology of the Cell* , 3 (2), pp.189–196. Available at: http://www.molbiolcell.org/content/3/2/189.abstract.

Roma, P., 2001. Letter to the Editor Mosaic (Segmental) Neurofibromatosis Type 1 (NF1) and Type 2 (NF2): No Longer Neurofibromatosis Type 5. , 180(May), pp.178–180.

Ross, J., 1995. mRNA stability in mammalian cells. *Microbiological reviews*, 59(3), pp.423–450.

Rutkowski, J.L. et al., 2000. Genetic and cellular defects contributing to benign tumor formation in neurofibromatosis type 1. *Human molecular genetics*, 9(7), pp.1059–1066.

Samatar, A.A. & Poulikakos, P.I., 2014. Targeting RAS-ERK signalling in cancer: promises and challenges. *Nature reviews. Drug discovery*, 13(12), pp.928–942.

Sedani, A., Cooper, D.N. & Upadhyaya, M., 2012. An emerging role for microRNAs in NF1 tumorigenesis. *Human genomics*, 6(1), p.23. Available at: http://www.pubmedcentral.nih.gov/articlerender.fcgi?artid=3537581&tool=pmcentrez&rendertype=abstract.

See, J. et al., 2004. Oligodendrocyte maturation is inhibited by bone morphogenetic protein. *Molecular and cellular neurosciences*, 26(4), pp.481–492.

Sharif, S. et al., 2007. Women with neurofibromatosis 1 are at a moderately increased risk of developing breast cancer and should be considered for early screening. *Journal of medical genetics*, 44(8), pp.481–484.

Shen, M.H., Harper, P.S. & Upadhyaya, M., 1996. Review article Molecular genetics of neurofibromatosis (NFl). *Molecular Biology*, 6, pp.2–17.

Simonetti, S. et al., 2014. Schwannomas, benign tumors with a senescent phenotype. *Histology and histopathology*, 29(6), pp.721–730.

Singh, A. & Morris, R.J., 2010. The Yin and Yang of bone morphogenetic proteins in cancer. *Cytokine & growth factor reviews*, 21(4), pp.299–313.

Sobell, H.M., 1985. Actinomycin and DNA transcription. *Proceedings of the National Academy of Sciences* , 82 (16), pp.5328–5331. Available at: http://www.pnas.org/content/82/16/5328.abstract.

Spyra, M. et al., 2011. Cancer stem cell-like cells derived from malignant peripheral

nerve sheath tumors. *PloS one*, 6(6), p.e21099.

Subramanian, S. et al., 2010. Genome-wide transcriptome analyses reveal p53 inactivation mediated loss of miR-34a expression in malignant peripheral nerve sheath tumours. *The Journal of pathology*, 220(1), pp.58–70.

Sun, D. et al., 2013. RAS/MEK-independent gene expression reveals BMP2-related malignant phenotypes in the Nf1-deficient MPNST. *Molecular cancer research : MCR*, 11(6), pp.616–27. Available at: http://www.ncbi.nlm.nih.gov/pubmed/23423222.

Takahashi, K. et al., 1994. Multiple transcripts of the neurofibromatosis type 1 gene in human brain and in brain tumours. *Clinical science (London, England : 1979)*, 87(5), pp.481–485.

Tong, J. et al., 2002. Neurofibromin regulates G protein-stimulated adenylyl cyclase activity. *Nature neuroscience*, 5(2), pp.95–96.

Villapol, S., Logan, T.T. & Symes, A.J., 2013. Role of TGF-β Signaling in Neurogenic Regions After Brain Injury. , pp.3–36.

Vineis, P., Schatzkin, A. & Potter, J.D., 2010. Models of carcinogenesis: An overview. *Carcinogenesis*, 31(10), pp.1703–1709.

Vogt, J., Traynor, R. & Sapkota, G.P., 2011. The specificities of small molecule inhibitors of the TGF?? and BMP pathways. *Cellular Signalling*, 23(11), pp.1831–1842.

Voorneveld, P.W. et al., 2013. Reduced expression of bone morphogenetic protein

receptor IA in pancreatic cancer is associated with a poor prognosis. *Br J Cancer*, 109(7), pp.1805–1812. Available at: http://dx.doi.org/10.1038/bjc.2013.486.

Wang, X. et al., 2012. Breast Cancer and Other Neoplasias in Women with Neurofibromatosis Type 1: A Retrospective Review of Cases in the Detroit Metropolitan Area. *American journal of medical genetics. Part A*, 158A(12), pp.3061–3064. Available at: http://www.ncbi.nlm.nih.gov/pmc/articles/PMC3505236/.

Watson, A.L. et al., 2013. Canonical Wnt/beta-catenin signaling drives human schwann cell transformation, progression, and tumor maintenance. *Cancer discovery*, 3(6), pp.674–689.

Watson, G.H., 1967. Pulmonary stenosis, café-au-lait spots, and dull intelligence. *Archives of disease in childhood*, 42(223), pp.303–307.

Weiss, B. et al., 2015. Sirolimus for progressive neurofibromatosis type 1-associated plexiform neurofibromas: a neurofibromatosis Clinical Trials Consortium phase II study. *Neuro-oncology*, 17(4), pp.596–603.

Whyte, D.B. et al., 1997. K- and N-Ras are geranylgeranylated in cells treated with farnesyl protein transferase inhibitors. *The Journal of biological chemistry*, 272(22), pp.14459–14464.

Widemann, B.C., 2009. Current status of sporadic and neurofibromatosis type 1-associated malignant peripheral nerve sheath tumors. *Current oncology reports*, 11(4), pp.322–328.

Wilusz, C.J. et al., 2001. Poly(A)-binding proteins regulate both mRNA deadenylation

and decapping in yeast cytoplasmic extracts. *RNA*, 7(10), pp.1416–1424. Available at: http://www.ncbi.nlm.nih.gov/pmc/articles/PMC1370185/.

Wong, W.W. et al., 1998. Malignant peripheral nerve sheath tumor: analysis of treatment outcome. *International journal of radiation oncology, biology, physics*, 42(2), pp.351–360.

Wozney, J.M. et al., 1988. Novel regulators of bone formation: molecular clones and activities. *Science (New York, N.Y.)*, 242(4885), pp.1528–1534.

Wu, J. et al., 2014. EGFR-STAT3 signaling promotes formation of malignant peripheral nerve sheath tumors. *Oncogene*, 33(2), pp.173–180. Available at: http://www.ncbi.nlm.nih.gov/pmc/articles/PMC3923530/.

Wu, M.Y. & Hill, C.S., 2009. TGF-β Superfamily Signaling in Embryonic Development and Homeostasis. *Developmental Cell*, 16(3), pp.329–343. Available at: http://www.sciencedirect.com/science/article/pii/S1534580709000860.

Xu, G.F. et al., 1990. The neurofibromatosis type 1 gene encodes a protein related to GAP. *Cell*, 62(3), pp.599–608.

Yeh, T.C. et al., 2007. Biological characterization of ARRY-142886 (AZD6244), a potent, highly selective mitogen-activated protein kinase kinase 1/2 inhibitor. *Clinical cancer research : an official journal of the American Association for Cancer Research*, 13(5), pp.1576–1583.

Yu, P.B. et al., 2008. BMP type I receptor inhibition reduces heterotopic [corrected] ossification. *Nature medicine*, 14(12), pp.1363–1369.

Zehou, O. et al., 2013. Chemotherapy for the treatment of malignant peripheral nerve sheath tumors in neurofibromatosis 1: a 10-year institutional review. *Orphanet journal of rare diseases*, 8(1), p.127. Available at: http://www.pubmedcentral.nih.gov/articlerender.fcgi?artid=3766199&tool=pmcentrez&rendertype=abstract.

Zhang, H. & Bradley, A., 1996. Mice deficient for BMP2 are nonviable and have defects in amnion/chorion and cardiac development. *Development (Cambridge, England)*, 122(10), pp.2977–2986.

Zhang, R. et al., 2013. Wnt/β-catenin signaling activates bone morphogenetic protein 2 expression in osteoblasts. *Bone*, 52(1), pp.145–156. Available at: http://dx.doi.org/10.1016/j.bone.2012.09.029.

Zheng, H. et al., 2008. Induction of abnormal proliferation by nonmyelinating schwann cells triggers neurofibroma formation. *Cancer cell*, 13(2), pp.117–128.

Zhu, Y. et al., 2002. Neurofibromas in NF1: Schwann cell origin and role of tumor environment. *Science (New York, N.Y.)*, 296(5569), pp.920–922.

Zou, C. et al., 2009. Clinical, pathological, and molecular variables predictive of malignant peripheral nerve sheath tumor outcome. *Annals of surgery*, 249(6), pp.1014–1022.

ABSTRACT

THERAPEUTIC TARGETING OF BMP2 IN NF1-DEFICIENT MALIGNANT PERIPHERAL NERVE SHEATH TUMORS

by

SIDRA AHSAN

December 2015

Advisor: Michael A. Tainsky, Ph.D.

Major: Cancer Biology

Degree: Doctor of Philosophy

Neurofibromatosis type I (NF1)-deficient malignant peripheral nerve sheath tumor (MPNST) is an aggressive tumor for which the standard treatment is surgical removal with wide margins, often leaving behind cancer cells needing chemotherapy. RAS-GRD is the most widely studied functional target of NF1 implicated in tumorigenesis, however, therapeutic interventions targeting RAS activity have met with limited success. Using gene expression profiling, our lab identified BMP2-SMAD1/5/8 signaling pathway as a therapeutic target in MPNSTs, independent of the NRAS and MEK1/2 regulation. The overall goal of my research was to validate the significance of BMP2 in MPNSTs in novel cellular models, study the combinatorial effects of BMP2 and MEK1/2 inhibition, and use the regulation of BMP2 transcriptional control to define mechanism-based rational targets of BMP2 signaling, to treat NF1-related tumors.

Biological aggressiveness of MPNSTs is characterized by its highly motile and invasive nature. I presented a unique approach that targets not only the motility and invasive capability but also growth and proliferative potential of MPNSTs, by inhibition of BMP2-SMAD1/5/8 and RAS-MEK1/2-ERK1/2 signaling pathways in MPNST cell lines.

By using physiologically relevant cell models that simulate MPNST condition *in vivo*, I have shown that combinatorial targeting of BMP2 and MEK1/2 pathways results in reversal of malignant features of MPNST cell lines. Additionally, I have identified a novel regulatory mechanism by which NF1 mediates BMP2 transcript stability. The targeted inhibition of the molecular components involved in stability of the *Bmp2* 3' UTR by NF1, represents an alternative approach of genetic targeting in MPNSTs. In summary, I have presented two independent methodologies of therapeutically targeting BMP2-SMAD1/5/8 signaling in MPNSTs.

AUTOBIOGRAPHICAL STATEMENT

SIDRA AHSAN

EDUCATION:

2010-2015	**Ph.D.**	Graduate Program in Cancer Biology, Wayne State University School of Medicine. Molecular Therapeutics Program, Department of Oncology, Karmanos Cancer Institute, Detroit, MI.
2002-2007	**B.Sc.**	Major: Biological Sciences, Minor: Nutrition and Food Sciences. College of Liberal Arts and Sciences, Wayne State University, Detroit, MI.

PUBLICATIONS:

1. **Ahsan S**, Tainsky MA. Combinatorial Therapeutic Targeting of BMP2 and MEK1/2 in Nf1-null malignant peripheral nerve sheath tumors. In Process of Publication.
2. Kaplun L, Fridman A.L, Chen W, Levin N.K, **Ahsan S**, Petrucelli N, Barrick J. L, Gold R, Land S, Simon M.S, Morris R.T, Munkarah A.T, Tainsky M.A. Variants in the Signaling Protein TSAD are Associated with Susceptibility to Ovarian Cancer in BRCA1/2 Negative High Risk Families. Biomarker Insights 2012:7 151-157.
3. Rengachary S, **Ahsan S**. Sir Robert Boyle and his unique case report on depressed cranial fracture. Neurosurgery 2007; 61(3):633-9; discussion 640

HONORS & AWARDS:

- Poster Presentation Award, Annual Cancer Biology Research Symposium, March 2015
- Thomas C. Rumble University Graduate Fellowship, Wayne State University Graduate School, 2014-2015
- Broadening Experiences in Scientific Training (BEST) Fellowship Award, Wayne State University Graduate School, 2014
- Cancer Biology Travel Grant Award, Wayne State University School of Medicine, 2014
- Graduate Student Professional Travel Award, Wayne State University Graduate School, 2014
- DeRoy Testamentary Foundation Fellowship, 2013-2014
- Poster Presentation Award, Annual Cancer Biology Research Symposium, May 2012
- Cancer Research Intern Fellowship, Center for Cancer Research, NCI, NIH, 2010